University of Zurich[UZH]

Habitat mapping of East and West Shark Bay, Australia

GEO 511 Master's Thesis

Author
Luca Brüderlin
14-731-640

Supervised by
Prof. Dr. Alexander Damm

Co-Supervised by
Prof. Dr. Michael Krützen

31.01.2019
Department of Geography, University of Zurich

A. Table of contents

A. Table of contents I
B. Figure index III
C. Table index VI
D. Abstract VII
1. Introduction 1
2. Background 3
2.1 History 3
2.2 Water structure 5
2.3 Flora and fauna 6
2.4 Heatwave 7
2.5 Research Goals 8
3. Methods 9
3.1 Data 10
3.1.1 Sensor selection 10
3.1.2 Datasets 12
3.1.3 Pre-processing 13
3.2 Water quality parameters 13
3.2.1 Estimating chlorophyll content using the normalized difference chlorophyll index 14
3.2.2 Concentration of total suspended solids 15
3.2.3 Content of coloured dissolved organic matter 16
3.3 Habitat mapping 17
3.3.1 Support vector machine 18
3.3.2 Analysis 18
3.4 Statistical analysis 20
4. Results 22
4.1 Temperature 22
4.2 Normalized difference chlorophyll index 24
4.3 Total suspended solids 30
4.4 Coloured dissolved organic matter 34
4.5 Correlation 39
4.6 Habitat analysis 41
5. Discussion 43
5.1 Temperature 43
5.2 Normalized difference chlorophyll index 44
5.3 Total suspended solids 45
5.4 Coloured dissolved organic matter 47
5.5 Correlation 48
5.6 Habitat analysis 48

6. Conclusion and Future Work 49
7. Bibliography 51
8. Appendix 57
8.1 NDCI 57
8.1.1 Images 57
8.1.2 Plots 70
8.2 TSS 72
8.2.1 Images 72
8.2.2 Plots 85
8.3 CDOM 87
8.3.1 Images 87
8.3.2 Plots 100
8.4 Correlation 102
9. Personal declaration 102

B. Figure index

Fig. 1. Landsat 7 ETM image showing the Shark Bay area, taken 07.03.2018 (Modified after: USGS; Australian Interstate Quarantine 2017). 3
Fig. 2 Overview of the Shark Bay and its islands. Additionally, the geological surfaces are displayed (Playford et al. 2013). 4
Fig. 3 The median water temperature per month shows a distinct peak in 2011 indicating the heatwave (Data Source: MODIS). 7
Fig. 4 The current systems surrounding Australia. The Leeuwin Current which was exceptionally strong because of La Niña is highlighted in red (Modified after: Richardson et al. 2014). 8
Fig. 5 The chart shows an overview of the processing chain. 9
Fig. 6 NDCI difference image generated by subtracting Sentinel 2 from Landsat 8 data. It illustrates potential sensor differences. 11
Fig. 7. NoData stripes in the Landsat 7 ETM+ image because of the sensor malfunction (Source: USGS). 12
Fig. 8 The radiative transfer when observing water bodies. 14
Fig. 9. The absorption coefficient of pure water, chlorophyll, colored dissolved organic matter and non-algal particles. (Watanabe et al. 2017). 14
Fig. 10 Flowchart showing the classification process. 19
Fig. 11 The regions of interest chosen for the data extraction, displayed on the ENVI created NDCI image. 20
Fig. 12 The difference in temperature induced by the warm water inclusion. The left image was taken on the 15.01.2011, the right one on the 04.03.2011. In the middle the difference between the two is displayed. 22
Fig. 13 The four time series data with their respetive trend lines. The red dashed lines indicates the heatwave in 2011 (Data Source: Landsat 7 ETM+). 23
Fig. 14 A comparison of the NDCI estimated in June 2011(left) and 2012 (right). In the middle the difference map of the two, showing a negative change in red and a positive one in blue. The yellow structures in the right image are clouds. 24
Fig. 15 The time series data for the western (upper graph) and eastern bay arm (middle graph) per region of interest. At the bottom a zoom into the years 2003 to 2006 is displayed reveling an unsystematic structure in the western bay (lower left) whereas the eastern bay arm (lower right) seems to show gradual structures. 25

Fig. 16 The two intermediate products of the statistical analysis of the data at West 3. The outlier detection (left) and F-statistics (right) are calculated within the analysis and generate the displayed side products. 27
Fig. 17 The NDCI values at the regions of interest West 3 (upper left), West 4 (upper right) and West 5 (lower middle). Plotted are the trend line over the whole time series (blue) and the segment trend lines (red). 27
Fig. 18 The NDCI time series at East 1 (left) and East 2 (right). Displayed are the overall trend line (blue) and the trends in the two segments (red) found by the breakpoint detection. 29
Fig. 19 The NDCI data at Hamlin pool (East 5) over the 14 years of interest. Displayed are the overall trend line (blue) and the trends in the two segments (red) found by the breakpoint detection. 29
Fig. 20 A comparison of TSS concentration in gm^{-3} estimated in June 2011 (left) and 2012 (right). In the middle the difference map of the two, showing the change in between the two years. Negative values (red) indicate a decrease in TSS whereas the positive values (blue) show an increase 30
Fig. 21 The TSS time series data for the western (upper graph) and eastern bay arm (middle graph) per region of interest. At the bottom a zoom onto the years 2003 to 2006 is displayed reveling no significant gradient in the data. However, the eastern arm (lower right) seems to by little bit more structured than the western one (lower left). 31
Fig. 22 The TSS time series data in the western bay arm. West 2 in the upper left, West 4 upper right and West 5 in the lower middle. The blue line shows the trend over the whole time series whereas the red lines show the trends in the two segments found by the breakpoint detection. 32
Fig. 23 The TSS data from June plotted over 14 years for East 2 (upper left), East 3 (upper right) and East 5 (lower middle). Displayed are the overall trend line (blue) and the trends in the two segments (red) found by the breakpoint detection. 33
Fig. 24 Two images showing the natural logarithm of the absorption at 440 nm which corresponds to the amount of CDOM in the water. The left image was taken in June 2011, the right image in June 2012 The change from June 2011 to 2012 is displayed in the middle. Negative change is presented in red whereas positive values are blue. 35

Fig. 25 The CDOM values over the whole time series for the western (upper graph) and eastern (middle graph) bay arm, shown per region of interest. The bottom images display a zoomed in view to show potential gradients present in the western (bottom left) and eastern (bottom right) waters. 36
Fig. 26 The CDOM concentration shown every June at West 3 (upper left), West 4 (upper right) and West 5 (bottom middle). Displayed are the overall trend line (blue) and the trends in the two segments (red) found by the breakpoint detection. 37
Fig. 27 The CDOM values in June recorded in the eastern Shark Bay. Displayed are East 3 (upper left), East 4 (upper right) and East 5 (bottom middle). The coloured lines represent the overall trend line (blue) and the segment trend lines (red)..... 38
Fig. 28 The correlation between the three indices in the west, shown on three examples. Displayed are the R indicating the correlation and p which is the significance value. 39
Fig. 29 Some examples of the eastern bay arms correlation coefficients when looking at the three indices. R shows the correlation and p the significance value..... 39
Fig. 30 The western indices correlation coefficients with the water temperature extracted from MODIS. The type of correlation is indicated by the R-value, p shows its statistical significance. 40
Fig. 31 The Pearson correlation coefficient for sea surface temperature and the indices, calculated in the eastern bay arm. R indicates the correlation type and p its significance value..... 40
Fig. 32 The benthic map showing the seagrass extent for 2010 (left), 2011 (middle) and 2012 (right). 41
Fig. 33 The pixel count for the seagrass (left) and no seagrass class (right) over the whole Shark Bay area. Displayed are the overall trend line (blue) and the trends in the two segments (red) found by the breakpoint detection. 41
Fig. 34 The western seagrass extent (left)from 2000 until 2017. The right graph shows the pixel count for no seagrass. The blue line represents the overall trend, the red lines the segment trends. 42
Fig. 35 The pixel count of the seagrass (left) and no seagrass (right) extent in the eastern bay arm. The over all trend line is shown in blue, the detected segment trend lines are in red. 42

C. Table index

Table 1. The basic parameters of the available sensors (Source: NASA, ESA, USGS). 10
Table 2 The results of the statistical analysis of NDCI values. Significant values are in bold. 28
Table 3 The results of the statistical analysis of TSS values. Significant values are in bold. . 34
Table 4 The results of the statistical analysis of CDOM values. Significant results are bold. 38
Table 5 The statistical results of the seagrass cover changes. 43

D. Abstract

The Shark Bay in Western Australia has had an extreme heat event in 2011, resulting in water temperatures rising 5 °C over their usual levels. Subsequently, the diverse and delicate ecosystem was disturbed and the whole maritime flora and fauna suffered negative effects. The study at hand will focus on detecting behavioural changes of bottlenose dolphin schools and seagrass loss in respect to the heatwave with remotely sensed optical data. Using three water quality parameters, the normalized difference chlorophyll index, total suspended solids and coloured dissolved organic matter, the analysis tries to grasp the heatwaves influence on the bay system and link it to the changes reported by dolphin researches. A time series analysis of the last 18 years of Landsat 7 ETM+ data helps embedding the warm water inclusion in the bay's development over time. These results are supplemented by a benthic habitat map, classifying the seafloor using a support vector machine. The results indicate statistically insignificant results analysing the water quality parameters. The heatwave is hardly detectable in the data and does not stand out within the time series. No explanations for the dolphin's behavioural changes could be found. The benthic maps were insufficient for a habitat analysis, because the water column's dynamic absorption interfered with the seafloor classification algorithm. Consequently, no insights in the maritime system's complex response to such a drastic event were gained.

1. Introduction

The analysis of water ecosystems in a context of global climate change has become an essential tool in assessing the impact of the recent global development. Water poses a major part of the system, as it hosts a vast number of unique plants and animals which are crucial components. Especially because the plants and algae in the world seas remain a vital part in the carbon cycle. Without the deposition of carbon and conversion into oxygen, habitable conditions outside of water would not be possible. The most valuable regions are the very diverse nearshore ecosystems, such as seagrass meadows or mangrove forests, which are intensely affected by environmental changes and anthropogenic influences (Goodell et al. 2018). The amount of parameters impacting these fragile systems range from thermal stress, nutrient runoff and sedimentation up to overfishing, coastal development and pollution (Garcia et al. 2018; Goodell et al. 2018). As water systems are extremely complex it is hard to capture its properties, changes and trends in full extent. However, with the implementation of remote sensing into water analysis, a multifaceted tool has been introduced, which is capable of gathering a wide spectrum of information. Especially water physical parameters are accurately and easily obtained (Jaelani et al. 2016). The power of remote sensing lies in the amount of data that can be collected within a short time, while still providing a decent spatial resolution. Landsat 7 ETM+ for example samples with a resolution of approximately 30m and a repetition frequency of 16 days (U.S. Department of the Interior & U.S. Geological Survey 2018). This allows us to investigate much larger areas of interest in an extremely short time without having the need of large-scale field studies.

With such a great potential, it seems unsurprising, that remote sensing has become a crucial part in monitoring water bodies in recent years. In comparison to vessel-based research, airborne image systems have great advantages. As one can imagine the vessel-based monitoring is bound to transects and can only estimate the whole extent of a larger water body by interpolating data. Additionally, boats have a fixed depth of flotation and are thus extremely limited when measuring coastal ecosystems (Ohlendorf et al. 2011). The strength of remote sensing lies in its cost and time efficiency while giving consistent temporal and a broad spatial coverage (Slonecker et al. 2016; Misra et al. 2018). The data is gathered in a digital format which can be easily processed further and combined with additional computer based models (Lamaro et al. 2013). The potential of remote sensing in understanding water ecosystems is shown in the various studies already done on this subject all around the world. Assessing the so-called water quality parameters is hereby a common tool to estimate the state of the water system and its possible effects on flora and fauna. Jaelani et al. (2016), show us that parameters such as the chlorophyll content of water and the amount of total suspended solids can be calculated very precisely in sea water such as the Indonesian Sea. But also other water bodies, for instance rivers or lakes have been the centre of interest in research (see Olmanson et al. 2016). Looking at the vast amount of successful studies already conducted, the great potential of remote sensing becomes even clearer. However, one should never miss out the limitations remote sensing is

faced with. The main influence on remotely sensed data comes from varying atmosphere and surface properties and the resulting absorption, transmission and reflection (glint) (Jaelani et al. 2016; Ohlendorf et al. 2011). Thus, atmospheric correction models are crucial in processing the data, since the water leaving radiance often is extremely weak and potentially concealed by the multiple scattering in the water and the atmosphere (Eugenio et al. 2015). However, the correction still remains challenging as the optical parameters are constantly changing and every image needs to be corrected accordingly (Mishra & Mishra 2012). As it is of great importance to assess the water properties over space and time it is essential to correct data properly (Park 2007).
Exploring the possibilities when observing water surface properties, recent years have shown a shift from obtaining surface properties, such as the chlorophyll content, to gathering bathymetry data, through the water column down to the sea floor. The conventional method of assessing benthic data and water parameters of coastal areas is ship based (Misra et al. 2018; Pattanaik et al. 2015). With costly echo-sounding an time-consuming infield measurements data is gathered (Gao 2009). Because benthic data is a crucial component in understanding the state of marine ecosystems, the marine life present, nutrient, habitats and sea surface properties, remote sensing has become increasingly important in recent years when looking at marine systems (Eugenio et al. 2015). Earth observation sensors record in their raw data, a reflection of the surface and, if strong enough, also one of the sea floor. The water between surface and ground naturally absorbs and scatters light according to its specific properties (Ohlendorf et al. 2011). The unique signals of the water column and the ground are valuable information sources, which allow us to understand depth distributions of the above named water physical properties, but also map the sea ground cover and structure (Pattanaik et al. 2015; Roy 2003; Gao 2009). But, this new field of observations also brings new challenges. In addition to atmospheric correction, the absorption of the water column needs to be considered. As the water absorbs and scatters light with increasing depth also the ground signal gets weaker. Several studies tried to estimate the limiting water depth and proposed estimates from 15 meters (Ohlendorf et al. 2011) up to 70 meters (Gao 2009). Nevertheless, remote sensing provides a very efficient, precise and time-saving approach in comparison to the used sounding systems (Gao 2009; Roy 2003). As both, the water physical parameters and the bathymetric analysis, hold crucial information on water systems the following approach tries to combine the two methods to provide an even better picture. By studying water bodies using a combined approach a broader analysis can be conducted and thus show us possible additional interconnections between the two. This is of particular interest, as the study aims on finding connections in between the distribution and dynamics of dolphin habitats, social structures and behaviour, and their link to water quality parameters and changes caused by climatic shifts. The study will focus on a heatwave event in 2011, where water temperatures in the Shark Bay rose 5 °C over their normal level (Arias-Ortiz et al. 2018; Caputi et al. 2014). The analysis is built around reports from the Dolphin Research Alliance, which indicate behavioural changes, potentially connected to the warm water inclusion, in the dolphin schools present in the bay. The study will be based on those findings and

tries to supplement and explain the observations brought forward by those scientists. At the same time, it will help the understanding of possibilities and limitations in water remote sensing while using it on a case study which is still research ongoing.

2. Background

The Shark Bay lies on the West Australian coast approximately 800 kilometres north of Perth. The bay area is roughly 11'000 km^2 and is separated into two parts by the Peron Peninsula reaching 100 km into the bay (see Fig. 1 and Fig. 2). On its westerly side the Shark Bay is separated from the open water by the Edel Land Peninsula, the Dirk Hartog island and several other, smaller islands. The surface of Shark Bay's landmasses is characterized by Holocene sand dunes (see Fig. 2), small shrubs and other thermophile vegetation (Playford et al. 2013). Underneath the sandy surface lays the bedrock, which is not particularly remarkable as mostly sand and limestone can be found (Playford et al. 2013). Hence the geology of the Shark Bay is not very special, even though geological processes such as faults and anticlines are present throughout the whole bay area, being the major factor in forming the Shark Bay into what it looks like today (Playford et al. 2013). What makes the Shark Bay unique is its extremely diverse and specialized flora and fauna, which has been the centre of scientific research for decades.

2.1 History

The first European to reach the coast of Western Australia was the Dutch seaman Dirk Hartog, setting foot onto Australian ground in the Shark Bay area in 1616 (Parks and Wildlife Service 2018b; Playford et al. 2013). However, the Dutch sailors where not the first people to visit the bay, as the area has been populated by Aboriginal people of the tribes Malgana, Nanda and Yinggarda for at least 40'000 years (Parks and Wildlife Service 2018b; Bowdler 1990). 83 years later, in the year 1699, the English geographer, explorer and sailor William Dampier visited Western Australia to study its coast (Playford et al. 2013). Landing at Shark Bay's western shoreline he explored the area, its animals and vegetation. Besides many other things, he observed great numbers of sharks subsequently giving the bay its name (Parks and Wildlife Service

Fig. 1. Landsat 7 ETM image showing the Shark Bay area, taken 07.03.2018 (Modified after: USGS; Australian Interstate Quarantine 2017).

2018b). The first European settlements were established in the 1850s, when the guano industry gained interest (Playford et al. 2013). Because of its high phosphate content, guano, bird's excrements, was collected to be used as fertilizer in Europe (Playford et al. 2013). Besides guano, the Shark Bay area also held a great amount of oysters, which were of interest for the pearling industry (Hart et al. 2016).

Today Shark Bay county is the home of 952 residents mainly working in the fishery as well as accommodation and food services (Australian Bureau of Statistics 2018; Shire of Shark Bay 2016). As the natural environment in the area is extraordinary, tourism is one of the main sources of income present. Hence the service industry is of great importance for the whole county. Luckily the bay is very popular with tourists because of its diverse flora and fauna, beautiful landscape and mild climate.

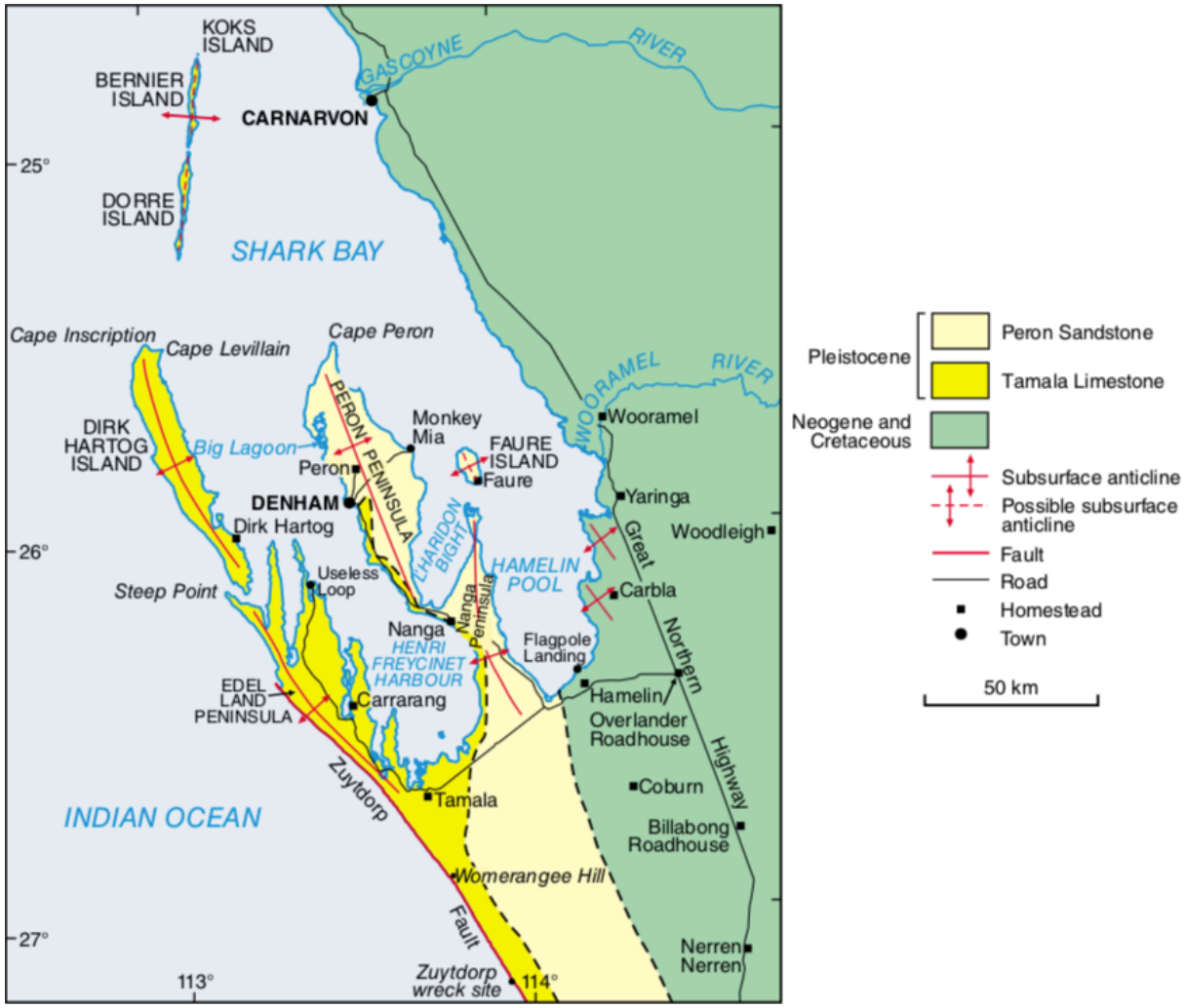

Fig. 2 Overview of the Shark Bay and its islands. Additionally, the geological surfaces are displayed (Playford et al. 2013).

2.2 Water structure

Laying at 25° south, Shark Bay is in a semi-arid climate zone with warm temperatures and little rain. Averaging at 26.5 °C the temperature ranges from approximately 10 °C to 35 °C throughout the year (Parks and Wildlife Service 2018a). However, the temperature and precipitation regimes are diversely distributed and thus generate small habitat niches for rare plant and animal species. In addition to the terrestrial species, the Shark Bay waters hold one of the most interesting marine systems and thus stands as a perfect study area.

Its shallow water is characterized by different salinity levels hence supporting the diversity of organisms present. Logan (1974) defined three regimes present in the Shark Bay waters. Hamlin Pool and L'Haridon Bright are classified as hypersaline with a salinity ranging from 55 – > 40‰. The northern part of the eastern Shark Bay and the western part are metahaline with 40 – 55‰. Roughly at the end of the Peron Peninsula the salinity regime changes into oceanic (35 – 40‰). However, the boundaries of these classes are dependent on the rain fall, evaporation, wind and tides. Especially Henri Freycinet Harbour is subject to varying salinity, depending on the parameters present, it changes from metahaline into hypersaline (Playford et al. 2013; Logan 1974). On the other hand, as the bay area is shielded towards the ocean by the peninsula and islands, the interchange and mixing of water is inhibited, thus stabilizing the salinity regimes and supporting hypersaline ponds (Playford et al. 2013).

In this context, Hamlin Pool needs be looked at closer, as it is the only region with a stable hypersaline environment giving very unique life forms a niche to live in. Within the high salinity levels, fishes, mussels and seagrass can hardly survive which is why stromatolites were able to developed uninterruptedly in these waters (Reid et al. 2003). Stromatolites are microbiological communities consisting mainly of cyanobacteria (Playford et al. 2013). They are of particular interest in understanding the origin of life as theories suggest that these mineral structures, hosting very primitive organisms, could be one of the starting points of life (Schweizer Radio und Fernsehen 2018). The organisms developed in the tidal zones of Hamlin Pool and are still actively growing today.

The tidal movement is rather complex as it consists not only of an astronomical component but also a meteorological one. Interestingly, the meteorological influence on the tides is much greater than the astronomical one (Burling et al. 2003). The local pressure regimes and the winds connected to them define the tides within the Shark Bay waters (Playford et al. 2013). However, the effect then again varies on a smaller scale. Hamlin Pool was found to be stronger affected by meteorological factors than Denham thus having the highest water level changes in the whole Shark Bay (Maximum: 1.59m in 1979) (Playford et al. 2013; Burling et al. 2003).

2.3 Flora and fauna

Looking at the diversity of habitat characteristics present in the Shark Bay, it is of no surprise, that it holds a substantial number of different lifeforms. Combined, the whole area has more than 660 animal species and over 900 corals and plants of which some are listed as most endangered animals such as dugongs or green turtles (Tourism WA 2018). This diversity combined with the historical importance, stromatolites and remarkable landscape led to the acceptance of the whole area as UNESCO world heritage in 1991 (UNESCO World Heritage Center 2018).

One of the most valuable species present, especially in a global context, is the extremely diverse seagrass ecosystem in the bay. Covering around 4'300 km^2, the seagrass beds are considered to be one of the largest and most significant ones in the world (Arias-Ortiz et al. 2018). Having these underwater meadows has a positive influence on the water quality and increases the value of the whole bay ecosystem. First, seagrass poses as a perfect habitat for many species. It does not only give shelter but also is a vital component within the oceanic food chain (Reynolds 2018). In addition to that, it protects the shoreline and holds together the sediments with its root structure while also improving the water quality (Duarte 2002). In a global context, however, the carbon sequestration is the most valuable function of a seagrass ecosystem. Like trees, seagrass has the ability to store carbon within their leaves and roots, when the plants die and decay it gets buried and subsequently stored in the seafloor (Fourqurean et al. 2012). It is estimated, that per year the meadows take up to 80 million tons of carbon worldwide, which leads to the fact that up to 0.65 – 1.2% of all carbon is stored within water plants (Reynolds 2018; Arias-Ortiz et al. 2018).

But, as many other ecosystems, also seagrass beds have been influenced by global warming and human activity negatively, resulting in a constant loss of their extent worldwide. The resulting consequences are immense and range from loss of habitat, water quality and hence biodiversity to the loss of great amounts of stored carbon (Duarte 2002). Arias-Ortiz et al. (2018) estimate that the Shark Bay has already lost about 22% of its meadows and their extent is steadily declining further. The influence of carbon being released into our atmosphere is widely known and seagrass plays a major role in our climate system and its constant change. It is estimated, that until the year 2051 the Shark Bay will release 10 to 52 MgC ha^{-1} in the atmosphere greatly influencing local but also global climate systems (Arias-Ortiz et al. 2018).

As stated, the large meadows provide nutrients, feeding grounds and habitat for animals and plants in the coastal region (Knudby & Nordlund 2011). One of the most noteworthy animal species living in the area are bottlenose dolphins or Tursiops (lat.). Tursiops is the genus describing three species of dolphins of which the most common one, tursiops truncatus also known as the common bottle nose dolphin, can be found nearly world-wide (Encyclopedia of Life 2013). The bottlenose dolphin species however, do vary strongly in their appearance and develop different characteristics depending on their habitats (Connor et al. 2000).The ones present in Western Australia are approximately 2 – 4 meters long and may reach weights around

200 kg (Grzimek 1969). Tursiops truncatus are extremely interesting creatures as they are known to be very social and have distinct structures in their groups. In the Shark Bay the dolphins have developed a diverse set of social structures and specific specialisations, such as using sponges as tools, depending on their local habitat (Shark Bay Dolphin Research Alliance 2018; Connor et al. 2000). These have been monitored and analysed in combination with water and weather parameters by the Shark Bay Dolphin Research Alliance since 1982.

2.4 Heatwave

The research is focused on an extreme heatwave in the year 2010/2011, when water temperatures were rising 2 to 5 °C above their average (see Fig. 3) (Arias-Ortiz et al. 2018; Caputi et al. 2014). The heatwave seems to be the result of an unusual strong Leeuwin current (see Fig. 4) which was built up by a strong La Niña system (Caputi et al. 2014). The consequences of this abnormally warm summer were drastic. The whole West Australian coast area suffered severe changes regarding their habitats, environment and subsequently biodiversity. Shark Bay however, was hit stronger than any other site along the west coast. The heatwaves effects, within the Shark Bay waters, were intensified because the western land tongue isolates the bay, hindering the flow of warm water and exchange with the open sea (Caputi et al. 2014). At the same

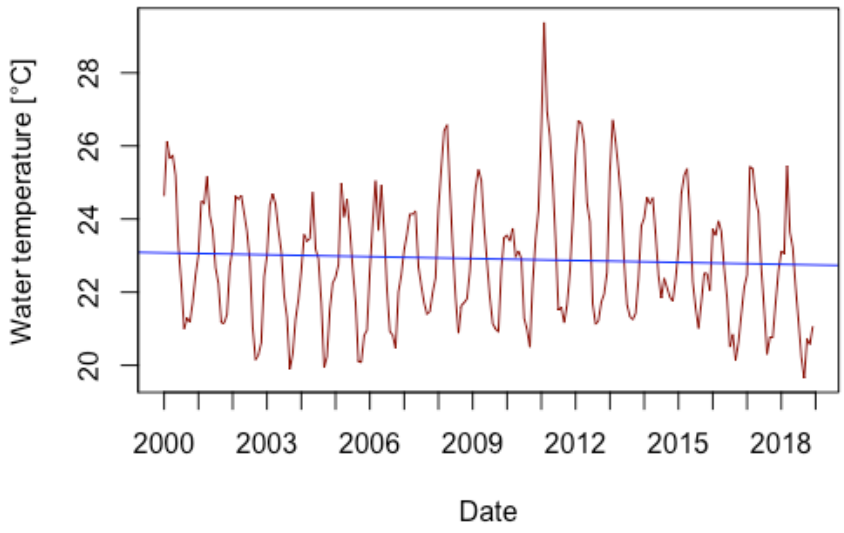

Fig. 3 The median water temperature per month shows a distinct peak in 2011 indicating the heatwave (Data Source: MODIS).

time, the comparatively shallow water structures further promote warming. Animals and plants present in the bay area were affected by the sudden inclusion of warm water into the bay area, because of changes in nutrient and oxygen availability in the water. Consequently, experiencing higher mortality and reduced fertility. These influences have been documented by the researches of the Shark Bay Dolphin Research Alliance. Since the heatwave, dolphins changed in their behaviour and diurnal activity, their social structures and specialisations are changing while having higher mortalities and lower fertility. In addition, the warmer water gave non-native tropical species perfect reproduction conditions which further weakened the already

groggy local species (Caputi et al. 2014). Besides many aquatic animals, mainly the seagrass meadows, posing one of the central components of the habitats in the bay area, were damaged. Arias-Ortiz et al. (2018) estimate that 36% of the seagrass present was harmed and its sediment C stock was exposed to oxic conditions, resulting in the release of CO_2. The ground cover directly or indirectly also influences the whole habitat, nutrition and biodiversity in the bay's water (Arias-Ortiz et al. 2018).

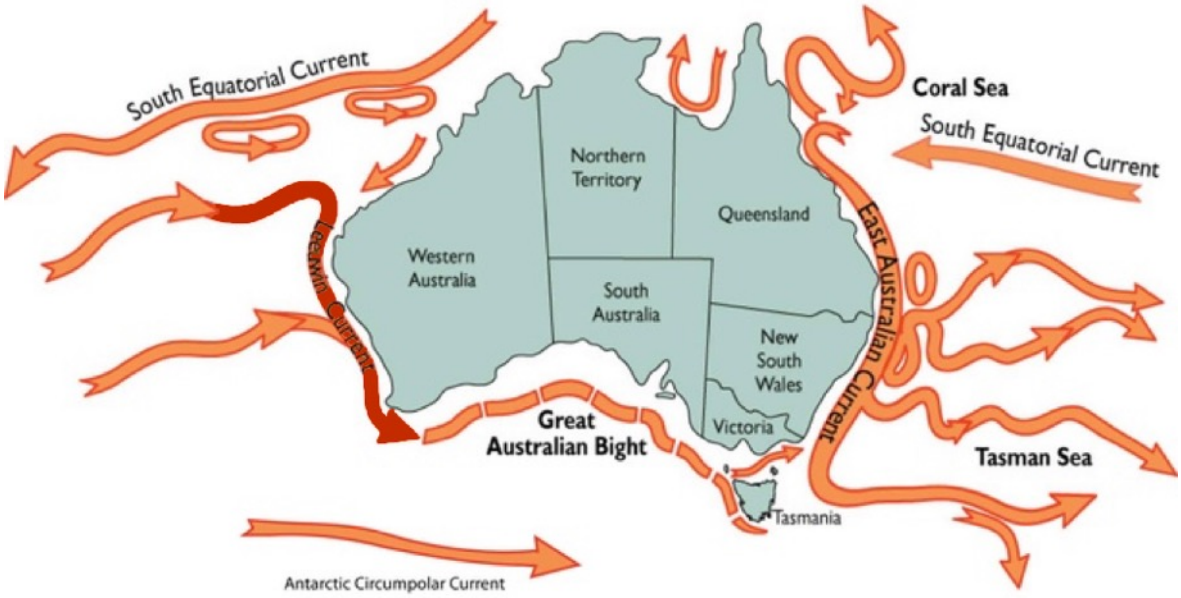

Fig. 4 The current systems surrounding Australia. The Leeuwin Current which was exceptionally strong because of La Niña is highlighted in red (Modified after: Richardson et al. 2014).

2.5 Research Goals

This study aims to investigate the water physical parameters in combination with a benthic habitat map to assess the influences of the warm water inclusion in summer 2010/2011. Remote sensing will be used to quantify the extend of changes in the region and finding explanations for the dolphin's behavioural changes. Additionally, connections between distinct parameters and specific changes in the ecosystem or animal and plant life will be examined.
The research goals are as follows:

- To examine the possibilities to generate spatial information and water information based on remote sensing methods and use those for a thorough study in the Shark Bay area
    - What are the possibilities and limits of remote sensing data and data analysis when examining water bodies?
    - Is the 2010/2011 heatwave detectable in the data?
    - Is it possible to understand the post-heatwave changes of dolphin's behaviour with remote sensed benthic data?
    - Does the data support the in situ observations conducted by the dolphin alliance?
    - Are there different changes between the diverse parts of the Shark Bay area?

The goal is to establish a connection between the data gathered by the researches in field and the remotely sensed data, while searching for the limitations of the remote sensing data in water and benthic analysis. It is expected, that a significant change, related to the heatwave, is detectable in the data. Water physical parameters will show a decrease in food availability for dolphins combined with a rising concentration of suspended solids and coloured dissolved organic matter. This will be connected to growth inhibitors for plants on the seafloor and their higher mortality. This development will most likely be linked to the summer heatwave in 2010/2011 and support the findings of the Shark Bay Dolphin Research Alliance. The questions will be tackled with a time series analysis of the water physical parameters back to the year 2000. This will ensure well understood results, as long term trends and short term changes can be distinguished easily. Additionally, a time series allows to estimate a potential recovery of the bay area and future trend predictions. Furthermore, the seafloor will be mapped to detect changes in the dolphin's habitat conditions. The combination of the two approaches will provide a fuller understanding of the processes happening in the bay area since 2000, and the magnitude of the heatwave within the long-term development.

3. Methods

The approach used in this study to identify the water physical parameters and benthic data in the Shark Bay area is composed of several different methods already applied in previous analyses. The combination helps to grasp the wide variety of an interdisciplinary field such as water quality parameters in connection with the bottlenose dolphin's habitats and social structures. The data however, is aggregated from one source, the USGS database. The data was then processed with ENVI Classic 5.4 (64-bit) and SNAP Desktop 5.0.8 using their built-in tools. The three indices were calculated and subsequently statistically analysed for a trend analysis. Additionally, a benthic habitat analysis of the seafloor properties was conducted using the ENVI provided support vector machine classification. In a final step, the water quality parameters

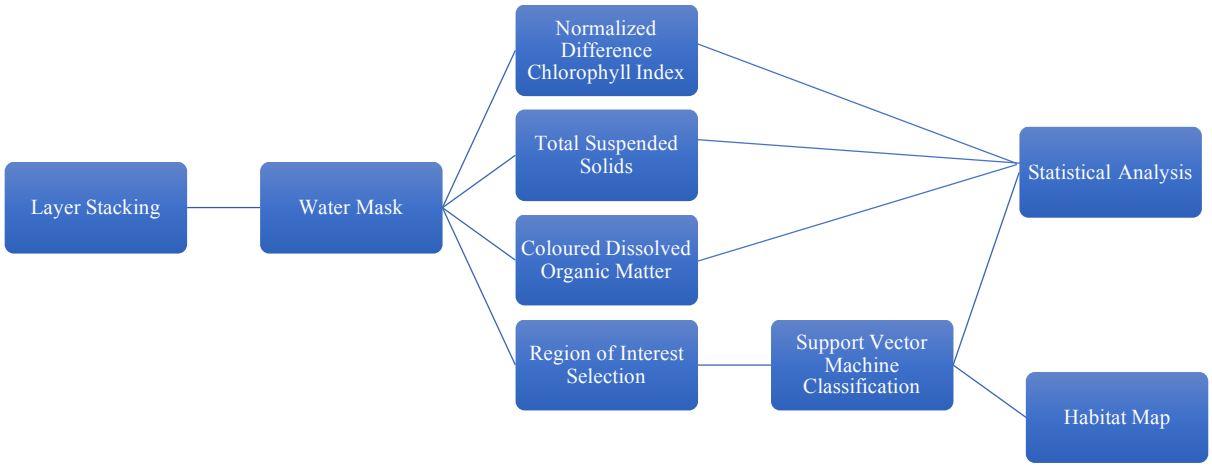

Fig. 5 The chart shows an overview of the processing chain.

were analysed in respect to the benthic data set, to find potential connections between the remotely sensed data and the observations made by the marine biologists in field.

3.1 Data

Before the selection of the Landsat 7 ETM+ as the matching sensor, a thorough comparison of the potential satellites in all their facets had to be conducted, to find the best fitting sensor for the analysis. The sensors available were ESA's Sentinel 2, NASA's Landsat 5, Landsat 7, Landsat 8 or MODIS (Part of the Terra Satellite). These sensors were chosen to be suitable because of their potential for a time series analysis and their spatial and spectral resolution. Table 1 shows a broad overview on the essential characteristics of the sensors.

Table 1. The basic parameters of the available sensors (Source: NASA, ESA, USGS).

Satellite	Sensors	Spectral resolution	Spatial resolution	Revisit frequency	Operation time
Sentinel 2	Multi Spectral Instrument (MSI)	12 Bands 0.45 – 2.19 µm	10 m, 20 m, 60 m	5 Days	Since June 2015
Landsat 5	Multi Spectral Scanner (MSS)	4 Bands 0.5 – 1.1 µm	57 x 79 m	16 Days	March 1984 – June 2013
	Thematic Mapper (TM)	7 Bands 4.5 – 2.35 µm	30 m, 120 m		
Landsat 7	Enhanced Thematic Mapper Plus (ETM+)	8 Bands 0.44 – 0.9 µm	15 m, 30 m, 60 m	16 Days	Since April 1999, Sensor Malfunction July 14, 2003
Landsat 8	Operational Land Imager (OLI)	9 Bands 0.43 – 2.3 µm	15 m, 30 m	16 Days	Since February 2013
	Thermal InfraRed Sensor (TIRS)	2 Bands 10.3 – 12.5 µm	100 m		
Terra	Moderate-resolution Imaging Spectrometer (MODIS)	36 Bands 0.4 – 14.39 µm	100 m, 250 m, 500 m	1 – 2 Days	Since December 1999

3.1.1 Sensor selection

To choose the best fitting senor(s), the main focus was on their time coverage, which is crucial for the time series analysis. Data of the last approximately 20 years are needed for a proper trend analysis. Terra MODIS would be a good fit since it is in space for 19 years and still operating normally. Additionally, its fast repetition frequency could be interesting to have, in case of incidents happening in a short time scale. Sentinel 2 on the other hand, does also have a very fast repetition frequency, however its operation time is too short to have a proper time series. Landsat data has the lowest repetition frequency, of only two pictures per month. Yet,

with more than 30 years, Landsat is the longest active satellite mission looking at Earth's surface parameters (Roy et al. 2016). Especially Landsat 7 and Landsat 8 hold a large potential when combined since they do not have large compatibility issues, as their sensors are strongly related. Additionally, the two sensors are also offset by 8 days, thus the revisit frequency decreases when combined (Roy et al. 2016).

A second parameter taken account of is the spatial resolution. Spatial resolution is of importance as it may influence the results greatly by generalizing small scale changes. Because the Shark Bay is a very diverse environment and dolphin habitats are changing in very small scales, a coarse resolution would not be able to grasp the structures properly. Consequently, by peer reviewing some images of the sensors, the MODIS data was ruled out because of its spatial resolution. Sentinel and Landsat data however, were held to be capable of illustrating the study area in its diversity.

To understand the influence of spatial resolution on the results even better, a comparison of the indices was conducted. For a Sentinel 2 (resolution 10 meters) and a Landsat 8 image (resolution 30 meters) all indices where calculated and the results compared by generating difference maps. This step is necessary to rule out possibly unfitting sensors but also to evaluate potential additional data sources, namely ultra-high resolution commercial satellites such as Worldview or Rapid Eye. To visualize the disparities of the two sensors the Normalized Difference Chlorophyll Index values of the Sentinel image were subtracted from the Landsat values. As both values are normalized between –1 and 1 a direct comparison of the two is possible. Fig. 6 shows the result of the subtraction. Obviously, the overall differences are rather small and thus the spatial resolution does not seem to affect the results immensely. What is interesting however, is the fact that the Sentinel image seems to find higher values throughout the whole image. A sensor specific underestimation of NDCI values might be an issue which needs to be taken account of. As the bands of the two sensors used in the calculation are not exactly congruent, different spectral resolution might have induced an underestimation of values. Nevertheless, the analysis showed, that the influence of spatial resolution at this level does not influence the data significantly. Thus, the Landsat satellites were chosen as the main data source, because their sensor characteristics seem to be the best fit for the analysis. Furthermore, images in lower spatial resolution also mean fewer gigabytes of data that need to be processed, subsequently resulting

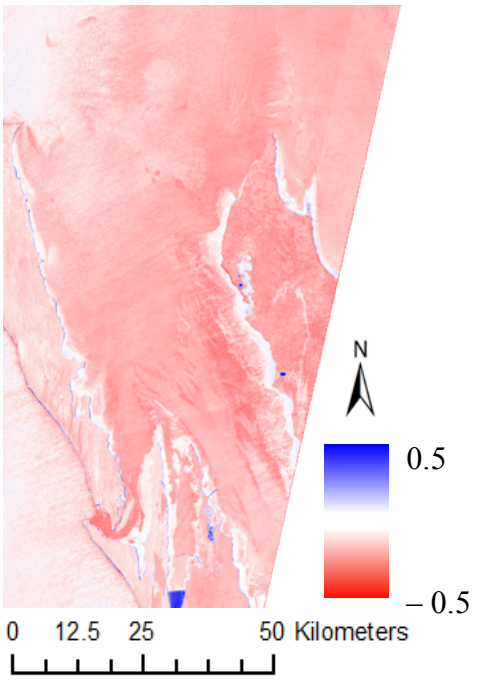

Fig. 6 NDCI difference image generated by subtracting Sentinel 2 from Landsat 8 data. It illustrates potential sensor differences.

in lower computation time. Within the Landsat missions, Landsat 7 was chosen as the key sensor, because of its time coverage perfectly fitting with the times of interest. The other Landsat satellites however, are potential supplementary sources for more precise analysis or in case of no available data (e.g. clouds covering the bay).

3.1.2 Datasets

All data used in the study was provided by USGS Earth Explorer. Luckily, the image in path 115 and row 78 of Landsat 7 ETM+ covers the Shark Bay area perfectly and thus the processing effort regarding composites was greatly reduced. The images were downloaded as level 2 processed data, which means they were atmospherically corrected and represented surface reflectance. Especially for water quality research the atmospheric correction is of great importance (Slonecker et al. 2016). Surface reflectance means that the data is corrected for atmospheric gases and particles influencing the recorded signal (Roy et al. 2016). As these parameters vary greatly over space and time atmospheric correction models are rather complex but also obligatory for any multi-sensor and multi-temporal study (Varma et al. 2016). The atmospheric correction for the level 2 data was executed by USGS with their Landsat Ecosystem Disturbance Adaptive Processing System (LEDAPS). The LEDAPS is based on MODIS routines and corrects for the following parameters: Water vapour, aerosol optical thickness, gases like ozone and elevation (Slonecker et al. 2016). With these parameters, for each acquisition a signal is simulated, which is used to calibrate and correct the data according to the respective conditions (Louvres et al. 2006; Roy et al. 2016). Besides correcting the data several other outputs are generated such as cloud masks (Slonecker et al. 2016). As the LEDAPS model is specifically used for Landsat datasets its atmospheric correction is very precise and greatly enhances the data quality for ETM+ but also OLI (Roy et al. 2016).

Besides having very good datasets provided, the Landsat 7 ETM+ has a major drawback. Unfortunately, Landsat 7 fell victim to a sensor malfunction in 2003, which was not corrected for in the provided USGS data. Since early summer 2003 there are gaps of NoData values in the image as the scan line corrector failed (Misra et al. 2018). The corrector would compensate the forward movement of the satellite (Wang et al. 2009). Approximately 22km in the middle of the image are not affected by the failure, the rest of the image contains stripes around 400 meters wide which tend to get thicker towards the border of the image (Misra et al. 2018). It is estimated, that 22% of the data is lost due to the failure, however reviewing the images (see Fig. 7) and looking at other studies

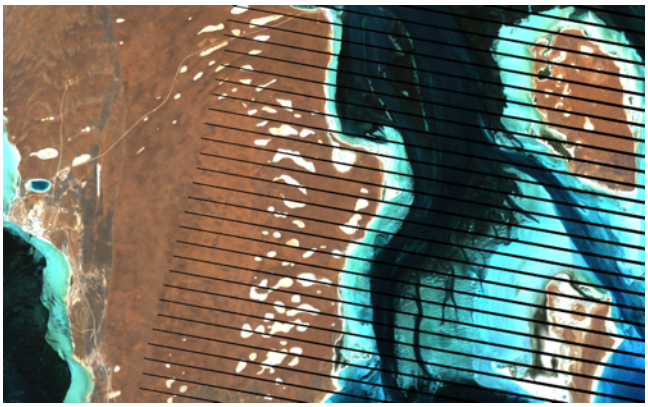

Fig. 7. NoData stripes in the Landsat 7 ETM+ image because of the sensor malfunction (Source: USGS).

conducted, it is clear that the radiometric and geometric quality is not reduced (Wang et al. 2009; Misra et al. 2018).

To ensure a proper time series analysis four pictures per year were taken. The heatwave had its highest effects in the end of February and beginning of March, hence the pictures were taken in three month intervals starting in March (Caputi et al. 2014). March was preferred to February as three months later, in June, algae bloom reaches its peak (Feng et al. 2009). This event is of great importance for the ecosystem and should therefore be part of the study. Thus, the analysis will use images from March, June, September and December, trying to cover the most interesting parts of the year. Each month the picture with the fewest cloud cover will be chosen. If several images are available, the one closest to the beginning of the month will be the one taken into the analysis. However, peer reviewing the potential images, in most cases only one picture seems to be suitable.

3.1.3 Pre-processing

As the USGS provides every band of the sensor individually in a TIF format, the images first had to be pre-processed to make them usable for the further analysis. So, in a first step the bands are stacked, using ENVI's built-in tool 'layer stacking', it assembles the bands in a proper geometry and saves them in a single image for further processing. As the data is already provided in UTM projection using the North American Datum the same settings were used for stacking the images (Louvres et al. 2006). ENVI exports a data and a header file, containing the information needed for SNAP to open it.

In a next step the stacked images are imported into SNAP were the land is masked out to reduce the amount of data and ensure a proper water analysis. The built-in masking tool of SNAP proved to be suitable for this task. Using all spectral bands as inputs, a new masked image was generated. The resulting image is saved in SNAP's own .dim format to reduce potential compatibility issues within the program. The water quality parameters were calculated in SNAP by using simple band math. The habitat mapping on the other hand, was conducted in ENVI with the stacked and unmasked images, because of the information needed to train the support vector machine algorithm.

3.2 Water quality parameters

As one can imagine water is a very complex medium to study. Not only do the particles throughout the whole water column influence the signal but also the water bottom albedo (Misra et al. 2018; Pattanaik et al. 2015). A simplified equation by Mahasandana et al. (2009) shows the parameters of interest when assessing water quality parameters:

$$a = a_{Chl\,a} + a_{tripton} + a_{CDOM} + a_{water}$$

where a represents the absorption of chlorophyll (Chl a), non–algal particles (tripton), coloured dissolved organic matter (CDOM) and the water itself. While Mahasandana et al. (2009) show us the influences throughout the water column only, the signal is also affected by its path

through the atmosphere which cannot be neglected (see Fig. 8). The absorption processes are very complex and influence the whole spectra. As described above the atmospheric correction was already provided. The water influence however was neglected, as some of the particles shown in the equation will be looked at in detail in the indices.

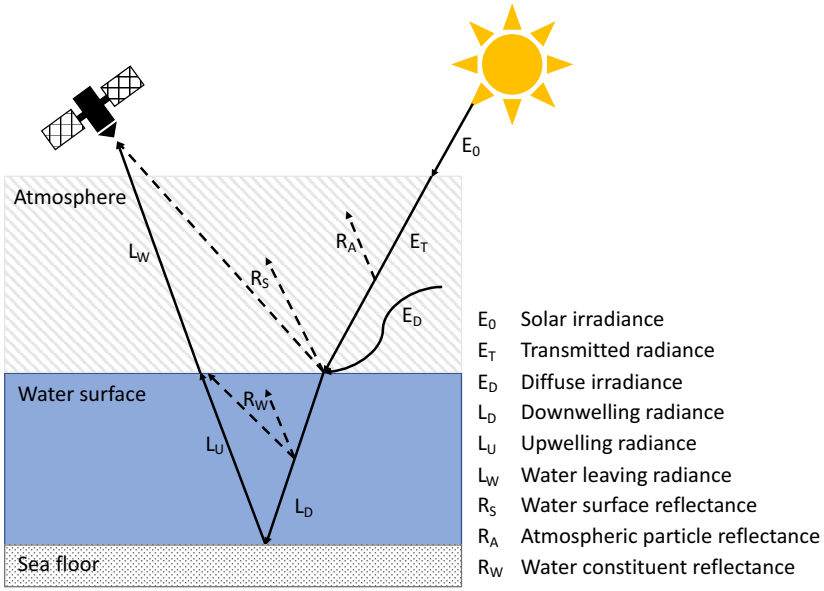

Fig. 8 The radiative transfer when observing water bodies.

In the following study, three water physical parameters have been chosen to be essential to assess the water quality in the Shark Bay area. These were selected because of their potential connection to habitat extents and dolphin behaviour. For each parameter, several indices have been evaluated to guarantee a decent result. Using band math equations, it was possible to quantify the chlorophyll content, total suspended solids and coloured dissolved organic matter. It was of great importance to choose multispectral indices to grasp the complexity of water parameters (Odermatt et al. 2012; Misra et al. 2018). The indices are all calculated using the band math tool within the SNAP application. It allows to formulate those rather simple mathematical expressions without difficulty and save the equations to use them repeatedly. Following the three indices will be explained in detail.

3.2.1 Estimating chlorophyll content using the normalized difference chlorophyll index

Chlorophyll is the key component of photosynthesis-based life forms. It is used to process sunlight and to generate essential energy for organisms. Thus the mapping of chlorophyll holds the potential of understanding global nutrient cycles but also biochemical and climatic processes (Mishra & Mishra 2012).

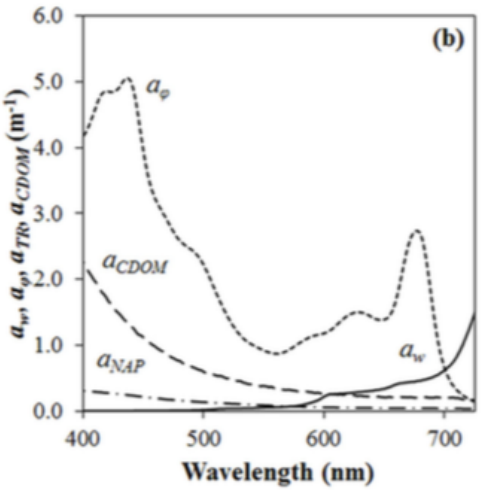

Fig. 9. The absorption coefficient of pure water, chlorophyll, colored dissolved organic matter and non-algal particles. (Watanabe et al. 2017).

In the ocean, the most fundamental photosynthetic lifeform is phytoplankton as it builds up the basis of the food chain in marine environments (Mahasandana et al. 2009). These creatures are known to have very distinct reflection patterns (Watanabe et al. 2017). Fig. 9 shows very strong absorption values in the range from 640nm up to 690nm and low values at 520nm to 560nm. Calculating a ratio of these two spectral regions will allow assessing the number of phytoplankton present in the water. The values will be mathematically normalized to have a distribution from –1 to 1. These normalized values are a great advantage of this index as they allow qualitative mapping without having field data at hand (Mishra & Mishra 2012). The lower the value the higher the chlorophyll content present. Lower reflectance values at 655nm mean strong absorption and result in a negative NDCI in the equation. The following equation was used:

$$NDCI = \frac{\lambda_2(655nm) - \lambda_1(560nm)}{\lambda_2(655nm) + \lambda_1(560nm)}$$

The displayed bands are the first two of the Landsat 7 ETM+ sensor. Band 2 ranges from 631nm to 692nm with a centre wavelength at 655 nm and thus was inserted as variable λ_2. The values at around 665 nm are widely used in estimations of Chl-a absorption models, as there is a specifically strong absorption in the red band (Watanabe et al. 2017). Photosynthesis is based on the energy received in the red spectral regions, while most of the green light is reflected by the chlorophyll. Thus, the second band λ_1 represents the low absorption in the green spectral region (see Fig. 9). Band 1 has a spectral bandwidth from 519 nm to 601 nm with a centre wavelength at 560 nm, perfectly covering the low absorption feature (U.S. Department of the Interior & U.S. Geological Survey 2018). Although this equation was developed using Landsat 8 OLI datasets, it was found to be suitable because of the sensor's similarities. Additionally, the used equation seems to generate as stable pictures in complex water systems as with Landsat 8, because indices with more than one band are known to help secure results (Mahasandana et al. 2009).

3.2.2 Concentration of total suspended solids

Total suspended solids, are as the name suggests, suspended organic and mineral particles in the water (Park 2007). They are distinguished from dissolved particles by their size, solids bigger than two microns are considered suspended (Fondriest Environmental 2014). Thus water constituents such as soil particles, algae microbes and other similar solids are considered to be part of the total suspended solids (United States Environmental Protection Agency 2012). Total suspended solids are of great importance for the water system. They limit light penetration, transport substances and thus influence habitat and food availability structures (Park 2007). Influencing photosynthesis by light inhibition consequently reduces the amount of oxygen produced and available in the water. Furthermore, TSS absorb heat and are thus able to raise water temperature which will subsequently reduce the dissolved oxygen present in the water (United States Environmental Protection Agency 2012). Additionally they can be used as an indication for erosion, stream flows in the water and deposits in the water (Park 2007). The total suspended

solids have an extreme variety of effects on the local system which also depend on the local circumstances. However, one needs to keep in mind, that the TSS particles and chlorophyll content may have some correlation as they look at similar water constituents. To estimate the total suspended solids in the Shark Bay area the following equation developed by Jaelani et al. (2016) is used:

$$\log(TSS) = 1.5212 \cdot \left(\frac{\log(\lambda_1)}{\log(\lambda_2)}\right) - 0.369$$

λ_1 corresponds to band 1 of Landsat 7 ETM+ with a centre wavelength at 478 nm, λ_2 to band 2 with a centre wavelength at 560 nm. These bands were chosen to be the equivalent to the Landsat 8 OLI bands 2 (482 nm) and 3 (561 nm) for which the equation originally was made. Looking at the OLI sensor as the successor of ETM+ the differences were determined to be negligible. Jaleani et al. (2016) validated their equation in the waters of eastern Java Timor, Indonesia and came up with the empirical parameters present in the equation above. As the Shark Bay area does not differ significantly from the study site chosen by Jaleani et al. (2016) the index was found to be good enough for qualitative estimations. Especially because there was no possibility to alter the empirical parameters since no in situ data is present.

3.2.3 Content of coloured dissolved organic matter

Coloured dissolved organic matter is definitely the most difficult to calculate. As seen in Fig. 9 it does not have a distinct absorption pattern but a gradual slope from the ultraviolet to the red spectral bands (Slonecker et al. 2016). Thus, it is rather complicated to formulate an equation which is capable of estimating the amount of coloured dissolved organic matter. This is further hindered by the Chl-a concentration which also has its maximum absorption in the same bands (Odermatt et al. 2012). However, Olmanson et al. (2016) have run several models and compared them to choose the best algorithm depending on the sensor. The best fit, which is specifically validated for Landsat 7 images, is a linear equation. The results scored a satisfying R^2 of 0.74 which is the highest value achievable with Landsat 7 images.

$$\ln(a440) = 20.3 + (-10)\left(\frac{\lambda_2}{\lambda_3}\right) + (-2.4)\left(\frac{\lambda_3}{\lambda_4}\right)$$

This equation calculates the absorption at 440 nm, where coloured dissolved organic matter does have very strong absorption features and was found to be the best spectral region for determination of coloured dissolved organic matter (Mahasandana et al. 2009). The bands used are band 2 with a centre wavelength of 560 nm, band 3 with 661 nm and band 4 with 835 nm. These aim to approximate the absorption through a regression model with specifically derived coefficients (Olmanson et al. 2016). The above used values were validated in lakes in the state of Minnesota and Wisconsin, however as they are explicitly for Landsat 7, they were chosen to be good enough for the salt water of Shark Bay.

Coloured dissolved organic matter describes one significant fraction (up to 90%) of all dissolved organic matter (Twardowski et al. 2004; Olmanson et al. 2016). CDOM are induced

into the water system mainly by terrestrial inputs, for this reason they are of particular interest in coastal regions (Branco & Kremer 2005). However, a small portion is also created in situ by biological processes (Branco & Kremer 2005). It is of specific interest as it is known to have extremely diverse influences on the water system especially in the optical spectral regions (Branco & Kremer 2005). The particles affect water quality directly by influencing the availability of metals and hydrophobic materials which are crucial for photolysis, thus playing a major role in carbon cycling even on a global scale (Olmanson et al. 2016). In addition, coloured dissolved organic matter, like the total suspended solids, do inhibit light penetration and influence photosynthesis and subsequently growth of microorganisms (Slonecker et al. 2016). However, the blocking of light does have a major advantage, as the CDOM strongly shield ultraviolet light (see Fig. 9) which could potentially harm organism's DNA (Olmanson et al. 2016; Zepp et al. 2008). Adding to the complexity of coloured dissolved organic matter, their absorption changes with the water depth. At the surface the absorption of UV light is dominant, whereas it shifts to general light blocking with increasing depth (Slonecker et al. 2016). It needs to be stated that no depth correction in any of the indices has been conducted.

3.3 Habitat mapping

In a second approach the Shark Bay area has to be mapped to understand the extent of dolphin habitats. One of the very crucial parameters for dolphins is seagrass cover. Seagrass does not only influence the food availability but also the specific specialisations of dolphins, for example sponging. However, the most significant factor influencing the specialisation of bottlenose dolphins in the Shark Bay is the water depth (Tyne et al. 2012). Anyway, the seagrass distribution is of particular importance for the flora and fauna in the region and also a good indicator for potential climatic changes in the area. Thus, mapping the seagrass coverage over the last 18 years allows a very detailed analysis of the climatic impacts on the diverse Shark Bay area. Additionally, it is possible to integrate the heat event of 2010/2011 in a longer trend or at least put it into relation to long term development of the waters. To ensure a proper analysis, the data had to undergo some simple pre-processing. All water pixels outside of the bay should not be included in the classification as they would seriously distort the results, because the water there is far too deep for a benthic analysis. Thus, a first step was to mask all data west of Dirk Hartog Island and Edel Land Peninsula, in the north the bays extent is cropped by the image boundaries. As a positive side effect, this procedure resulted in fewer data and consequently lower computation time for the classification algorithm. If the northern part of the bay is usable for a benthic classification is debatable because of its depth. However, peer reviewing the images and several test runs showed no significant changes in the performance of the classification algorithm when excluding the water north of Cape Peron. Ohlendorf et al. (2011) propose a threshold for benthic analysis at 15 meters, as the bays northern area reaches depths around 12 meters with maximum values of 20 meters, it was chosen to be suitable. Subsequently the whole bay area was used for the support vector machine classification.

3.3.1 Support vector machine

With in situ measurements present for several transects in the western Shark Bay, a supervised classification method was chosen to be suitable. Supervised classification gives us the possibility to choose specific training samples for the algorithm to classify the seafloor properly. Within the potential supervised classifiers, the support vector machines poses to be a perfect fit to classify remote sensing data (Varma et al. 2016; Zhan et al. 2003). Support vector machines are efficient and rather simple to implement, especially with ENVI's built-in tool. The classifier relies on the principle of constantly minimizing the training error to ensure the results are not influenced by effects such as overfitting (Zhan et al. 2003). It does so by generating hyperplanes in a multidimensional space based on the training data. These hyperplanes are then constantly evaluated by minimizing the distance of classified pixels to their respective plane thus controlling its own classification (Varma et al. 2016; Zhan et al. 2003). As the classification relies on margin maximization and structural risk minimization and not on the statistical distribution of the training samples, the classification should generate better results especially regarding generalization (Melgani & Bruzzone 2004; Zhan et al. 2003). Thus, support vector machines are thought to very efficient and good classifiers for heterogeneous remote sensing data (Varma et al. 2016; Melgani & Bruzzone 2004). However, support vector machine were initially developed to classify binary problems and thus the usability might shrink with rising number of classes (Melgani & Bruzzone 2004).

3.3.2 Analysis

To study the extent of seagrass meadows in the Shark Bay, the ENVI built in support vector machine tool was used. The machine was trained mainly with regions of interest chosen based on the in situ measurements conducted by Tyne et al. (2012). The problem with Tyne et al. (2012) data is, that it only covered a very small part of the western bay area at one single point in time and thus held too few data points to generate good results especially for a time series. Subsequently, supplementary training data, based on the provided transect data, was added by reviewing the satellite images. Based on the spectra and location from the training data set, other pixels similar to those were searched for every image in the time series. This way the training error was kept as small as possible throughout the time series. However, reviewing the spectral response revealed that the water column does have an unneglectable influence on the seafloor reflection which might distort the data. To tackle this issue, it was essential to split the basic classes up into deep and shallow water pixels, even though the testing of several combinations of classes showed, that fewer classes generate better results. However, to account for the constantly changing water environment the compromise to distinguish between different depths and re-joining the classes afterwards was of great importance. This way it was possible to overcome the changing environment of over 20 years of images and also represent the regions not present in the transects of Tyne et al. (2012). The final classes will distinguish between no seagrass, seagrass, bare sand and land. No seagrass will contain all pixels not having seagrass

but all other potential surfaces such as corals and maerl. The seagrass class contains all the pixels of seagrass on the seafloor, regardless of their species and density. The bare sand pixels will contain the very bright sandbanks on the seashore as they have a very distinct spectrum which needed to be separated from the other rather dark pixels. The land pixels will contain all the pixels not covered by water.

As outlined, the training data was based on the camera drop data provided. These pixels were then used to aggregate around 220 pixels per class by drawing regions of interest within ENVI. The ROI's had to be drawn for every image by hand and were thus evaluated for every image separately by eye. ENVI's support vector machine tool directly imports the regions drawn into the algorithm as training data sets. The settings were left at default as they were fitting for the analysis conducted. The radial basis function was preferred to a linear kernel type, since a non-linear dependency within the data could not be ruled out. However, this choice resulted in a greater processing effort. The penalty parameter was not changed, as a higher accuracy and reduction of the generalization was not needed. The pyramid levels, defining the iterations of the training with different resolutions, proved to have a negligible influence on the result.

The analysis was conducted on one image per year. The images were preferably taken in June, however several images do have clouds interfering with the classification algorithm because of their extremely high reflectance. If this was the case, the September image was chosen as a backup. Unfortunately, there were years with no suitable images neither in June nor in September resulting in the classification being executed on the images of march. June was chosen to be the best month as it marks the peak of growth season, but having a mix of different months throughout the time series should not have a major impact on the analysis as the change in seagrass cover is happening over a period of months.

The classified images were then exported into ArcMap where the deep and shallow water classes were reunited. In a final step the habitat maps where then coloured to visualize the potential changes.

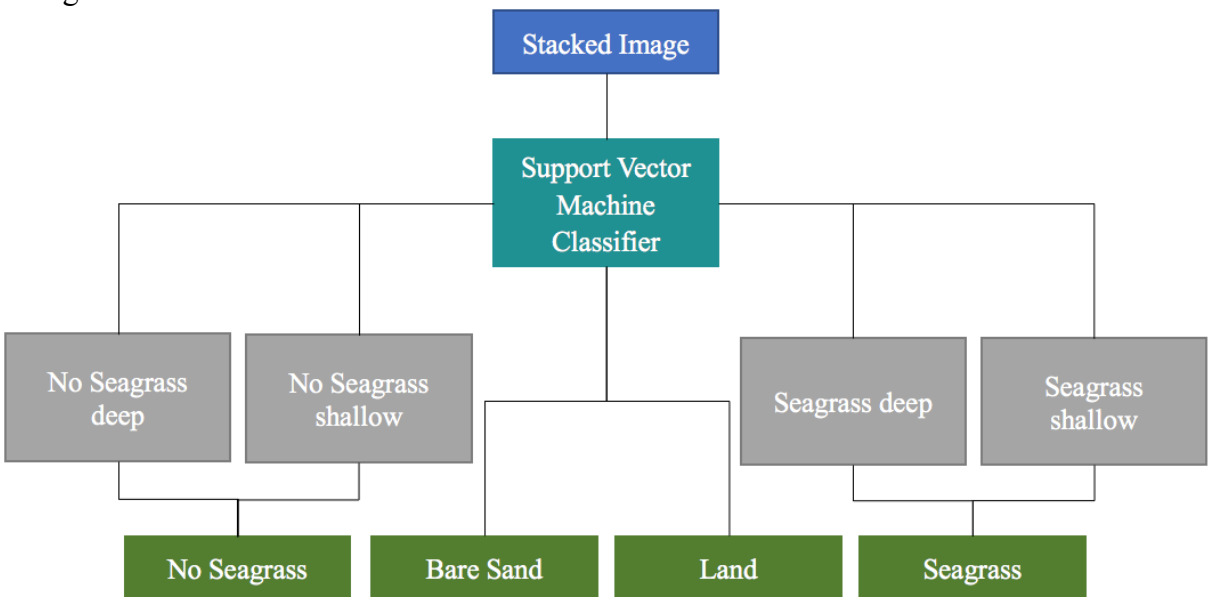

Fig. 10 Flowchart showing the classification process.

3.4 Statistical analysis

To statistically evaluate the results generated and analyse significant trends and outliers, very basic statistical methods were used. Using an analysis of variance, the trends of the indices over the years were quantified. To statistically determine a shift in the system an additional search for a breakpoint within the data was made. The trends before and after this point were then calculated separately.

In a first step, the data to use in the statistical analysis needed to be chosen. Averaging the data over the four months per year was not an option as there are several years which do have missing data thus distorting an averaged value. Subsequently the data of a single month had to be used. Like the habitat analysis, the month June poses as a good fit for the thorough statistical evaluation. Having the peak in algae bloom and marking the most productive month in the year, it makes sense to use its values for further analysis. However, like any other month, June unfortunately does not have a complete series of data as clouds sometimes made it impossible to gather information. These holes were treated as NA and thus appear as blanks in the plots and analysis.

The analysis was conducted once in the western and once in the eastern bay-arm, to be able to compare the two. Because of the water dynamics and hindered exchange within the bay waters, a gradient from the inlet down to Henri Freycinet Harbour and Hamlin Pool respectively, might be present. To account for this, the data was extracted from five regions of interest covering the bay arm from top to bottom (see Fig. 11). The regions of interest cover approximately 60'000 pixels which were then extracted in the raw data format for all four months each year. The .txt datasets were then processed to import them into Microsoft Excel. This program was used to extract and group the data of the four months using simple cell functions. In a last data preparation step, the data was rudimentarily corrected for atmospheric influences. Several pixels, assumed to be constant over the years, were chosen throughout the satellite image. The index values were then extracted over the whole time period. The first value was chosen to be the bench mark, any deviation from the value is due to other effects influencing the reflectance. Now, for each year the difference between the constant value and the measured one was calculated. These correction values were then averaged per image trying to account for possible variability. To correct the calculated indices, the

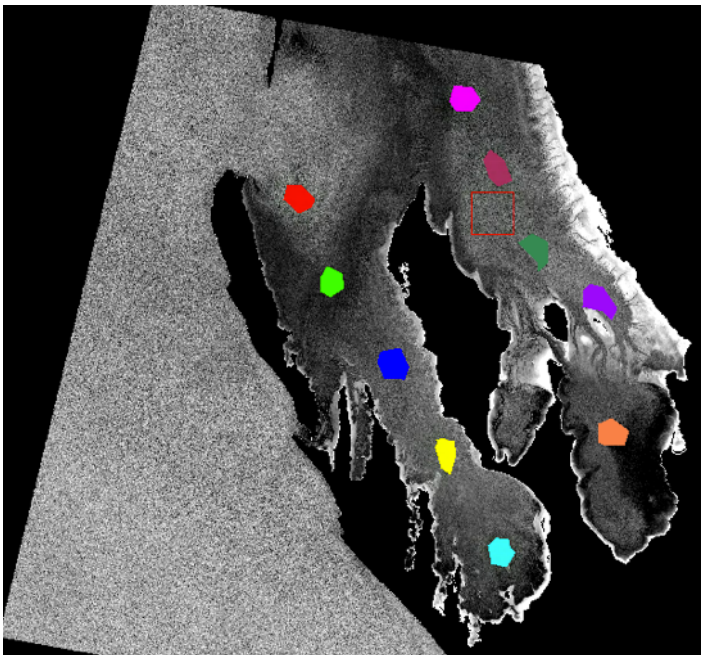

Fig. 11 The regions of interest chosen for the data extraction, displayed on the ENVI created NDCI image.

averaged correction factor was then either added or subtracted from the index values to rule out potential external influences on the data. The prepared data was then imported into R Studio to run the thorough analysis, providing us with all statistical parameters per trend line and plots for visualization. First a linear model was built combined with an analysis of variance to calculate the significance level of a trend over the 18 years. The null hypothesis states, that the changes or trends in the data are caused randomly. The α-value is set at 0.05, if the calculated P-value is lower, H_0 will be refused and the trends are assumed to be significant. Following the linear model, data is analysed for outliers which would then be replaced by other numeric values. Using the strucchange package, the data is searched for any structural changes as these could indicate a breakpoint in the data. The analysis is based on the standard linear regression model (Zeileis et al. 2002):

$$y_i = x_i^{\mathrm{T}} \beta_i + u_i \qquad (i = 1, \dots, n)$$

The y_i represents the dependent variable, while x_i^{T} is the independent variable. x_i^{T} is multiplied with β_i representing the regression coefficients. By adding an error term u_i the bias due to noise can be reduced (Zeileis et al. 2002). Now, the β_i is compared to β_0, if they can be assumed to be equal no structural change is present in the data. If the two values are not equal the script will give us a breakpoint in the data. Based on the provided point of change, the data is then split up in two segments which are then tested again for significance using an ANOVA. The whole statistical analysis leaves us with a trend over the whole time series, an eventual breakpoint and the trend for the resulting two segments.

Additionally, the indices were exported specifically over the years 2010/2011 in 3 month steps to assess the direct influence of the heat wave. Here the data was plotted per index from September to June to visualize the effect of the summer heat wave per region of interest. This analysis can highlight possible changes happening in a shorter timescale throughout the heat event. In combination with the whole data series this analysis allows to understand a potential gradient and possible differences between the impact on the two bay arms.

In a last step, the indices are analysed on potential relationships using the Pearson correlation coefficient. It is used to measure the correlation between two variables and generates coefficients indicating the type of dependency from +1 positive to -1 negative. This is then statistically evaluated using an α-value of 0.05. As before, a P value will be calculated indicating if the detected correlation is of statistical significance.

The habitat maps were statistically processed by looking at the pixel count per class. However, not the whole images were used. Because of depth restrictions in benthic analysis the data north of Cape Peron was not considered. Ohlendorf et al. (2011) propose a threshold of 15 meters were the influences of the water column start distorting the data gravely. Peer reviewing the images and the classifications, masking out the northern part of the bay proved to be a good idea. The boundary was set in a west-south-westerly direction, crossing Cape Peron. Following the same procedure as when analysing the indices, an analysis of variance of the amount of

seagrass pixels per year was conducted. As a counterpart, also the no seagrass class was analysed for a better understanding. In addition to the normal ANOVA, again the potential breakpoints in the data were searched und subsequently the significance for the two segments was calculated. To grasp potential differences in the seagrass changes between the eastern and the western arm, they were also looked at separately.

4. Results

The statistically analysed results are split up in different parts as they try to look at the potential gradient from inlet to the bay, the time series but also the heat event itself. The data will be presented per index. For a better understanding, the data is always split into western and eastern data, which are then split up into the respective regions of interest. The regions have been numbered from one to five, top to bottom (see Fig. 11). To better comprehend the whole process, the statistical results for the analysis of West 1 NDCI will be displayed step by step. For the other indices, however only the final results will be displayed, as the process is similar for each region of interest.

4.1 Temperature

To visualize the general extent of the heatwave of 2011, the sea surface temperature (SST) was mapped based on the available Landsat 7 images. The at sensor brightness temperature has been used to estimate the heatwave's impact on the water system. Fig. 12 shows a difference map, comparing SST in January and beginning of March. One can clearly see, that the change is visible throughout the Shark Bay. Fig. 12 indicates that the water is around 5 °C warmer than one and a half month earlier. This is supported by measurements done in the region (Arias-

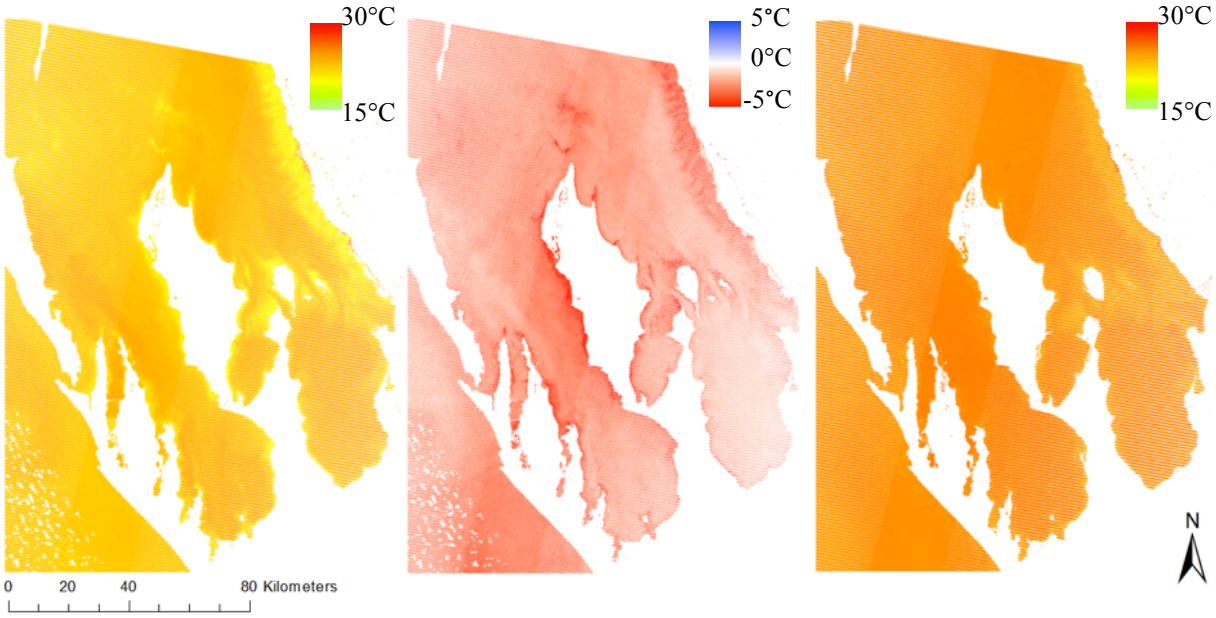

Fig. 12 The difference in temperature induced by the warm water inclusion. The left image was taken on the 15.01.2011, the right one on the 04.03.2011. In the middle the difference between the two is displayed.

Ortiz et al. 2018; Caputi et al. 2014). Mainly coastal regions had a significant change in temperature as the difference map shows the most negative values in the shallow water regions. There are two hotspots north of Cape Peron, which are the result of very low temperatures recorded there in January. However, they do not seem to be related to any water structure, hence they could also be data errors. The white spots in the lower left are clouds, which were masked by the program. There are also some values displayed outside of the water, these are the result of imperfect water masking.

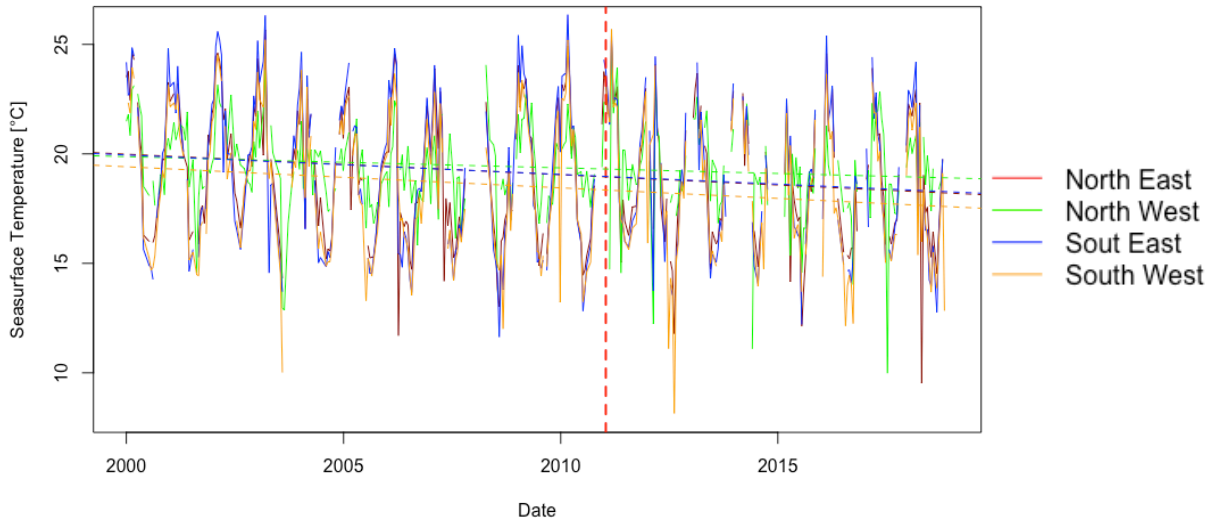

Fig. 13 The four time series data with their respetive trend lines. The red dashed lines indicates the heatwave in 2011 (Data Source: Landsat 7 ETM+).

The two bay arms seem to be affected similarly by the heatwave, but the eastern arm appears to record slightly weaker influences. It also looks like Faure Sylt shielded Hamlin Pool from the water inclusion, as the temperature change in there is not as strong as in the rest of the bay arm. But one needs to keep in mind, that the picture is also distorted by the scan line error, which makes it difficult to spot such minor differences. Especially because the influence on the difference map is doubled as two images with scan line errors were subtracted from each other. In an attempt to locate the heatwave within the whole time series, all at sensor brightness temperature values were analysed. Using the mean value of four regions of interest in the Shark Bay, an analysis of variance was executed. The regions are used to spot potential differences in between individual parts of the bay in respect to their water temperature regime. They were placed in the northeast, northwest, southeast and southwest. Fig. 13 shows the seasonal temperature pattern of all four regions of interest. There are only minor differences between the four parts of the bay thus indicating that no gradients are present. The heatwave shows as a strong peak in the time series, however there are other summers with similar or even higher outliers. 2003 and 2010 are the other two years showing very high temperature values. Besides very high temperatures, there are also cold winters with extremely low values recorded. Winter 2012 stands out, showing water temperatures around 8 °C. Interestingly, these were only recorded in the southwestern part of the bay, in Henri Freycinet Harbour. The overall trends of all four

regions are slightly negative, but mathematically insignificant. This would indicate, that the temperature has slightly decreased over the last 18 years.

4.2 Normalized difference chlorophyll index

To gain a first insight into the effects of the heatwave onto the whole bay system, a difference map from June 2011 and 2012 was calculated. By subtracting the 2012 image from the one in 2011 change can be detected and thus a first visual estimation of the potential impacts can be conducted. The calculation done results in an image with values ranging from -1 to 1. Positive difference values, displayed in blue, indicate a positive change in NDCI. Negative values however show a decrease in NDCI from 2011 to 2012. It is clear, that most of the area is affected negatively by the heatwave resulting in a decrease in chlorophyll content in the bay. Some of the very reddish pixel, especially at the inlet, are due to clouds present in one image (See the

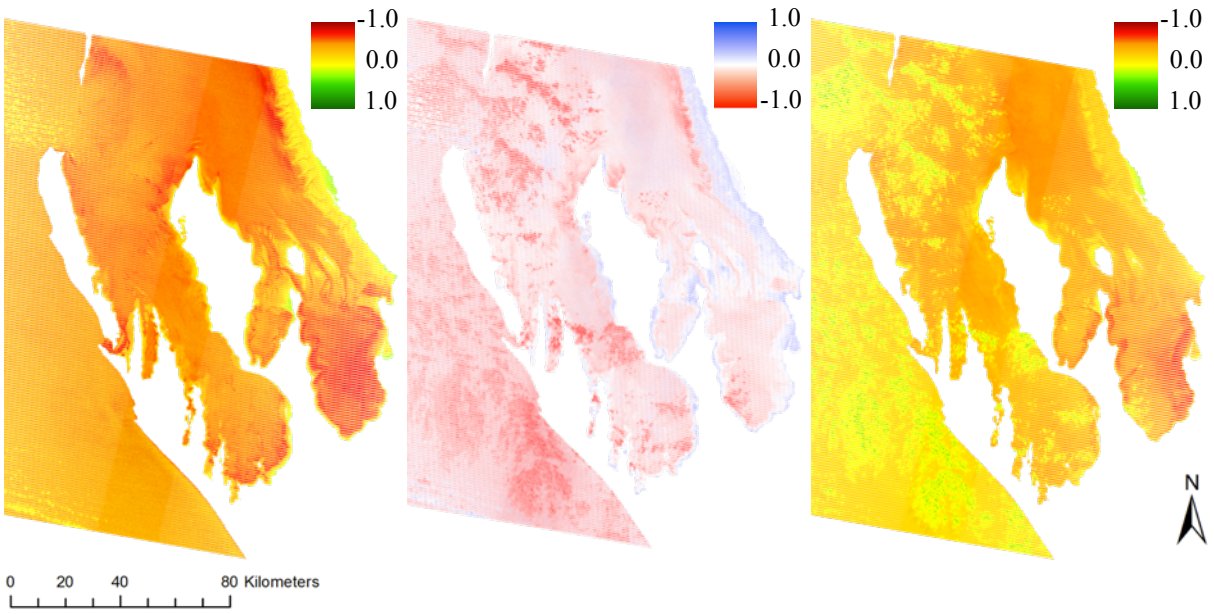

Fig. 14 A comparison of the NDCI estimated in June 2011(left) and 2012 (right). In the middle the difference map of the two, showing a negative change in red and a positive one in blue. The yellow structures in the right image are clouds.

right image of Fig. 14). The negative trend seems somehow evenly distributed, the only highlight present being in the north-eastern part of the bay. Interestingly, the very shallow shorelines seem to have a positive response to the water temperature change. Especially the eastern coast seems to profit from the warming, as the highest positive change is recorded there. The eastern arm in general seems to have benefitted more than the western one, although one needs to bear in mind the clouds are covering part of the bay. By visually analysing the index an impact seems clear. However, to quantify the extent of influences on the Shark Bay's chlorophyll levels a thorough statistical analysis is needed.

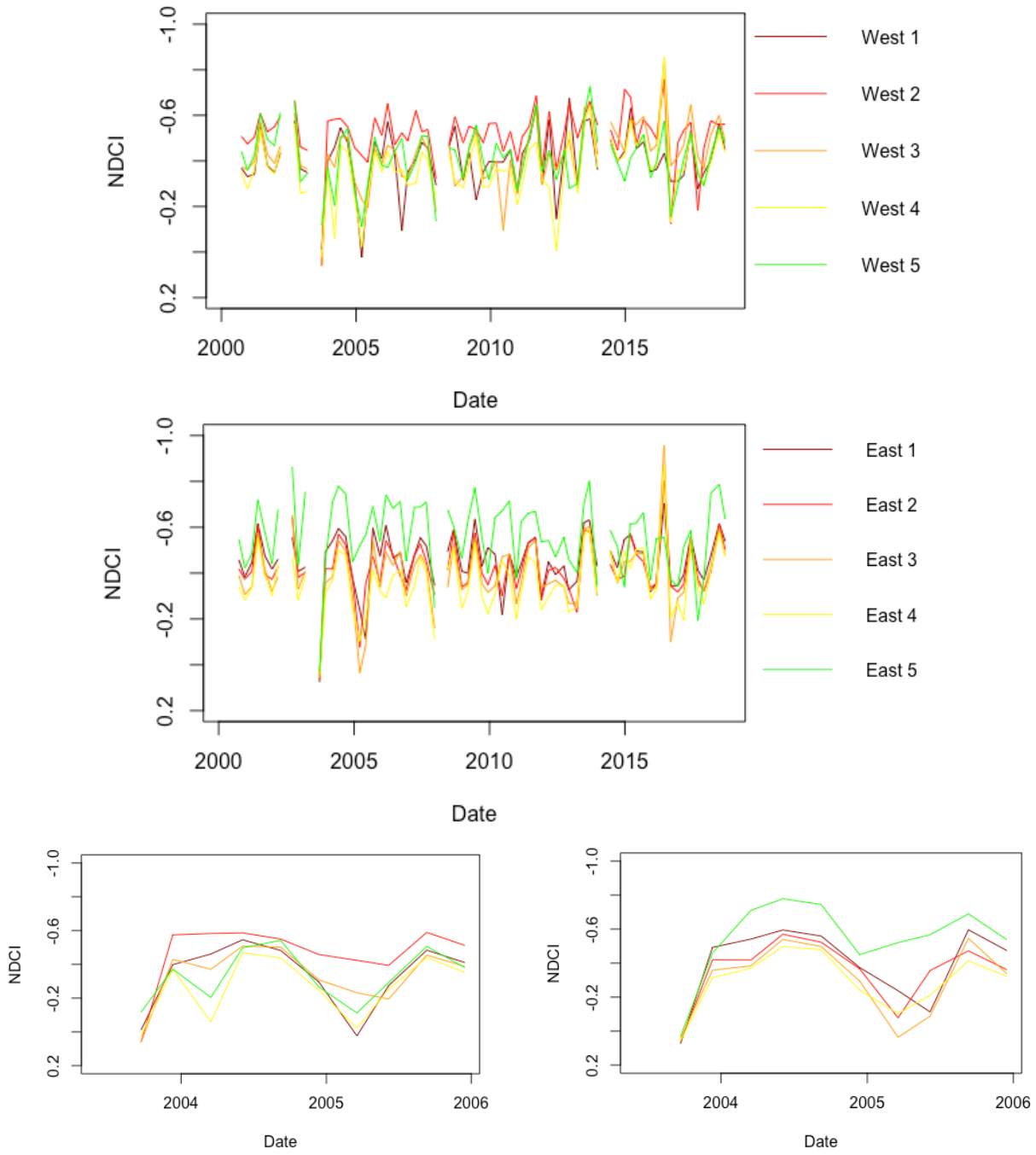

Fig. 15 The time series data for the western (upper graph) and eastern bay arm (middle graph) per region of interest. At the bottom a zoom into the years 2003 to 2006 is displayed reveling an unsystematic structure in the western bay (lower left) whereas the eastern bay arm (lower right) seems to show gradual structures.

First, the data throughout the whole time series is shown to give a broad overview of the dataset. The NDCI is displayed four times a year and shows some very distinct features with significant decrease in chlorophyll content (see Fig. 15). The eastern and western bay arms have some similar outliers, however in both areas, the seasonality affects the data greatly and subsequently reduces the information content displayed. Interestingly in both regions, the decrease at 2004 and 2005 as well as the peak in 2016 are visible. Remarkably, the heatwave in 2011 is not observable as a major change in the presented data. The two time series show an increase in

2011 with a rather steep decrease in 2012 in chlorophyll. Nevertheless, the change seems insignificant within the whole time series, as such short changes seem to occur from time to time. An overall trend is hardly noticeable, as the data varies greatly over time. The ANOVA of the eastern bay shows a slightly negative trend overtime, whereas the p-value of 0.6512455 shows no statistical significance. This is confirmed by the analysis of the western bay arm which has the same trend and significance present. But one needs to bear in mind, that the whole data set is affected by seasonality. Additionally, it is clear that not all the outliers are in the same months over the years. Other influences, such as clouds, have been removed as good as possible, several pictures have been removed completely, shown as blanks in the series.

Zooming in on the different regions of interest could reveal potential gradients in the data. As the data is analysed from the inlet down to the shore and keeping in mind the water structure and inhibited mixing, such gradual changes might be possible. Having a closer look at the data series from 2003 to 2006 the eastern bay arm shows somehow decreasing NDCI values from East 1 to East 4. East 5, located in Hamlin pool, has an apparent different regime as it shows higher values throughout the displayed time series and does not fit the gradient of the other four (see Fig. 15). Looking at the whole data series again, this structure seems to be present not only in the zoomed part. It gets even clearer that Hamlin pool needs to be looked at separately, as it does not react in the same way the others do. While always having higher values, it also has some anticyclical behaviour. In the western bay arm, such structure is not present. Although the five regions of interest show similar data, no gradient is evident. The highest value is scored by West 2 most of the time, the other four regions of interest vary greatly and change their structure over time.

To untangle the seasonal data, the thorough statistical analysis was only conducted on the data from June. Reducing the data to June has a major drawback, because of repeated cloud cover from 2000 to 2004 only one image is available. Consequently, the first 4 years were not integrated in the analysis and the time series now starts at 2004.

For a better understanding of all the statistical results generated, the whole process will be discussed on the example of West 3, as West 1 and 2 did not have any outliers. As outlined, in a first step the outlier detection runs through the data and returns potential values to correct the influence of extreme pixel. Fig. 16 shows the three detected data points and their effect within the time series. However, the outliers have not been corrected as they were of interest for the analysis. But it is interesting to see, where outliers are located in time, as they could be caused by potential external effects. Hereafter, the break detection is run to search for a change influencing the trend analysis. Fig. 16 shows the F statistics for each point, indicating potential breakpoints. The redline marks a significance threshold, points reaching above are of particular importance. In the example of West 3, the year 2012 shows a significant breakpoint which is then used to split the date for the further analysis. Having these results, the final ANOVA for the two segments is calculated and following all the data is brought together. The final result is a time series with a trend line for the whole dataset and the two segments (see Fig. 17).

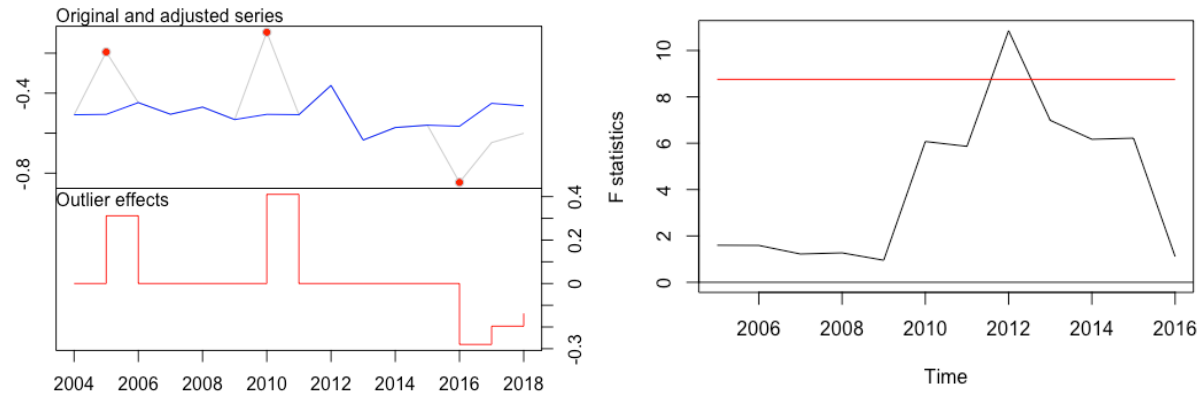

Fig. 16 The two intermediate products of the statistical analysis of the data at West 3. The outlier detection (left) and F-statistics (right) are calculated within the analysis and generate the displayed side products.

The data shows a significant drop in 2010 indicating a severe loss of productivity. 2011 does not seem to have a distinct value, however a second drop can be seen after the heat event in 2012 which also marks the breaking point. The segment trends do not have significant characteristics, nevertheless the trend before the breakpoint is slightly negative whereas the one afterwards is slightly positive. The overall trend shows a rather strong and statistically significant positive trend, indicating increasing chlorophyll content since the beginning of the data series. Similar results are generated within the whole western bay arm (see Table 2). Four out of five regions of interest show their breakpoint in the year 2012, while most of them do not have any trends of statistical significance. The whole dataset can be found in the appendix. However

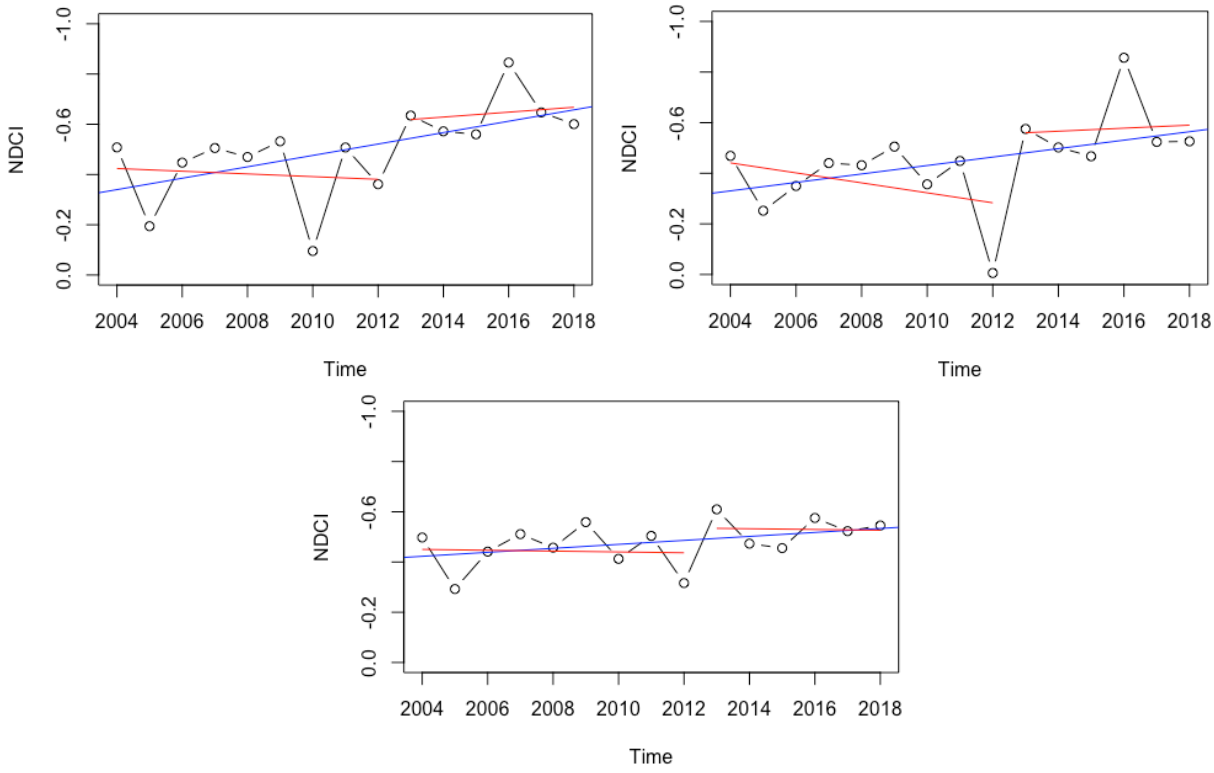

Fig. 17 The NDCI values at the regions of interest West 3 (upper left), West 4 (upper right) and West 5 (lower middle). Plotted are the trend line over the whole time series (blue) and the segment trend lines (red).

West 4 stands out as it registered the strongest decrease in chlorophyll content (see Fig. 17). The data shows an extreme drop from 2011 to 2012, still the system recovers fast and 2013 is at a normal level again. Compared to the West 3 data, the year 2012 at West 4 shows a reduction of an extent not seen in any other graph. On the other hand, the low value in 2010 at West 3, which has a comparable extent, is only small at West 4. The two datasets however agree on a short increase in chlorophyll content in 2016. A totally different image can be seen when looking at West 5. One can see, that the influence on water in the rear of the bay seems to be weaker. The data has no outliers and is rather uneventful. Even though the breakpoint is also found in the year 2012 the segment's trend lines nearly correspond to the overall trend. The slight drop in 2012 with its following increase in 2013 is the biggest change in the sequence, whereas the beforehand mentioned peak in 2016 is of no importance. Hence, the western data describes a general positive trend in chlorophyll content with two negative (2010, 2012) and one positive outlier (2016).

Table 2 The results of the statistical analysis of NDCI values. Significant values are in bold.

ROI	P-Value	Break	S1 P-Value	S2 P-Value	Segment 1	Segment 2
West 1	0.3258258	2012	0.250754	0.9546764	2004 – 2012	2013 – 2018
West 2	0.1547701	2015	0.9019929	0.3013142	2004 – 2015	2016 – 2018
West 3	**0.02984172**	2012	0.80914	0.7414323	2004 – 2012	2013 – 2018
West 4	0.1242962	2012	0.3544353	0.8820777	2004 – 2012	2013 – 2018
West 5	0.1383445	2012	0.8965696	0.9298396	2004 – 2012	2013 – 2018

ROI	P-Value	Break	S1 P-Value	S2 P-Value	Segment 1	Segment 2
East 1	0.1397248	2012	0.9797005	0.6390841	2004 – 2012	2013 – 2018
East 2	0.130466	2015	0.9614892	0.4995839	2004 – 2015	2016 – 2018
East 3	**0.03909867**	2015	0.2171778	0.4560198	2004 – 2015	2016 – 2018
East 4	**0.01674979**	2015	0.1518184	0.3747891	2004 – 2015	2016 – 2018
East 5	0.3911035	2011	0.9645487	0.2388737	2004 – 2011	2012 – 2018

The eastern data shows similar outcomes. Again, the years 2010 and 2012 have major decreases in NDCI both followed by a rapid recovery in the following year. Interestingly, the low values in 2010 are only observable at East 1 and East 2, the following regions of interest do only have a small reduction in 2012 (see Fig. 18). However, the most striking data point is in June 2016 where a peak is visible throughout the whole eastern part of the bay. The amplitude is growing until East 3, where it reaches its maximum extent, at the same time the other outliers get smaller. This is also reflected in the breakpoints. While at East 1 2012 still splits the data, even though statistically insignificant, the breakpoint then shifts to 2015. The segment trend lines subsequently forfeit their meaning as they spread over most of the data range thus aligning with the overall trend. The data suggests an overall increase in chlorophyll supporting the findings in the west. The positive trend at East 3 and East 4 is even statistically significant (see Table 2).

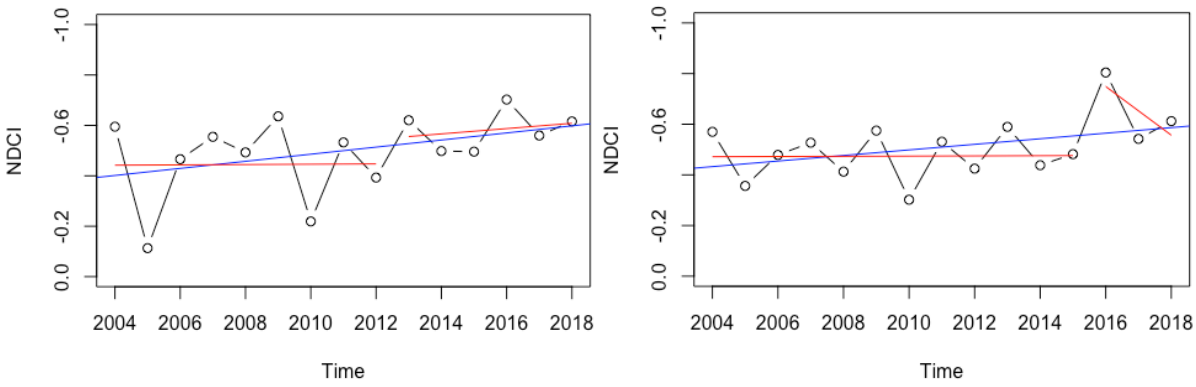

Fig. 18 The NDCI time series at East 1 (left) and East 2 (right). Displayed are the overall trend line (blue) and the trends in the two segments (red) found by the breakpoint detection.

These analyses however do not apply when looking at East 5. Similar to West 5, the bay's rearmost region of interest shows a different pattern. The insignificant negative overall trend at East 5 opposes to the other findings in the eastern bay. On one hand 2012 again marks the breakpoint as it is the most significant change present in the data. From 2012 onward the trend, in contrast to the overall trend, is positive. On the other hand 2016 does not have an influence whatsoever. While the rest of the bay has its peaks in 2010, 2012 and 2016, the fifth region of interest again indicated contrasting data.

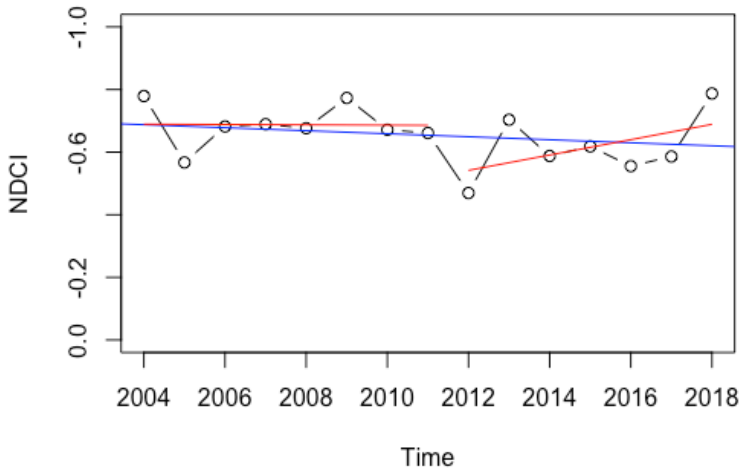

Fig. 19 The NDCI data at Hamlin pool (East 5) over the 14 years of interest. Displayed are the overall trend line (blue) and the trends in the two segments (red) found by the breakpoint detection.

4.3 Total suspended solids

The total suspended solids have a potential influence on the light availability and subsequently on photosynthesis and other processes connected to nutrition in water. Looking at the difference map (Fig. 20), the two images do not show significant changes induced by the heatwave. The overall picture shows a slight negative tendency in the deeper waters and a positive one on the bays shorelines. Interestingly, the eastern shorelines, in both bay arms, seem to score higher TSS concentration than the ones on the western side. Additionally, a gradient might be present, as the results tend to get more positive the further back they are in their respective arm. Again, part of the sea surface is occluded by clouds, where also the highest values in the image are generated. The distribution of pixel values of the change map shows a Gaussian shape around zero indicating little change and no trend to either side. Thus, a very low threshold of 0.22 was chosen to colour the difference map, further underlining the rather small change. This can also be confirmed visually, as the difference between the left and right image in Fig. 20 seem to be minor.

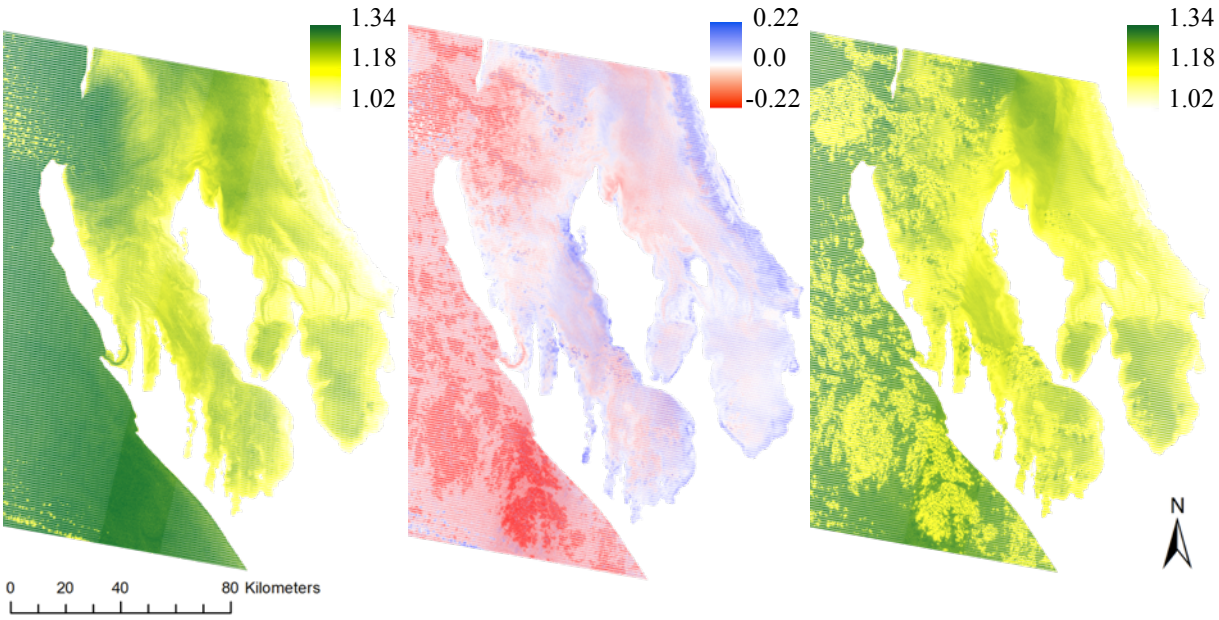

Fig. 20 A comparison of TSS concentration in gm^{-3} estimated in June 2011 (left) and 2012 (right). In the middle the difference map of the two, showing the change in between the two years. Negative values (red) indicate a decrease in TSS whereas the positive values (blue) show an increase.

The whole time series data does not help to support the findings indicated by the difference map. Similar to the NDCI values, the TSS series has a very chaotic distribution of values affected by seasonal changes and other external effects. The western dataset seems to have a particular outlier in 2003 followed by a strong drop the following year. However, the rest of the extreme values seem to be part of seasonal fluctuations. What is interesting, is the fact, that West 1 and West 2 seem to have higher values throughout the whole time series, while the other three regions of interest seem to have a similar distribution. Nevertheless, they still show comparable features. On the other hand, the eastern bay arm shows more packed lines with outliers

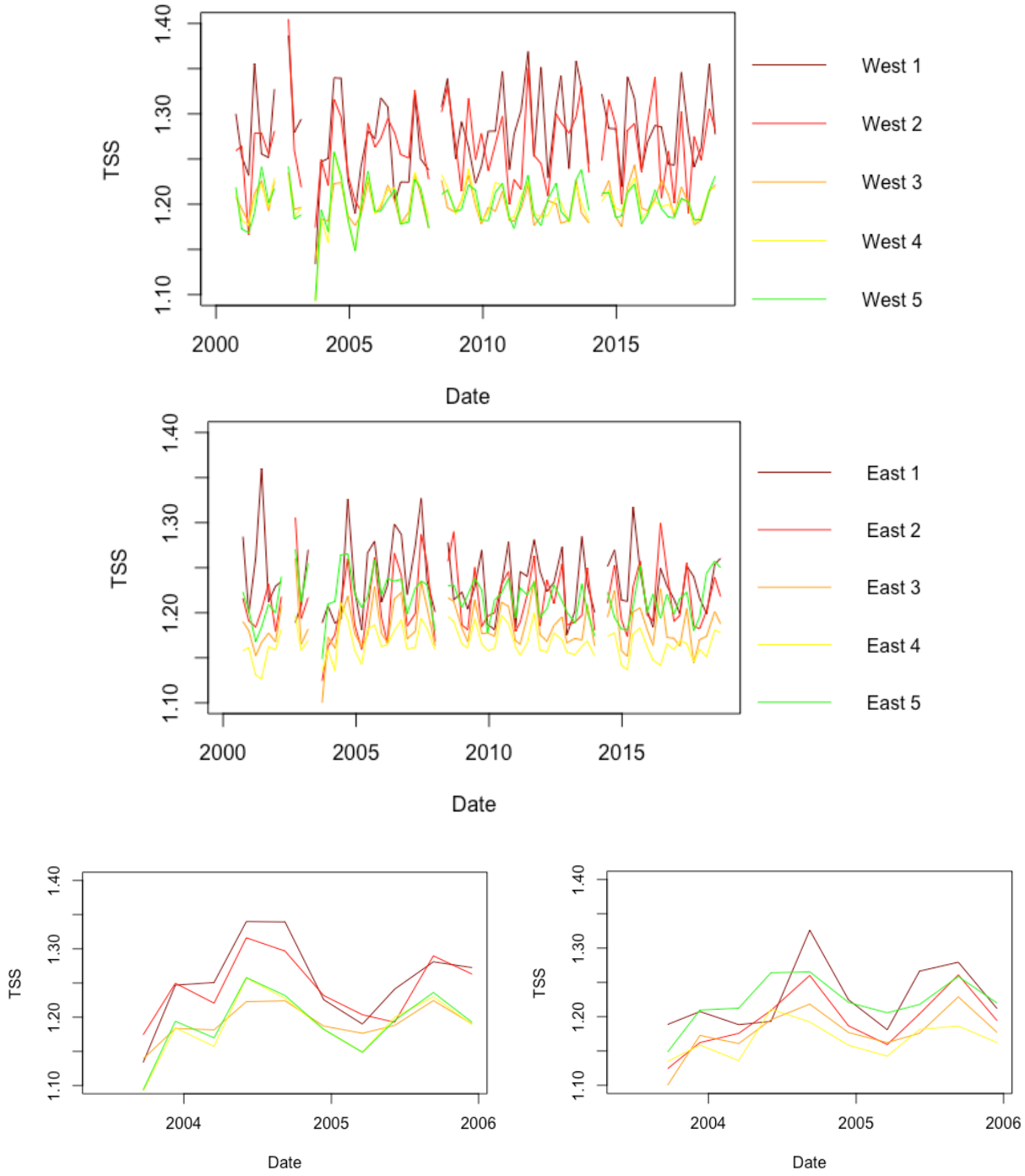

Fig. 21 The TSS time series data for the western (upper graph) and eastern bay arm (middle graph) per region of interest. At the bottom a zoom onto the years 2003 to 2006 is displayed reveling no significant gradient in the data. However, the eastern arm (lower right) seems to by little bit more structured than the western one (lower left).

at 2001, 2004, 2007 and 2015. The highest value is scored in 2001, however it is only recorded at East 1. There are some vague similarities between the western and eastern time series, but nothing strikingly. Looking at the zoomed images (lower images of Fig. 21) of the western regions of interest, no structure seems to be present. West 1 and 2 have higher concentration values while the other three seem to be extremely close to each other. Even though the

TSS concentration decreases from West 1 to West 4, no clear gradual structure is present. Interestingly, West 4 and West 5 follow each other very closely. Like the NDCI values, the TSS data only seem to show a gradual decline in the eastern bay arm. East 5 again needs to be treated separately, as it seems to be behaving in a different manner than the rest of the bay.
The western and eastern time series shows no significant trends. The overall trend appears to be sometimes positive and other times negative, without showing any distinct patterns. The only trend which is significant, is recorded at East 4 which shows a strong negative tendency (see Table 3). However, as this result is not confirmed by any other region of interest, it needs to be treated with caution.
At West 2 and 4 a gradual reduction of TSS is visible (see Fig. 22), which can also be seen in some of the eastern data. This reduction starts around four years after an extreme drop recorded in 2005. Because of its starting point in 2009, it cannot be associated with the heatwave, even though it has its lowest value in 2012. Following this feature, the TSS concentration at West 2 has a strong increase ending in a peak in 2016. The peak corresponds to the already mentioned high values in NDCI recorded in the same year. Although, these findings indicate some similarities between the western regions of interest, looking at the plots it is visible, that the results vary greatly. West 4 does not show a strong increase after 2012. In this region of interest the concentration seems to stabilize itself in the following years. Again, West 5 shows a disimilar distribution. The reported gradual decline is of very small extent and the peak in 2013 is one of

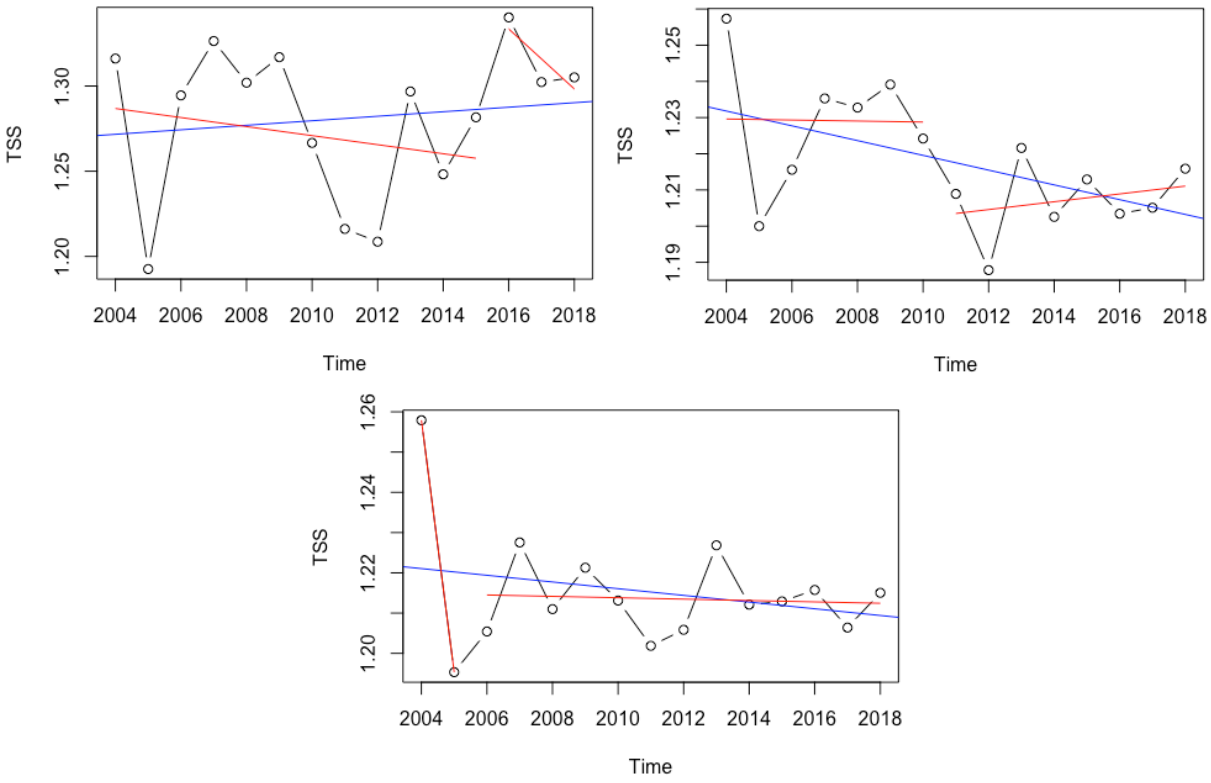

Fig. 22 The TSS time series data in the western bay arm. West 2 in the upper left, West 4 upper right and West 5 in the lower middle. The blue line shows the trend over the whole time series whereas the red lines show the trends in the two segments found by the breakpoint detection.

the most significant features present. These observations further underline the apparent differences between the western regions of interest. This claim is also supported by the detected breakpoints, which are distributed randomly over time, not matching with the heatwave in 2011. Every region of interest recorded a different breakpoint while none of the results are statistically significant. This implies that the results in the west are not only influenced by the water temperature but possibly by another, more important, parameter.

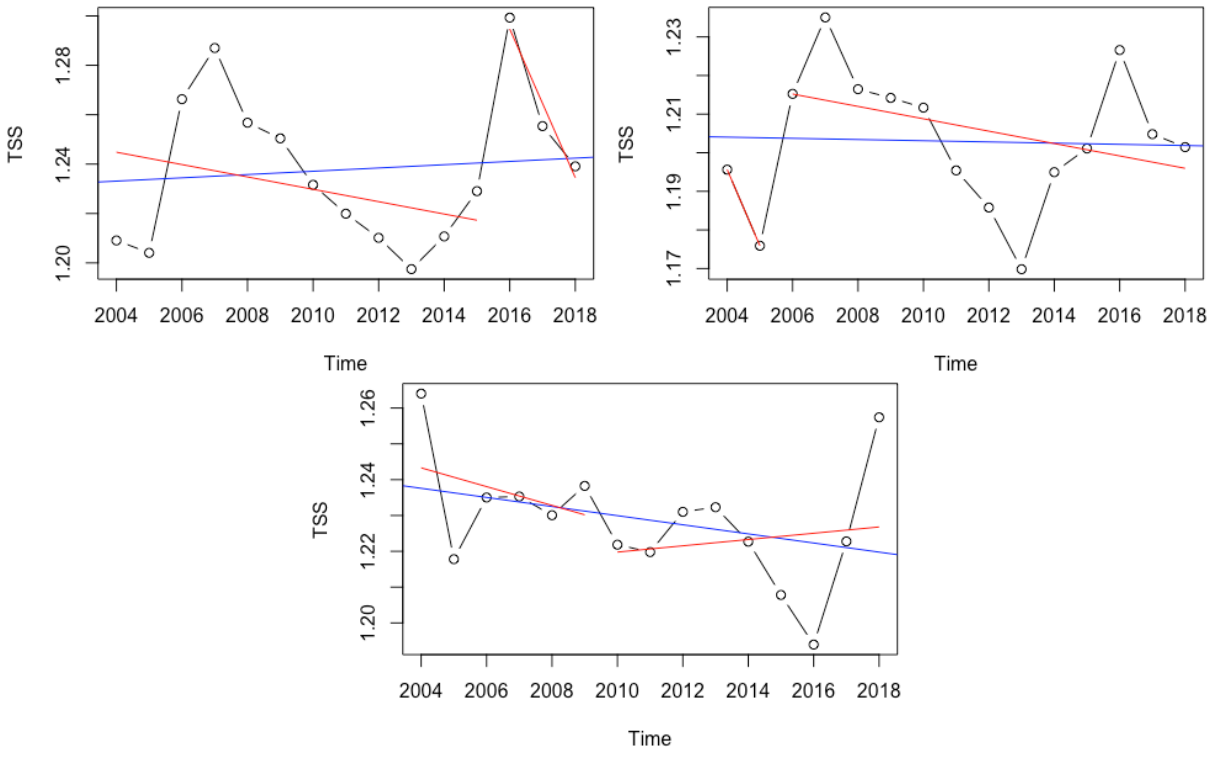

Fig. 23 The TSS data from June plotted over 14 years for East 2 (upper left), East 3 (upper right) and East 5 (lower middle). Displayed are the overall trend line (blue) and the trends in the two segments (red) found by the breakpoint detection.

As already briefly touched, the gradual decrease has also been recorded in the eastern data set. However, the lowest value here is shifted one year to 2013 (see Fig. 23). Like in the western bay arm, the continuous decrease is following an extremely low TSS value in 2005. The difference to the western data lays in the peak recorded in 2007. Unlike the values displayed in Fig. 22, the East shows a very distinct high value in-between the two drops. Again, a very significant feature is 2016, scoring a single, very high value in TSS. Once more, the breakpoint detection fails to find a tipping point coinciding with the heatwave. The segments vary greatly and show no significant values whatsoever. The values recorded at the rearmost region of interest, East 5, do not support the findings discussed above, as the water there seems to be behaving differently. No gradual decrease can be seen and contrary to the other time series 2016 marks the lowest value recorded.

The trend over the whole time series shows no significant decrease or rather increase except for East 4. The ANOVA shows us some negative as well as positive trends which do not indicate

a pattern or gradient within the data. To conclude, the western as well as the eastern TSS concentration does not have significant results which could be the outcome of influences induced by the heatwave of 2011.

Table 3 The results of the statistical analysis of TSS values. Significant values are in bold.

ROI	P-Value	Break	S1 P-Value	S2 P-Value	Segment 1	Segment 2
West 1	0.1937847	2012	0.2279734	0.9907208	2004 – 2012	2013 – 2018
West 2	0.6408402	2015	0.5143931	0.3750605	2004 – 2015	2016 – 2018
West 3	0.8104061	2009	0.2450476	0.07350291	2004 – 2009	2010 – 2018
West 4	0.05326065	2010	0.9717326	0.5361287	2004 – 2010	2011 – 2018
West 5	0.3612596	2005	NaN	0.7852973	2004 – 2005	2006 – 2018

ROI	P-Value	Break	S1 P-Value	S2 P-Value	Segment 1	Segment 2
East 1	0.8933276	2005	NaN	0.3803399	2004 – 2005	2006 – 2018
East 2	0.7336916	2015	0.3098097	0.1648975	2004 – 2015	2016 – 2018
East 3	0.8889981	2005	NaN	0.2233539	2004 – 2005	2006 – 2018
East 4	**0.006540292**	2010	0.9746918	0.9056879	2004 – 2010	2011 – 2018
East 5	0.2329018	2009	0.5327331	0.7232442	2004 – 2009	2010 – 2018

4.4 Coloured dissolved organic matter

The coloured dissolved organic matter shows a very strong positive change in between the years 2011 and 2012. The difference map indicates that over the whole bay area the CDOM was increased significantly. The only areas negatively affected are the eastern shorelines, especially in very shallow water the CDOM seems to have decreased greatly. The change is so big, that it is easily visible by just comparing the two images in Fig. 24, however one needs to keep in mind that the view is obstructed again by some clouds. There is no difference observable in between the eastern and western bay arm. Also, no gradient is present, as the waters do not show differences from the inlet down to the shorelines. CDOM seems to be the only index showing a positive reaction to the heatwave.

The data of the whole time series presented in Fig. 25, gives a general overview on how the data is structured in their respective part of the bay. In the western bay, a first outlier is recorded in 2004, where West 2 and West 5 both have an extreme value. However, they are contradictory as they point in different directions, which can be seen even better in the zoomed picture (bottom left of Fig. 25). Following this year, the data series is rather balanced having only seasonal fluctuations. The heatwave in 2011 shows a decline in CDOM followed by an increase normalizing the concentration. 2016 and 2017 show two extremely low values, posing as the biggest outliers in the whole data. However, the different regions of interest seem to be affected differently. While West 1 and West 5 seem to have no extreme value, the other three show a gradient with the lowest value recorded at West 4. In 2017 no clear gradient is present, however the

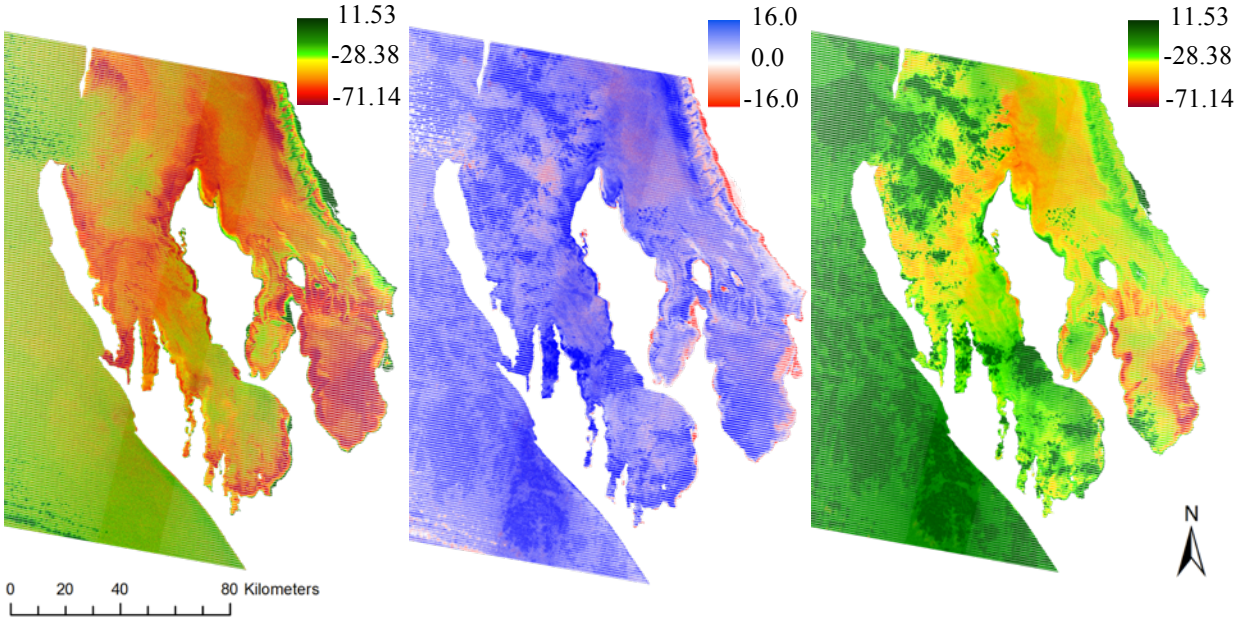

Fig. 24 Two images showing the natural logarithm of the absorption at 440 nm which corresponds to the amount of CDOM in the water. The left image was taken in June 2011, the right image in June 2012 The change from June 2011 to 2012 is displayed in the middle. Negative change is presented in red whereas positive values are blue.

regions are not affected equally. Whereas the western bay arm has a rather stable data distribution the eastern one shows some more distinct patterns. The first outlier is also the most extreme one. It is recorded in 2003 but, as well as the one in 2004, only region East 5 is affected. In comparison to the western data the following years show more extreme seasonal changes, however they seem to be more or less systematic. 2010 yet again, East 5 has a negative outlier, while all other regions show a slight positive value. The heatwave in 2011 shows a decrease in CDOM, however it does not seem extraordinary within the whole series. Its extent is comparable to the one shown in the western bay. The decline in CDOM concentration is followed by a rapid normalization in the following year. In 2013 the eastern as well as the western data show a similar feature starting with a positive CDOM value which is followed by a sharp decline. The last three years of the two data sets look rather similar. The eastern data also has an outlier at 2016. While East 1 and East 5 are not affected, the other three regions of interest have a strong outlier. However, the data does not present such a clear gradual influence as it can be seen in the western bay. Further comparing the most recent years of the two data sets, the outlier in 2017 seems to shifted by approximately one vegetation period in the eastern data.

Zooming in, the western bay does not show a significant structure. While the values seem to gradually decrease from West 4 to West 2 the other two regions, West 1 and West 5 seem to behave differently, even though they follow the overall trend. The eastern data shows a gradient, as the concentration decreases from East 4 to East 1. The structure is more evident in this part of the bay as in the other one. Like with every other index, the southernmost region of interest,

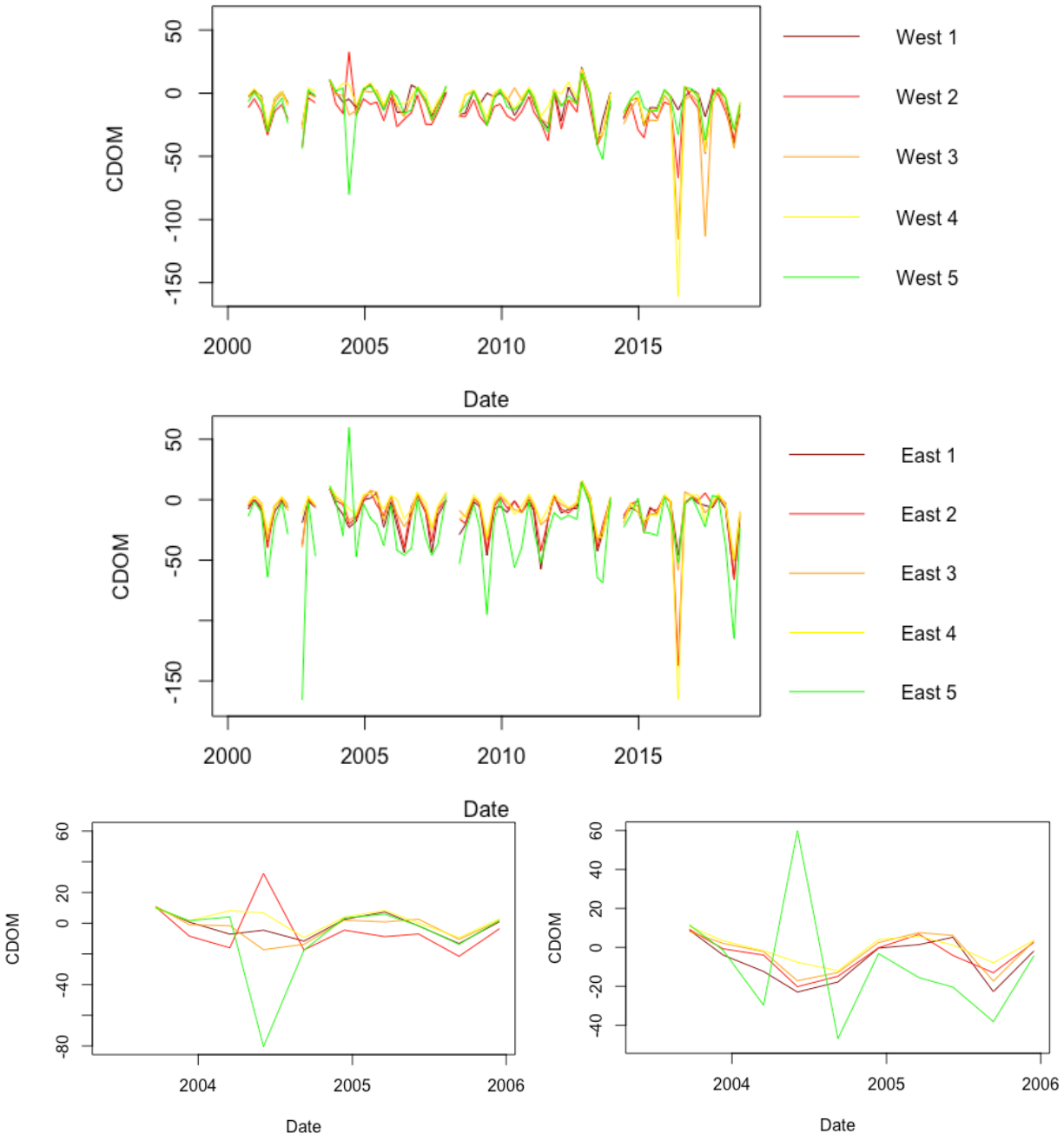

Fig. 25 The CDOM values over the whole time series for the western (upper graph) and eastern (middle graph) bay arm, shown per region of interest. The bottom images display a zoomed in view to show potential gradients present in the western (bottom left) and eastern (bottom right) waters.

East 5, shows a different pattern, also indicating strong outliers which are not recorded in the other parts. Nevertheless the overall distribution of data corresponds to the other four regions. For the in-depth analysis of the data, the time series was untangled and only the data from June is examined (see Fig. 26). One can see that the data at West 3 and West 4 show similar behaviour. West 2 (see Appendix) has some comparable features, but West 1 as well as West 5 show a different picture, confirming what has been observed above. West 2 has a small peak in 2005 which is also visible at West 5, however no other region of interest shows this feature. Until 2009 the data series is very stable, which is also observable at East 4. 2009 however some

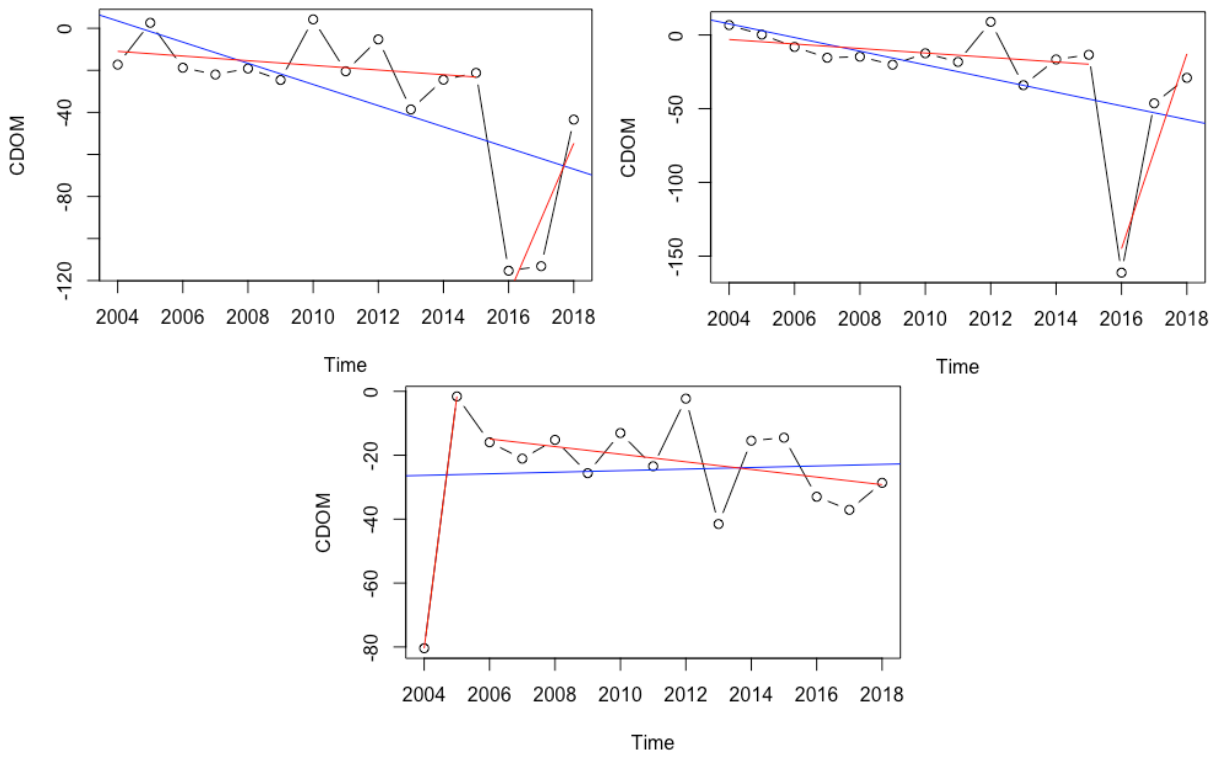

Fig. 26 The CDOM concentration shown every June at West 3 (upper left), West 4 (upper right) and West 5 (bottom middle). Displayed are the overall trend line (blue) and the trends in the two segments (red) found by the breakpoint detection.

fluctuations start and the values change constantly. The variations stop in 2016 where an extremely low value is recorded. The following year the CDOM concentration stays on a very small level only to return to a more positive one in 2018. The overall trend of the data describes a significant negative tendency over the 14 years' time. This is confirmed by other significant results at West 2 and West 4. Looking at the data set, it seems logical that West 3 has its breakpoint in 2015. However, no segment is statistically significant. Table 4 shows that the ANOVA calculated very similar results at West 3 and 4, where the breakpoint yet again is 2015. It is noteworthy however, that the outlier recorded at West 4 only lasts one year and not two and recovers fast to a normal level. West 5 again confirms the distinctive regime present in its water, as it behaves differently than the other regions of interest. It has an extremely low value in 2004 distorting the breakpoint detection. From 2005 onwards, the values are distributed around a nearly neutral trend line. The only interesting feature left is the increase from 2011 to 2012 which is followed by a rapid decline in the year 2013 which might be linked to the heatwave. After this the system normalizes and follows the known pattern.

Looking at the eastern Shark Bay, the June values seem to be like the ones recorded in the west. East 3 shows bigger fluctuation with strong changes from year to year, however the overall distribution is equal to the one at West 3 (see Fig. 27). Again, one can observe the peak in 2005 followed by the mentioned oscillations. The drop in 2013 is also present in the time series. The most extreme outlier is in 2016, in contrast to the western bay, the region of interest shows

another severe drop in 2018. East 4 is very similar to West 4. The data shows a very stable environment until 2016 where yet again a major decline in CDOM concentration is registered. The system recovers in the following year and shows no other significant features. In both time series, 2015 is detected as a breakpoint, however no result is statistically significant (see Table 4). East 5 differs in its behaviour not only from all other eastern regions of interest but also the western ones. It shows a gradual decrease from 2004 until 2009. The following years show some variability in the data, however no outliers are present. This rather stable phase ends in another very low value in 2018.

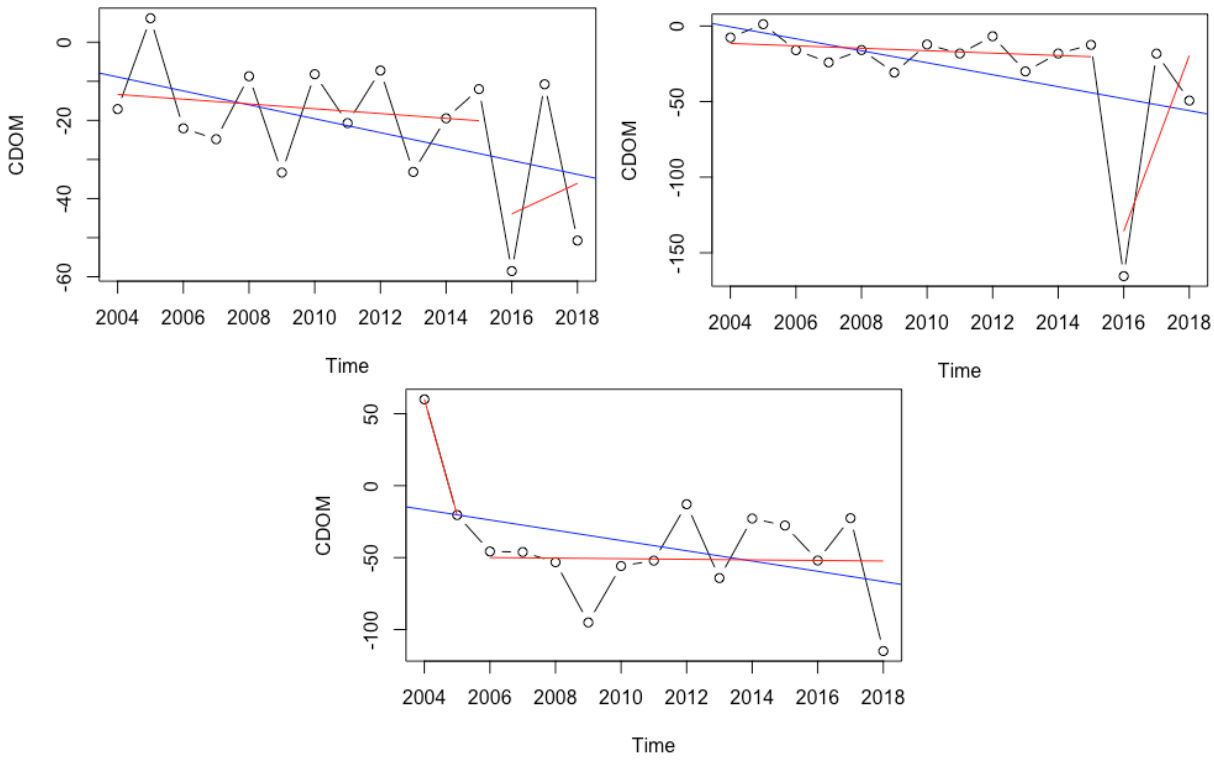

Fig. 27 The CDOM values in June recorded in the eastern Shark Bay. Displayed are East 3 (upper left), East 4 (upper right) and East 5 (bottom middle). The coloured lines represent the overall trend line (blue) and the segment trend lines (red).

The western as well as the eastern data do not have any results of particular interest regarding the 2011 heatwave. Even though some results are statistically significant, none coincide with the event. Although the slight increase shown in the difference map is also visible in most of the datasets, it does not stand out within the time series.

Table 4 The results of the statistical analysis of CDOM values. Significant results are bold.

ROI	P-Value	Break	S1 P-Value	S2 P-Value	Segment 1	Segment 2
West 1	0.07343378	2012	0.9338035	0.9529229	2004 – 2012	2013 – 2018
West 2	**0.006369324**	2005	NaN	0.08557402	2004 – 2005	2006 – 2018
West 3	**0.01193272**	2015	0.2945463	0.3164951	2004 – 2015	2016 – 2018
West 4	**0.04992529**	2015	0.1347007	0.256489	2004 – 2015	2016 – 2018
West 5	0.8400314	2005	NaN	0.1489988	2004 – 2005	2006 – 2018

Table 4 (Continued) The results of the statistical analysis of CDOM values. Significant values are in bold.

ROI	P-Value	Break	S1 P-Value	S2 P-Value	Segment 1	Segment 2
East 1	0.6649834	2005	NaN	0.7285264	2004 – 2005	2006 – 2018
East 2	0.2899349	2015	0.7562706	0.6664245	2004 – 2015	2016 – 2018
East 3	0.07816512	2015	0.5474517	0.9027401	2004 – 2015	2016 – 2018
East 4	0.09612118	2015	0.3318149	0.4615351	2004 – 2015	2016 – 2018
East 5	0.1350914	2005	NaN	0.9290838	2004 – 2005	2006 – 2018

4.5 Correlation

To examine potential interconnections of the indices the correlation coefficient was calculated. The Pearson correlation will provide a significance value to see if there are any indices influencing one another and test the dependency from water temperature changes.

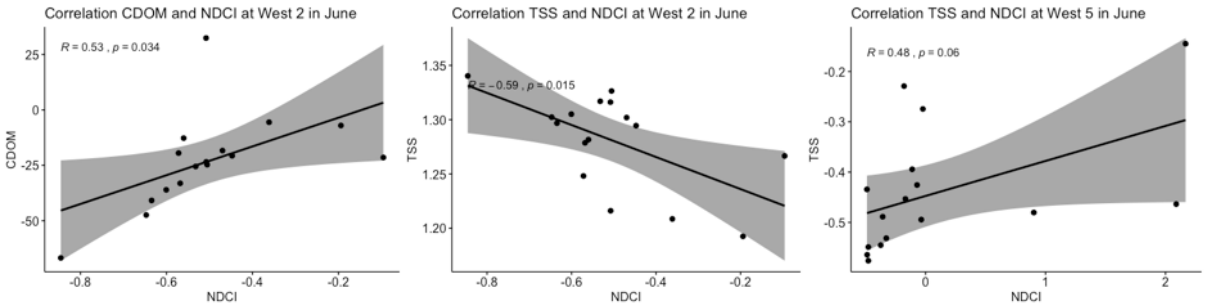

Fig. 28 The correlation between the three indices in the west, shown on three examples. Displayed are the R indicating the correlation and p which is the significance value.

Looking at the western bay arm it can be observed, that the data shows a slight positive correlation between CDOM and NDCI (see Fig. 28). Several other analysed regions of interest also show statistically significant results. However, CDOM and NDCI show the only conclusive correlations found in the western bay. Even though there are other statistically significant results, those are only recorded at one or two specific regions of interest which indicates that a third factor might be inducing this correlation (see Fig. 28). Interestingly, the TSS and NDCI which could be linked positively, because of the particles they are looking at, show no correlation supporting this claim. The eastern data shows a similar picture. Again, the relationship

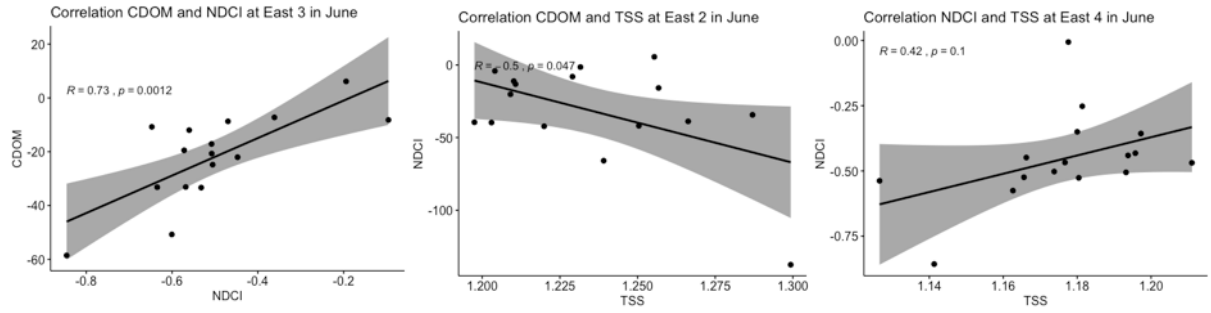

Fig. 29 Some examples of the eastern bay arms correlation coefficients when looking at the three indices. R shows the correlation and p the significance value

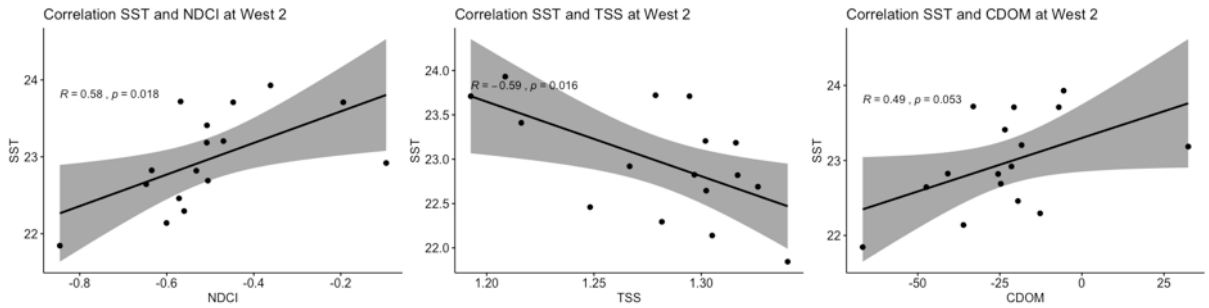

Fig. 30 The western indices correlation coefficients with the water temperature extracted from MODIS. The type of correlation is indicated by the R-value, p shows its statistical significance.

between CDOM and NDCI seem to be the most significant. The other indices show comparatively low connections and have only one noteworthy result (see Fig. 29). However, such low correlations in between the indices support the results as they are proven to be independent.
Looking at the correlation with the water temperature extracted from MODIS the western NDCI values show a strong positive correlation in the first three regions of interest. Indicating that higher water temperatures subsequently meant higher productivity resulting in higher chlorophyll content in the water. NDCI seems to be the index which is closest related to the water temperature (see Fig. 30). Looking at the total suspended solids no relationship seems to be present, only West 2 shows a significant negative correlation. The CDOM values also score significant positive correlation values, which puts the NDCI values into perspective as there might still be a third parameter influencing the system, as both parameters show similar results.

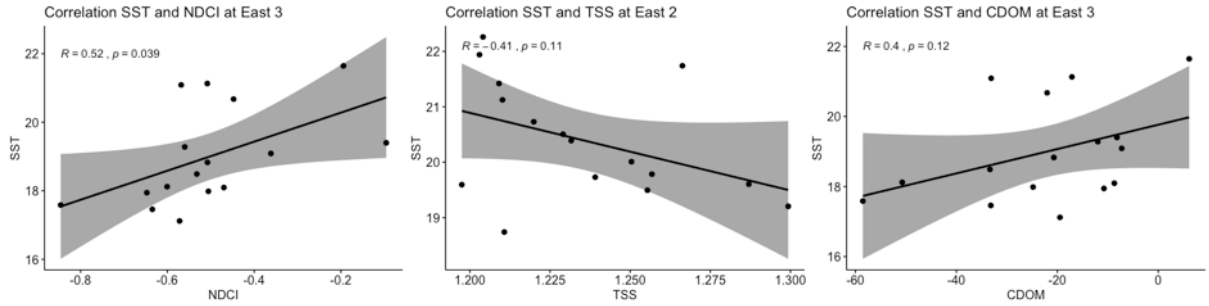

Fig. 31 The Pearson correlation coefficient for sea surface temperature and the indices, calculated in the eastern bay arm. R indicates the correlation type and p its significance value.

The eastern data yet again shows a similar outcome; however, it seems to be less driven by water temperature as the results are less significant. Only the NDCI shows a dependency whereas TSS and CDOM have no results indicating a relationship (see Fig. 31). The correlation direction of the ones recorded point in the same directions as in the west. NDCI is positively influenced by higher sea surface temperature. TSS has a negative direction and CDOM a positive one, but none are of statistical importance. The fact, that in the eastern bay the CDOM values and NDCI do not correspond needs to further looked at. Because if a third parameter influences their relationship it would only be present in the western bay arm, which seems unusual but not totally unlikely.

4.6 Habitat analysis

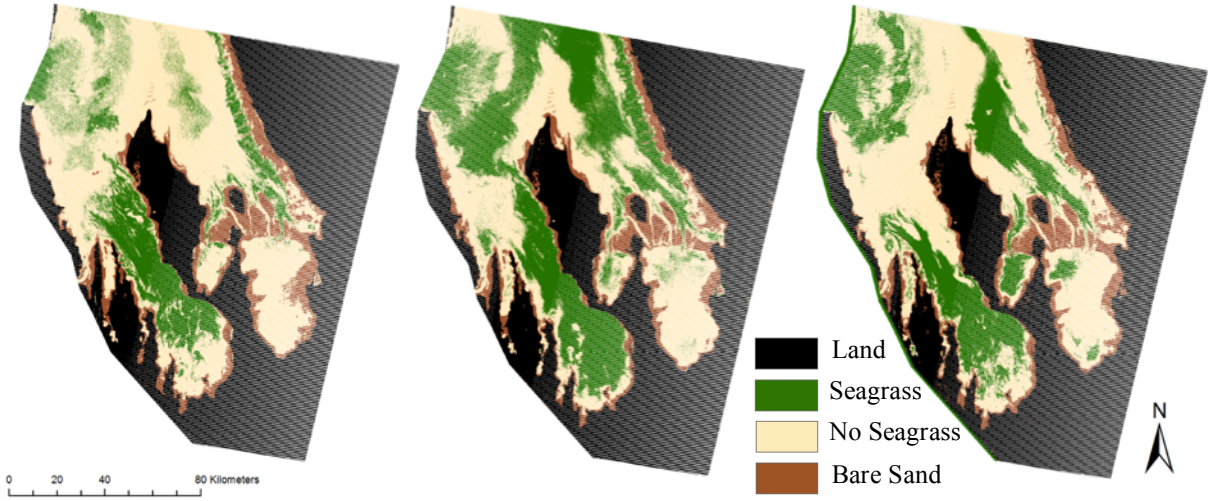

Fig. 32 The benthic map showing the seagrass extent for 2010 (left), 2011 (middle) and 2012 (right).

Similar to the water quality parameters, the seagrass extent was statistically validated. Again, the eastern and western bay were analysed separately. However, to have a first overview of the data, the whole area was studied. Fig. 32 shows a comparison of three years and their respective seagrass extent. The image displays a very diverse and fast changing environment which seems unlikely, as one can assume the seagrass meadows to be rather constant and changing gradually over time. The data seems to be very unprecise, because of the diversity present. Nevertheless, a statistical analysis was conducted.

Fig. 33 shows the time series data of the whole bay area indicating a slight negative trend in seagrass cover over the years. However, the decrease is not statistically significant. As one can see, the data varies greatly throughout the 18 years, with sudden drops and subsequent recoveries, though no structure is present. The breakpoint is detected in 2007, but the break as well as the two segment trend lines are of no statistical significance. The data shows a very fast changing environment, like Fig. 32 also suggested. Looking at the no seagrass data, a similar picture is presented. As expected, the time series is more or less anticyclical to the seagrass

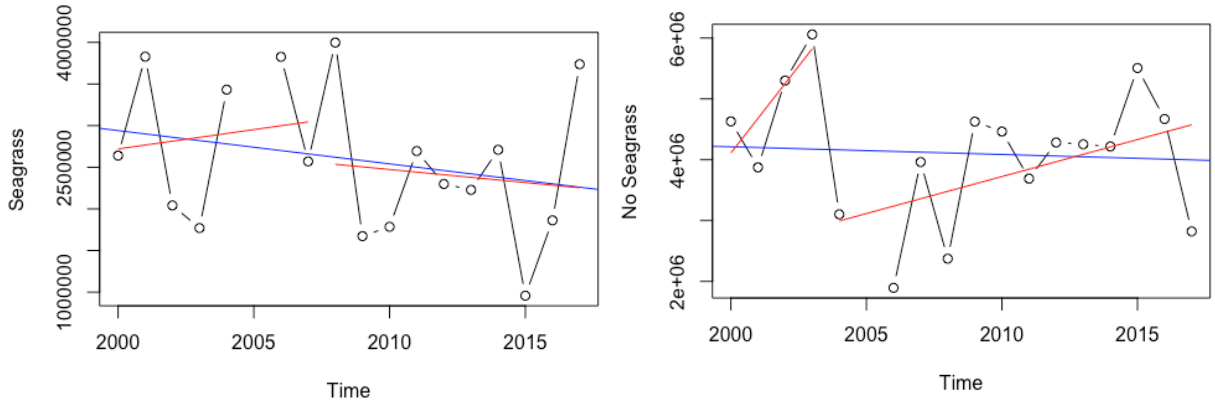

Fig. 33 The pixel count for the seagrass (left) and no seagrass class (right) over the whole Shark Bay area. Displayed are the overall trend line (blue) and the trends in the two segments (red) found by the breakpoint detection.

data, yet again no significant features or trends are visible. The overall trend conversely shows a nearly neutral tendency. The breakpoint detection shows a structural change in 2003, but as before all features are insignificant (see Table 5).

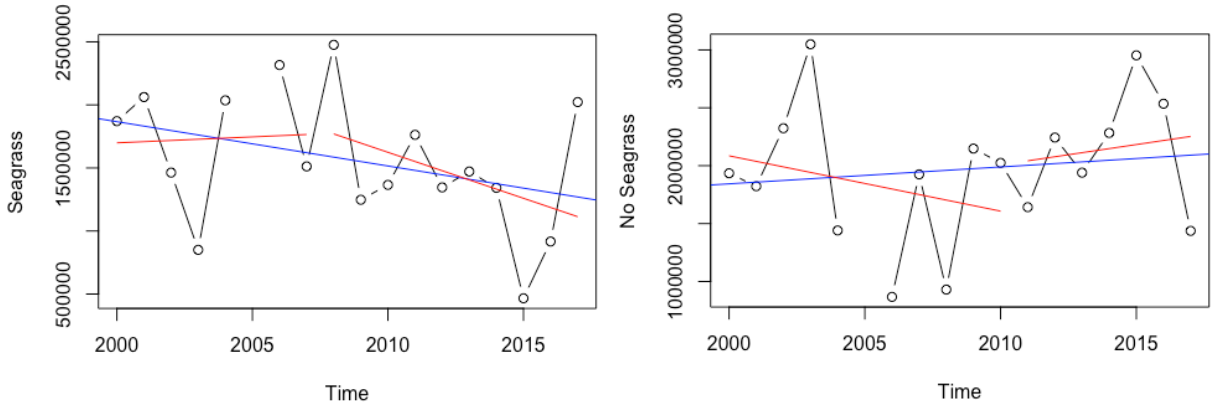

Fig. 34 The western seagrass extent (left)from 2000 until 2017. The right graph shows the pixel count for no seagrass. The blue line represents the overall trend, the red lines the segment trends.

Focusing on the western time series strong similarities to the overall data become evident. In both, the seagrass and no seagrass class, the same data progress with comparable features is observable. This means, that a subset of the whole bay area is still not capable of erasing the extreme diversity in in the data, indicating a fundamental issue. The two main features are a drop in 2003 and another one in 2015 both followed by a fast recovery of the benthic system. The highest seagrass extent was recorded in 2008, however a single peak indicating a fast growth in one year seems unlikely. The no seagrass class supports the seagrass data set by presenting a mirrored data series. This makes sense as more seagrass consequently means less surface not covered by water plants. However, no changes can be linked to the heatwave in 2011 or the gradual decrease in seagrass cover recorded by other studies (Arias-Ortiz et al. 2018). The breakpoints in 2007 and 2010 divide the data into two statistically insignificant segments. The overall trend, even though negative as expected, is not of statistical significance (see Table 5).

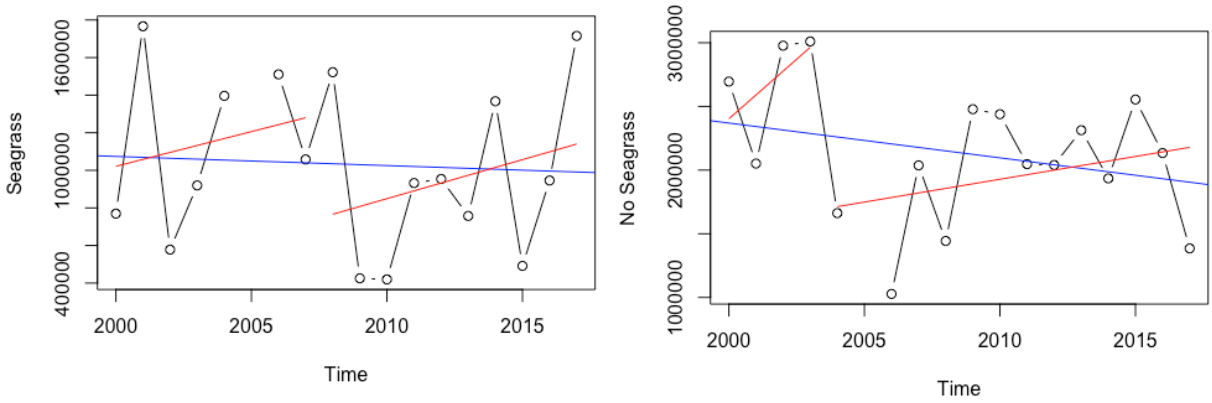

Fig. 35 The pixel count of the seagrass (left) and no seagrass (right) extent in the eastern bay arm. The overall trend line is shown in blue, the detected segment trend lines are in red.

A somewhat different development of the seafloor cover can be seen in the eastern by arm (see Fig. 35). The seagrass extent shows the basic features that were also present in the western bay, however the data has even more and stronger changes from year to year. An extreme peak in 2001 is followed by a negative outlier, indicating a shift by one year comparing it to the one in 2003 in the west. In contrast to Fig. 33 and Fig. 34 the lowest value in the east is recorded in 2010, where a two-year depression is present. The last feature in the time series is yet again a low value in 2015 which is followed by a rapid seagrass growth in the next two years. Additionally, the different behaviour is underlined by the fact, that the no seagrass class does not fit as well as before. Even though, an increase in seagrass subsequently provokes a decrease in no seagrass pixels, the connection is not apparent. Especially the time before the no data value, e.g. 2003 to 2004, do not correspond as expected. While the seagrass shows a growth in this year, the no seagrass class stays constant within this time period. Again, the breakpoints have no statistical significance in both classes. Most interestingly the seagrass extent is split up into two positive segments, while the no seagrass extent is also increasing in both its segments. This can only be explained by a decrease of the third class, bare sand. To conclude, the habitat data does not supplement any of the findings presented above and cannot be linked to the heatwave in any way.

Table 5 The statistical results of the seagrass cover changes.

Seagrass	P-Value	Break	S1 P-Value	S2 P-Value	Segment 1	Segment 2
Whole Area	0.5239291	2007	0.8271604	0.9736025	2000 – 2007	2008 – 2017
West	0.1606415	2007	0.916783	0.2575442	2000 – 2007	2008 – 2017
East	0.8185641	2007	0.6345989	0.443281	2000 – 2007	2008 – 2017

No Seagrass	P-Value	Break	S1 P-Value	S2 P-Value	Segment 1	Segment 2
Whole Area	0.5909715	2003	0.4425914	0.4181908	2000 – 2003	2004 – 2017
West	0.6137994	2010	0.4719852	0.7556408	2000 – 2010	2011 – 2017
East	0.2907667	2003	0.4565372	0.3008352	2000 – 2003	2004 – 2017

5. Discussion

5.1 Temperature

The temperature calculated using the at sensor brightness temperature showed the inclusion of warm water very clearly. The difference map supports other research and measurements conducted to estimate the extent of the heatwave (Arias-Ortiz et al. 2018; Caputi et al. 2014). The time series data however, is much less conclusive, shows a different picture and also has contradictory results to the MODIS sea surface temperature estimate. Besides the heatwave, several other, positive and negative outliers, are detected which cannot be explained by the data at hand. These might be due to the fact, that the data used is not very precise and not consistent. The at sensor brightness temperature is not corrected for any atmospheric influences, which have the

potential of greatly changing the results. A dynamic equation would be needed to correct for the constantly changing atmospheric parameters. But as this would have been too much work and the uncorrected results did not show huge variabilities, the data was approved as it is.
In addition, the time series data is only as good as the images available. There are only two images per month thus presenting us individual snapshots of the month. These images can then have clouds, water and atmospheric parameters influencing the recorded temperature values. Thus, the time series data needs to be treated with caution.

5.2 Normalized difference chlorophyll index

The overall data shows no results of any importance to the study conducted. The data is very unstructured and due to seasonal fluctuations not very useful in understanding the process. However, the zoomed in graph reveals a gradient in the eastern bay which is most likely present because of the water structure given by the bays properties. From the inlet down to the southern shoreline the NDCI slightly decreases in the years looked at. As water enters the bay in the north, less and less mixing happens the further it progresses into the eastern bay arm. Limited mixing has an influence on the water properties such as oxygen circulation and thus has an effect on the NDCI. East 5 in Hamelin Pond is cut off from the other part of the bay system by the Faure Sylt banks, which generate a very unique system. As the structure is not present in the western bay arm, one can argue that the western waters are better mixed or have a different chlorophyll regime.
Looking at the June time series and the heatwave of 2011, no concluding statements can be made. In the west the heatwave is better visible than in the east, which is also reflected in the breakpoints detected. Four out of five are in 2012 while the eastern ones are not as distinctive. The time series data shows, that except for West 4 the decrease in 2012 is the most extreme negative outlier present in the data. However, 2010 poses as another extreme year in several regions of interest. This is of importance, because even without a heatwave in the year 2009 it still had a strong La Niña weather system present, which might have an influence on the chlorophyll content in the water. This could be due to different current systems and atmospheric conditions present. The positive peak in chlorophyll in the year 2016 does not coincide with any meteorological or water parameters and cannot be explained by the data at hand. The only possible explanation are potential sensor issues as several images where generated by using Landsat 8 images as there were no others available. However, as argued above, there are only minor spectral difference between the two sensors as they are built to supplement each other. Additionally, part of the image is occluded by clouds, which were avoided as good as possible but might still influence the result.
In the east, the results do not seem to coincide with the heatwave. Even though several regions of interest show a slight decrease in NDCI from 2011 to 2012, the drop is of minor extent compared to other outliers, e.g. 2009 to 2010. Contrary to the western regions of interest the

drop at 2010 in the east is big compared to the other outliers in the time series. Again, the positive peak in 2016 can be seen, however no conclusive results are present.
The NDCI seems to be subject to several uncertainties affecting the data. On one hand, one must keep in mind, that the atmospheric correction executed is based on a model using external data to estimate the atmospheric conditions present. This holds a potential for minor errors influencing the resulting corrected datasets, which are then further progressed into the equations used (Mishra & Mishra 2012). Furthermore, the ratio used for the estimation is rather basic. Watanabe et al. (2017) report, that an overall understimation of chlorphyll-a content is possible when using the ratio at hand. Several effects affect the spectral response of chlorophyll-a and subsequently distort the resulting NDCI values. In the research conducted by Watanabe et al. (2017), their concentration increased while the absorption did not. This is due to the pigment package effect, which describes the fact, that phytoplankton does not necessarily increase its cell number, but can also change its cell volume or intercellular structure (Alcântara et al. 2016). This change does affect the absorption properties of phytoplankton and can lead to an inverse relationship between growth and chlorophyll-a concentration (Alcântara et al. 2016). This could have masked the influence of the heatwave on the maritime system, as the effect is known to be of particular importance in saline water (Wang et al. 2014). Additionally, the data used, are snapshots of one point in time, as Landsat 7 ETM+ does not provide more images. The assumption was, that the data of one image is representative for a longer time span. Phytoplankton however, is part of a dynamic system which is influenced by the bays environment on a very short time scale (Mishra & Mishra 2012).
To conclude, the heatwave seems to be visible in the data presented especially in the west whereas the east is not affected as much. However, one needs to evaluate the data also in respect to the approach used. The analysis is based on a simple band ratio which was never validated by ground truth data in the bay waters. Bearing this in mind, the results generated, especially as most of them are not statistically significant, should not be used to assess the behavioural changes of dolphins in the Shark Bay waters. The structural changes induced by the heatwave can never be fully accounted for by the analysis used as they are of extreme complexity. Nevertheless, by scratching the surface, the time series show decent results which can be used as a guideline for further in-depth studies. To improve the results, a thorough analysis of in situ data is needed to understand the errors in the time series at hand. The influence of masking effects related to phytoplankton growth and the weight of external effects such as currents and other changes on a short time scale need to be assessed. Using this knowledge, the equation can be altered to minimize errors in NDCI estimations.

5.3 Total suspended solids

Again, the non-filtered time series shows extreme variations over the years induced by seasonality and other fluctuations in the system. The zoomed in image confirms what was already seen when looking at the NDCI, namely that the eastern bay arm shows more structure than the

western one. The gradient present suggests a decrease from inlet down to Faure Sylt, while East 5 has a different regime. The western data also has decreasing values from the open sea southwards, however they are not as structured as the eastern ones supporting again the assumption of uneven mixing in the two arms.

Coinciding the TSS concentration with the heatwave in 2011 is not as straight forward as with the NDCI. Even though the difference image indicates a slight decrease in year, the results show a rather balanced regime. Following an inexplicable decrease in TSS in 2005, is a gradual decrease starting in 2009. As mentioned, this would coincide with another strong La Niña year, however this timely co-occurrence is only visible in some of the western and eastern regions of interest. It is noteworthy that it finds its end in 2012, indicating a possible turning point in the system. However, this is of no statistical significance and thus needs further examination. Yet again, 2016 poses as a strong positive outlier, but the results are not conclusive. Especially in the east, 2016 shows to be neutral or even has a negative influence in some regions of interest. The TSS can thus not be linked to the heatwave in any way. This might also be due to particles induced into the system by Gascoyne River. Park (2007) reported strong influences on the TSS analysis due to river based sedimentation and human pollution in the Korean Sea. As Gascoyne River is known to have had extreme floods in 2010 (which are not visible in the data), large amounts of material could have been flushed in to bay waters. Human pollution however, should not be of great importance, as there is little activity in the protected waters. Gascoyne River flows into the bay in the north and is known to carry many particles into the Shark Bay waters. The inlet of the river is north of the area looked at in the study, but might have had a delayed influence on the total suspended solid detection, depending on the currents present.

Again, the atmospheric correction model poses as a potential source of error. Jaelani et al. (2016) suggest, that the atmospheric correction provided by USGS has limitations which influence the results of TSS estimations. The correlation between in situ measurements and the calculated values show deviations, which were linked to insufficient atmospheric correction (Jaelani et al. 2016). If this problem exists in the Shark Bay waters, needs to be the looked at in further analysis of the bay's water. A thorough analysis of the water would also provide verified coefficients for the equation to improve its performance. These constants are of importance in natural waters to ensure proper concentration estimations (Gray et al. 2000).

In conclusion, the data is yet again based on a ratio calculating the total suspended solids in close proximity of the water surface. This analysis seems to be insufficient to be used in explaining dolphin's behavioural changes, especially because no significant results linked to the heatwave were found. With well-grounded in situ measurements the calibration of the equation could be altered to generate decent results. Nevertheless, it is also possible, that the TSS are not influenced by warm water induced in to the system, but in ways that the approach was not able to grasp.

5.4 Coloured dissolved organic matter

Yet again, the whole time series shows strong outliers over the years which are most likely due to seasonal changes, clouds and other external parameters influencing the system. The zoomed in image reveals again a gradient which is present in the eastern bay waters. In comparison to the other two indices, the CDOM values decrease from East 4 up to the East 1 and not the other way around. Nevertheless, this can still be the result of unequal mixing which might also accumulate CDOM in front of Faure Sylt which acts as a barricade. The western bay arm also shows an inverted gradient, but again the data is less structured indicating more mixing within the waters.

Looking at the heatwave, the difference map can be used as a starting point of the analysis. The coloured dissolved organic matter shows a strong increase throughout the whole bay area, which can be linked to the dying of seagrass. When decaying, the dead plants set particles free which are then detected as CDOM by our sensor. However, these promising results were not confirmed by the in-depth statistical analysis conducted. Neither the eastern nor the western data series show the heatwave in 2011, as the most influential feature. The western data has its two most extreme outliers in 2013 and 2016. The increase in 2012 which could be linked to the seagrass dying because of the warm water is of no significance within the whole time series. The drop in 2013 might be due to a delayed reaction by the water system, however it can be placed within the normal fluctuations of the CDOM concentration. The most drastic feature is recorded in 2016, where yet again the sensor might have had an influence. However, several regions of interest show another low value in the following year which stands in contrast with this argument. The eastern bay confirms these findings by presenting similar results. Again, 2013 shows a strong decrease in CDOM but the biggest outlier is found in 2016. Interestingly, 2009 appears to be another negative feature which seems to be followed by yet another increase in CDOM the following year. If the weather system was influenced negatively in 2009 and the following year particles of dying seagrass are detected, cannot be said. The magnitude of the oscillations varies throughout the time series and regions of interest, thus leaving us with no definite results. The CDOM seems to be the one the least affected by the heatwave showing no significant results coinciding with the induced warm water.

However, there are other parameters not taken into the analysis. Salinity, temperature and turbidity have the potential to influence the precision of CDOM absorption measurement (Branco & Kremer 2005; Slonecker et al. 2016). CDOM concentration tends to correlate especially with salinity, but also algal activity in the water, both are major components in the Shark Bay's water system (Branco & Kremer 2005). To improve CDOM mapping, newer satellites, such as Landsat 8, could prove to be very useful. Having better bands available, such as the ultra-blue band, helps in distinguishing CDOM from other water constituents (Olmanson et al. 2016). Further research thus needs to evaluate the potential of newer sensors with narrower bands.

Though, none will be helpful in generating time series analysis, because of their short operation time. To increase the precision of the older satellite used in the study at hand, the equation needs to be thoroughly calibrated using in situ measurements.

5.5 Correlation

The calculation of the correlation coefficient helped to disentangle potential interconnections between the indices. The results showed that CDOM and NDCI might have a third parameter influencing them, however which one this might be can only be speculated. The significant relationship of NDCI with sea surface temperature is reasonable, as up to a certain extent, higher water temperature raise productivity in the water. What cannot be seen by this analysis, is how the increase comes about. It is possible that tropical algae grow in such environment perfectly whereas the local species get oppressed.
The other two indices show no significant reaction to the changing temperature. One also needs to bear in mind, that even though an index might not follow the sea surface temperature, it can still be influenced by sudden environmental changes such as the heatwave in 2011. As such, the correlation did not greatly contribute to the overall data, nevertheless it adds to a greater understanding of the bay's water system.

5.6 Habitat analysis

The habitat analysis has no results which could be used for a deeper analysis as they are very imprecise. The aim was to map the seafloor without correcting for the water column, as this was successfully done in several other studies. However, this showed to be impossible in the Shark Bay waters. The fast changing environment has too many external parameters influencing the water column and subsequently the spectral signal received. The time series data shows fast changing seagrass meadows which is contrary to any other study conducted on the subject. All results are statistically insignificant and show no connection to either atmospheric or water physical conditions present. For a thorough analysis the above calculated water quality parameters would be needed to correct for particles in the water column. Additionally, the depth and other external influences are required to be corrected for, otherwise a precise seafloor map will not be possible. Especially water turbidity reduces the accuracy of a benthic analysis (Roy 2003; Garcia et al. 2015). Turbidity reduces light penetration and subsequently reflectance, thus masking the seafloor. The river in the north might be a potential source of material influencing the benthic mapping negatively. Additionally, water depth is the major component in defining a sensors ability to map the seafloor. The depth of coastal waters however is influenced by several processes such as tides, seasonal water level changes and waves, which were all not integrated in the analysis at hand (Roy 2003). Having all these potential error sources shows that the attempt at benthic mapping was not sophisticated enough to account for the dynamic and complex water system of the Shark Bay. Still, the results can be used as the basis for additional analysis, as the basic approach is working and proved to be suitable in such an environment.

In further research a correction for the water column is essential, all other parameters considered will improve the results. A combined approach could also increase the accuracy of a benthic analysis. Ohlendorf et al. (2011) suggest a combination of optical and SAR images to enhance the result. Additionally, the usage of precise training data, based on in situ measurements, would better the benthic map significantly.

6. Conclusion and Future Work

In examining water quality parameters using remotely sensed data, this study helps understanding the major advantages and disadvantages of such an approach. Using rather simple band math equations, indices were used to map the influence of an extreme heat event on a water system. Even though the water quality indices showed a potential in detecting fluctuations in the Shark Bay waters, they were not precise enough to be used in a thorough analysis of changes in the ecosystem. Remote sensing data, especially when used in water systems, is affected by environmental changes in all the media radiation passes through. Thus, for perfect results, it is necessary to correct the equations for the local system parameters, which was not possible in the study at hand. Subsequently the limits of satellite data lie in its adaption to the local circumstances. This is best shown by the benthic habitat maps that have been limited in their usability by the changing water parameters for which the classification algorithm was not corrected. Without a proper and dynamic water column correction, such an analysis will not generate reasonable results in the Shark Bay waters. Therefore, it was difficult to detect the heatwave in the data. The normalized chlorophyll index showed the best results having breakpoints coinciding with the heatwave event and clearly visible changes. However, these shifts were only short-term and the system went back to normal levels in the following years. Additionally, there are other outliers such as 2009 that could be explained by similar La Niña weather conditions, but this needs further investigation. The other data does not show conclusive results. It seems that the two bay arms have different reactions to the induced external effects however, the difference in reaction is not quantifiable or explainable by the presented data. Additionally, the indices suggest a gradual structuring of the data which could be sensible looking at the water structure present.

Nevertheless, all these findings do not suffice to understand the post-heatwave changes of the bottlenose dolphins reported by the Dolphin Research Alliance. In the way remotely sensed data was implemented, it cannot be used supplementary to the dolphin research done in the bay. It can be utilized as a guideline for further studies and giving summary data. But one needs to understand, that the full potential of remote sensing was never tapped in this application. With a more sophisticated approach, the complexity of the factors influencing dolphin habitat and dolphin behaviour could most likely be analysed. Thus it is evident, that the data cannot support the in situ observations conducted over the last decades by the Research Alliance.

Nonetheless, this study will pose as a potential starting point of further studies which will build on the information gathered in the thesis at hand. This is also why, as a side product, the whole

data generation was implemented in a simple application in Google Earth Engine. The three indices can be calculated everywhere the Landsat satellites gather data. It is a tool simple to use, as it does not only plot all the data one needs, but also prepares it to be exported as a data table for statistical analysis. Additionally, the whole code is accessible and editable, thus giving the possibility of altering the equations. This helps in improving the indices as local correction factors and/or better parameters can be used to generate perfect results in the respective regions. Providing this facile approach for a superficial analysis in waters around the globe might help in further studies on the subject. Also, because problems raised by climate change and subsequent shifts in balanced ecosystems are already a major issue, and will become even more important in the coming years. Here, remote sensing will pose as a major instrument in assessing the severity of environmental transformations.

7. Bibliography

Alcântara, E., Watanabe, F. & Rodrigues, T., 2016. An investigation into the phytoplankton package effect on the chlorophyll- a specific absorption coefficient in Barra Bonita reservoir , Brazil the chlorophyll- a speci fi c absorption coe ffi cient in Barra. *Remote Sensing Letters*, 7(8), pp.761–770. Available at: http://dx.doi.org/10.1080/2150704X.2016.1185189.

Arias-Ortiz, A. et al., 2018. A marine heatwave drives massive losses from the world's largest seagrass carbon stocks. *Nature Climate Change*, 8(4), pp.338–344.

Australian Bureau of Statistics, 2018. Data by Region. Available at: http://stat.abs.gov.au/itt/r.jsp?databyregion&ref=CTA2 [Accessed August 2, 2018].

Australian Interstate Quarantine, 2017. Interstate quarantine. Available at: https://www.interstatequarantine.org.au [Accessed June 16, 2018].

Bierwirth, P.N., Lee, T.J. & Burne, R. V, 1992. Shallow Water Mapping via the Seperation of Depth and Substrate Components from Multispectral Data. In *6th Australasian Remote Sensing Conference*. Canberra: Australian Geological Survey Organisation, Environmental Geoscience and Groundwater.

Bierwirth, P.N., Lee, T.J. & Burne, R. V, 1993. Shallow sea-floor reflectance and water depth derived by unmixing multispectral imagery. *Photogrammetric Engineering and Remote Sensing*, 59(3), pp.331–338.

Bowdler, S., 1990. *Archaeological research in the Shark Bay region, Western Australia: An introductory account.*,

Bowdler, S., 2018. The Excavation of Two Small Rockshelters at Monkey Mia , Shark Bay , Western Australia Author (s): Sandra Bowdler Source : Australian Archaeology , No . 40 (Jun ., 1995), pp . 1-13 Stable URL : https://www.jstor.org/stable/40287205 REFERENCES Linked r. , 40(40), pp.1–13.

Branco, A.B. & Kremer, J.N., 2005. The relative importance of chlorophyll and colored dissolved organic matter (CDOM) to the prediction of the diffuse attenuation coefficient in shallow estuaries. *Estuaries*, 28(5), pp.643–652.

Brown, A.M. et al., 2016. Site-Specific Assessments of the Abundance of Three Inshore Dolphin Species to Inform Conservation and Management. *Frontiers in Marine Science*, 3(February), pp.1–18. Available at: http://journal.frontiersin.org/Article/10.3389/fmars.2016.00004/abstract.

Burling, M.C., Pattiaratchi, C.B. & Ivey, G.N., 2003. The tidal regime of Shark Bay, Western Australia. *Estuarine, Coastal and Shelf Science*, 57(5–6), pp.725–735.

Caputi, N., Jackson, G. & Pearce, A., 2014. *The marine heat wave off Western Australia during the summer of 2010/11 – 2 years on Management implications of climate change effects on fisheries in WA: an example of an extreme event*,

Connor, R.C. et al., 2000. The Bottlenose Dolphin. In *Cetacean Societies: Field studies of whales and dolphins*. Chicago: University of Chicago Press, pp. 92 – 125.

Denman, P.D. & Geological Survey of Western Australia, 1985. *Wooramel, Western Australia (2nd edition): Geological Survey of Western Australia*,

Donlon, C. et al., 2012. The Global Monitoring for Environment and Security (GMES) Sentinel-3 mission. *Remote Sensing of Environment*, 120(2012), pp.37–57. Available at: http://dx.doi.org/10.1016/j.rse.2011.07.024.

Duarte, C.M., 2002. The future of seagrass meadows. *Environmental Conservation*, 29(2), pp.192–206.

Encyclopedia of Life, 2013. Tursiops – Brief Summary. *Encyclopedia of Life*. Available at: http://eol.org/data_objects/27112764.

ESA, 2018. Sentinel-2. Available at: https://sentinel.esa.int/web/sentinel/missions/sentinel-2 [Accessed June 14, 2018].

Eugenio, F., Marcello, J. & Martin, J., 2015. High-Resolution Maps of Bathymetry and Benthic Habitats in Shallow-Water Environments Using Multispectral Remote Sensing Imagery. *Geoscience and Remote Sensing, IEEE Transactions on*, 53(7), pp.3539–3549.

Feng, M., Waite, A.M. & Thompson, P.A., 2009. Climate variability and ocean production in the Leeuwin Current system off the west coast of Western Australia. *Journal of the Royal Society of Western Australia*, 92(2), pp.67–81.

Fondriest Environmental, I., 2014. Turbidity, Total Suspended Solids and Water Clarity. *Fundamentals of Environmental Measurements*. Available at: https://www.fondriest.com/environmental-measurements/parameters/water-quality/turbidity-total-suspended-solids-water-clarity/#Turbid1 [Accessed November 26, 2018].

Fourqurean, J.W. et al., 2012. Seagrass ecosystems as a globally significant carbon stock. *Nature Geoscience*, 5(7), pp.505–509. Available at: http://dx.doi.org/10.1038/ngeo1477.

Gao, J., 2009. Bathymetric mapping by means of remote sensing: Methods, accuracy and limitations. *Progress in Physical Geography*, 33(1), pp.103–116.

Garcia, R.A., Lee, Z. & Hochberg, E.J., 2018. Hyperspectral shallow-water remote sensing with an enhanced benthic classifier. *Remote Sensing*, 10(1).

Garcia, R. et al., 2015. A Method to Analyze the Potential of Optical Remote Sensing for Benthic Habitat Mapping. *Remote Sensing*, 7(10), pp.13157–13189. Available at: http://www.mdpi.com/2072-4292/7/10/13157/.

Goodell, W., Stamoulis, K.A. & Friedlander, A.M., 2018. Coupling remote sensing with in situ surveys to determine reef fish habitat associations for the design of marine protected areas. *Marine Ecology Progress Series*, 588(February 2018), pp.121–134.

Gray, J.R. et al., 2000. Comparability of suspended-sediment concentration and total suspended solids data. *Water-Resources Investigations Report 00-4191*, (August), p.20.

Grzimek, B., 1969. Säugetiere 2. In *Grzimeks Tierleben*. Zürich: Kindler Verlag AG.

Hart et al., 2016. *Western Australian Silver-lipped Pearl Oyster (Pinctada maxima) Industry Western Australian Marine Stewardship Council Report Series*, Available at: http://www.fish.wa.gov.au/Documents/wamsc_reports/wamsc_report_no_5.pdf.

Hsu, C.-W., Chang, C.-C. & Lin, C.-J., 2016. *A Practical Guide to Support Vector Classification*, Taipei 106, Taiwan.

Jaelani, L.M. et al., 2016. Estimation of TSS and Chl - a Concentration from Landsat 8 - OLI : The Effect of Atmosphere and Retrieval Algorithm. *IPTEK, The Journal for Technology and Science*, 27(1), pp.16–23. Available at: http://www.iptek.its.ac.id/index.php/jts/article/view/1217.

Knudby, A. & Nordlund, L., 2011. Remote sensing of seagrasses in a patchy multi-species environment. *International Journal of Remote Sensing*, 32(8), pp.2227–2244.

Lamaro, A.A. et al., 2013. Water surface temperature estimation from Landsat 7 ETM+ thermal infrared data using the generalized single-channel method: Case study of Embalse del Río Tercero (Córdoba, Argentina). *Advances in Space Research*, 51(3), pp.492–500.

Logan, B.W., 1974. Inventory of Diagenesis in Holocene-Recent Carbonate Sediments, Shark Bay, Western Australia. In *Evolution and Diagenesis of Quaternary Carbonate Sequences, Shark Bay, Western Australia*. pp. 195–249.

Louvres, M., Louvres, G. & Soleil, B., 2006. *Product Guide Version 8.3*,

Mahasandana, S., Tripathi, N.K. & Honda, K., 2009. Sea surface multispectral index model for estimating chlorophyll a concentration of productive coastal waters in Thailand. *Canadian Journal of Remote Sensing*, 35(3), pp.287–296.

Melgani, F. & Bruzzone, L., 2004. Classification of hyperspectral remote sensing images with support vector machines. *IEEE Transactions on Geoscience and Remote Sensing*, 42(8), pp.1778–1790.

Mishra, S. & Mishra, D.R., 2012. Normalized difference chlorophyll index: A novel model for remote estimation of chlorophyll-a concentration in turbid productive waters. *Remote Sensing of Environment*, 117, pp.394–406. Available at: http://dx.doi.org/10.1016/j.rse.2011.10.016.

Misra, A. et al., 2018. Shallow water bathymetry mapping using Support Vector Machine (SVM) technique and multispectral imagery. *International Journal of Remote Sensing*, 00(00), pp.1–20. Available at: https://doi.org/10.1080/01431161.2017.1421796.

Mobley, C., Boss, E. & Roesler, C., 2018. *Ocean Optics Web Book*, Available at: http://www.oceanopticsbook.info.

NASA, 2018. MODIS. Available at: https://modis.gsfc.nasa.gov/about/ [Accessed June 14, 2018].

Odermatt, D. et al., 2012. Review of constituent retrieval in optically deep and complex waters from satellite imagery. *Remote Sensing of Environment*, 118, pp.116–126. Available at: http://dx.doi.org/10.1016/j.rse.2011.11.013.

Ohlendorf, S. et al., 2011. Bathymetry mapping and sea floor classification using multispectral satellite data and standardized physics-based data processing. , pp.21–22.

Olmanson, L.G. et al., 2016. Comparison of Landsat 8 and Landsat 7 for regional measurements of CDOM and water clarity in lakes. *Remote Sensing of Environment*, 185, pp.119–128. Available at: http://dx.doi.org/10.1016/j.rse.2016.01.007.

Park, G.S., 2007. The role and distribution of total suspended solids in the macrotidal coastal waters of Korea. *Environmental Monitoring and Assessment*, 135(1–3), pp.153–162.

Parks and Wildlife Service, 2018. Shark Bay – History & Culture. Available at: https://www.sharkbay.org/culture-history/ [Accessed August 2, 2018].

Parks and Wildlife Service, 2018. Climate. Available at: https://www.sharkbay.org/about/climate/ [Accessed August 2, 2018].

Pattanaik, A., Sahu, K. & Bhutiyani, M.R., 2015. Estimation of Shallow Water Bathymetry Using IRS-Multispectral Imagery of Odisha Coast, India. *Aquatic Procedia*, 4(Icwrcoe), pp.173–181. Available at: http://linkinghub.elsevier.com/retrieve/pii/S2214241X15000255.

Peneva, E., Griffith, J.A. & Carter, G.A., 2008. Seagrass Mapping in the Northern Gulf of Mexico using Airborne Hyperspectral Imagery: A Comparison of Classification Methods. *Journal of Coastal Research*, 244, pp.850–856. Available at: http://www.bioone.org/doi/abs/10.2112/06-0764.1.

Playford, P.E. et al., 2013. *The Geology Of Shark Bay Geological Survey of Western Australia : Bulletin 146*,

Reid, R.P. et al., 2003. Shark Bay Stromatolites: Microfabrics and reinterpretation of Origins. *Facies*, 49, pp.299–324. Available at: file:///C:/Users/apaul/Documents/My EndNote Library.Data/PDF/1190527522/2003-Reid-Shark Bay Stromatolites_ Microfabric.pdf file:///C:/Users/apaul/Documents/My EndNote Library.Data/PDF/1131079428/art%253A10.1007%252Fs10347-003-0036-8.pdf.

Reynolds, P.L., 2018. Seagrass and Seagrass Beds. *Smithsonian Institution*. Available at: https://ocean.si.edu/ocean-life/plants-algae/seagrass-and-seagrass-beds [Accessed October 29, 2018].

Richardson, A.J. & Poloczanska, E.S., 2009. Australia's Oceans. *A Marine Climate Change Impacts and Adaptation Report Card for Australia 2009*, (June).

Roy, C., 2003. Coastal Bathymetric Mapping of the Upper Bay of Bengal Using Optical Satellite Mapping Coastal Bathymetry of the Upper Bay of Bengal Using Satellite ' S.

Roy, D.P. et al., 2016. Characterization of Landsat-7 to Landsat-8 reflective wavelength and normalized difference vegetation index continuity. *Remote Sensing of Environment*, 185, pp.57–70. Available at: http://dx.doi.org/10.1016/j.rse.2015.12.024.

Schweizer Radio und Fernsehen, 2018. Einstein – Sind Mineralien die Bausteine des Lebens? Available at: https://www.srf.ch/sendungen/einstein/sind-mineralien-die-bausteine-des-lebens.

Shark Bay Dolphin Research Alliance, 2018. Dolphin Alliance Project. Available at: http://www.sharkbaydolphins.org/dolphin-alliance-project/ [Accessed June 12, 2018].

Shire of Shark Bay, 2016. Population and People Characteristics. Available at: http://www.sharkbay.wa.gov.au/business/economic-profile/population-and-people.aspx [Accessed August 2, 2018].

Slonecker, E.T., Jones, D.K. & Pellerin, B.A., 2016. The new Landsat 8 potential for remote sensing of colored dissolved organic matter (CDOM). *Marine Pollution Bulletin*, 107(2), pp.518–527. Available at: http://dx.doi.org/10.1016/j.marpolbul.2016.02.076.

Smith, J.S., Chandler, J. & Rose, J., 2009. High spatial resolution data acquisition for the geo-sciences: kite aerial photography. *Earth Surface Processes and Landforms*, 34(March), pp.155–161. Available at: http://www3.interscience.wiley.com/journal/121517813/abstract.

Strasserf, R.J., Srivastava, A. & Govindjee, 1995. Polyphasic Chlorphyll a Fluoresence Transient in Plants and Cyanobacteria. *Photochemistry and Photobiology*, 61(1), pp.32–42.

Subramaniam, A. et al., 2002. Detecting Trichodesmium blooms in Sea WiFS imagery. *Deep-Sea Research II*, 49, pp.107–121.

Tourism WA, 2018. Shark Bay World Heritage Area. Available at: https://www.westernaustralia.com/de/Destinations/Australias_Coral_Coast/Shark_Bay_World_Heritage_Area/Pages/Shark_Bay.aspx#/ [Accessed June 12, 2018].

Twardowski, M.S. et al., 2004. Modeling the spectral shape of absorption by chromophoric dissolved organic matter. *Marine Chemistry*, 89(1–4), pp.69–88.

Tyne, J.A. et al., 2012. Ecological characteristics contribute to sponge distribution and tool use in bottlenose dolphins Tursiops sp. *Marine Ecology Progress Series*, 444, pp.143–153.

U.S. Department of the Interior & U.S. Geological Survey, 2018. Landsat Missions. Available at: https://landsat.usgs.gov [Accessed June 14, 2018].

UNESCO World Heritage Center, 2018. UNESCO World Heritage List – Shark Bay, Western Australia. Available at: https://whc.unesco.org/en/list/578 [Accessed October 29, 2018].

United States Environmental Protection Agency, 2012. 5.5 Turbidity. *Water: Monitoring and Assessment*.

Van de Graaff, W.J.E. et al., 1983. *Yaringa, Western Australia: Geological Survey of Western Australia*,

Varma, M.K.S. et al., 2016. Pixel-Based Classification Using Support Vector Machine Classifier. *2016 IEEE 6th International Conference on Advanced Computing (IACC)*, pp.51–55. Available at: http://ieeexplore.ieee.org/document/7544809/.

Wang, J.-J. et al., 2009. Retrieval of suspended sediment concentrations in large turbid rivers using Landsat ETM+: an example from the Yangtze River, China. *Earth Surface Processes and Landforms*, 34, pp.1082–1092.

Wang, S.Q. et al., 2014. Influence of the Changjiang River on the light absorption properties of phytoplankton from the East China Sea. , pp.1759–1773.

Watanabe, F. et al., 2017. Remote Sensing of the Chlorophyll-a Based on OLI/Landsat-8 and MSI/Sentinel-2A (Barra Bonita reservoir, Brazil). *An Acad Bras CiencAnnals of the Brazilian Academy of Sciences)*, pp.1–14.

Zeileis, A. et al., 2002. strucchange: an R package for testing for structural change. *Journal of Statistical Software*, 7(2), pp.1–38.

Zepp, R.G. et al., 2008. Spatial and temporal variability of solar ultraviolet exposure of coral assemblages in the Florida Keys: Importance of colored dissolved organic matter. *Limnology and Oceanography*, 53(5), pp.1909–1922.

Zhan, H., Shi, P. & Chen, C., 2003. Retrieval of oceanic chlorophyll concentration using support vector machines. *IEEE Transactions on Geoscience and Remote Sensing*, 41(12 PART II), pp.2947–2951.

8. Appendix

8.1 NDCI

8.1.1 Images

NDCI 05.03.2000	29.09.2000
	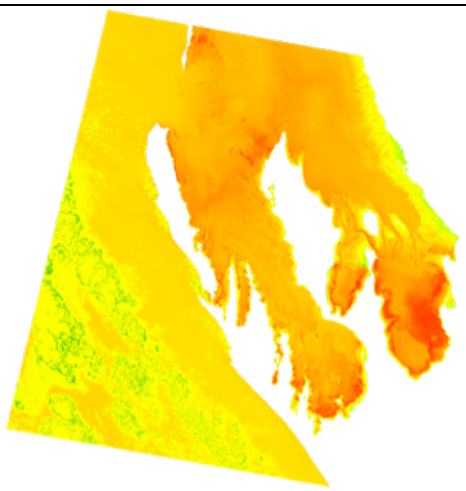
No Data	18.12.2000
24.03.2001	12.06.2001
	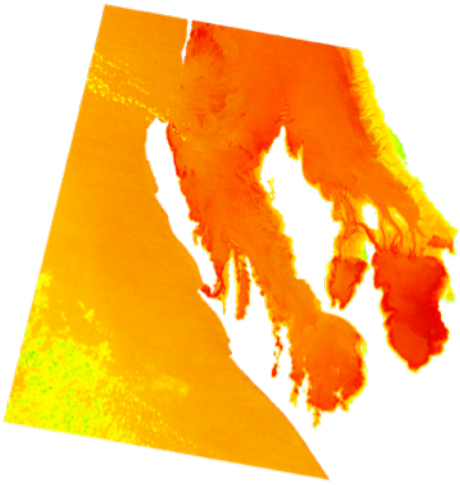

NDCI 16.09.2001	21.12.2001
11.03.2002	No Data
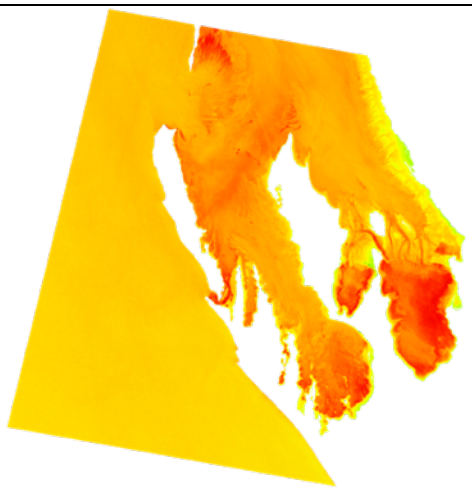	
19.09.2002	08.12.2002
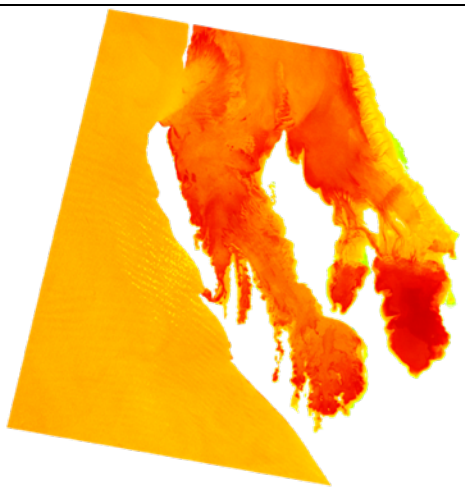	

14.03.2003	No Data
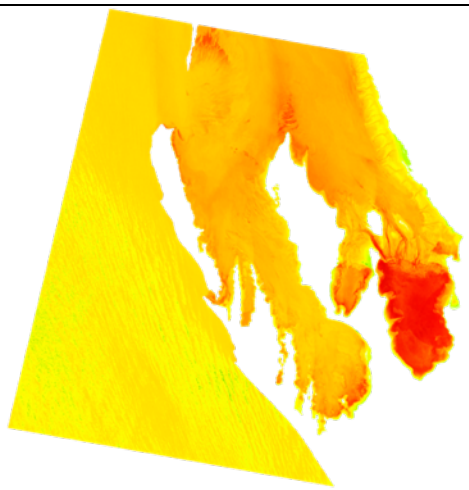	
22.09.2003 (Cloudy Sample)	11.12.2003
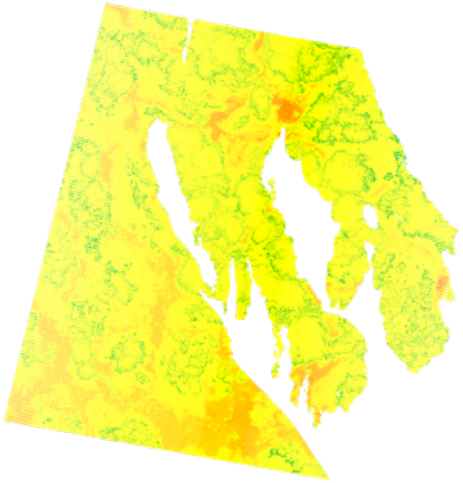	
16.03.2004	04.06.2004
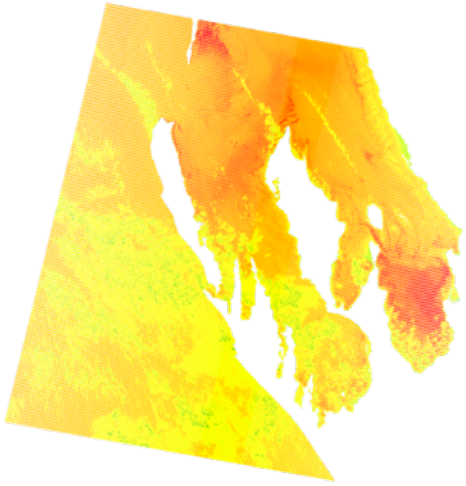	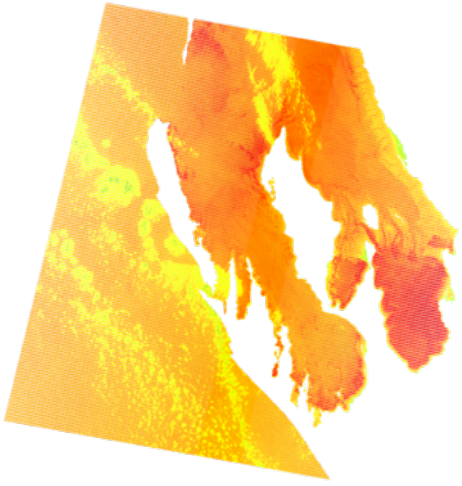

NDCI 08.09.2004	13.12.2004
19.03.2005	07.06.2005
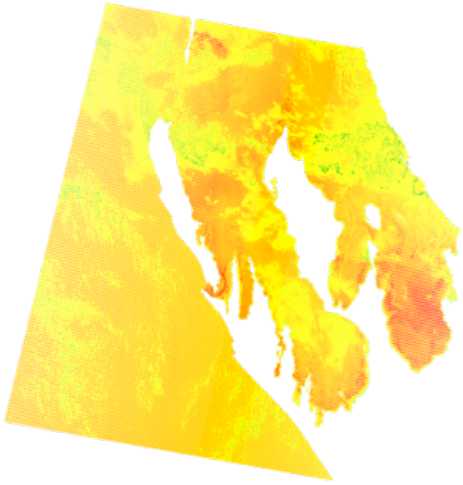	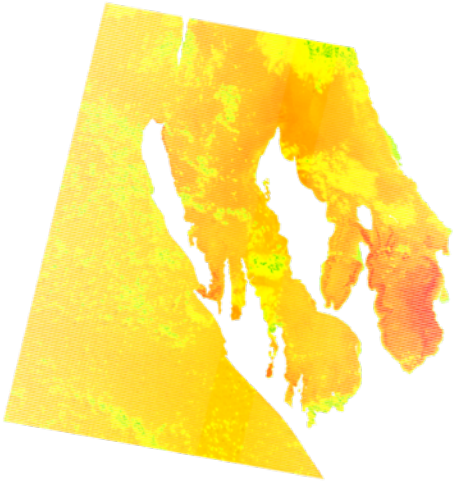
11.09.2005	16.12.2005

NDCI 06.03.2006	10.06.2006
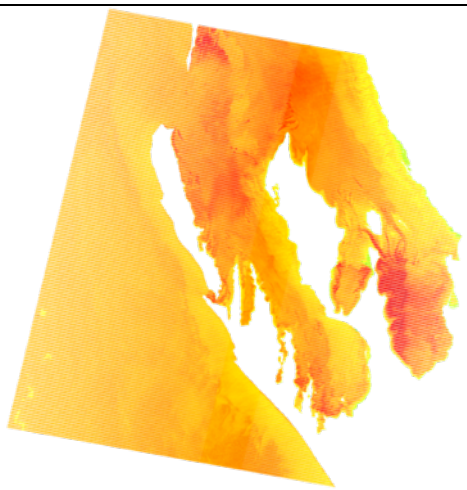	
14.09.2006	03.12.2006
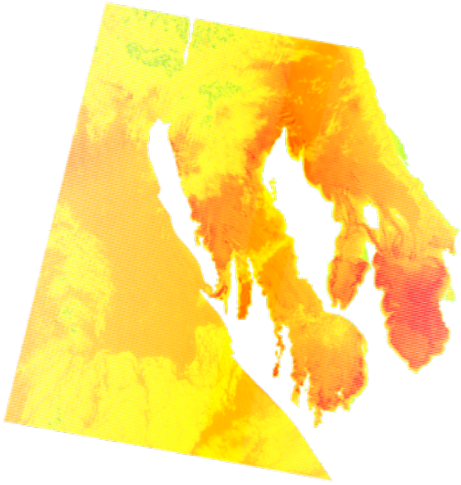	
25.03.2007	13.06.2007
	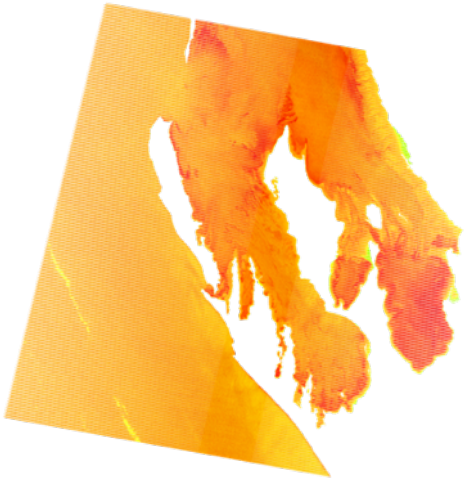

NDCI 01.09.2007	22.12.2007
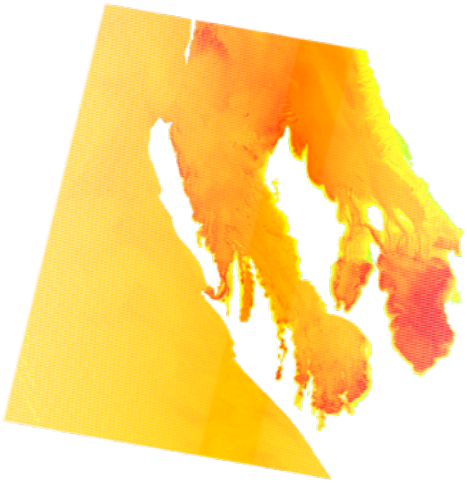	
No Data	15.06.2008
	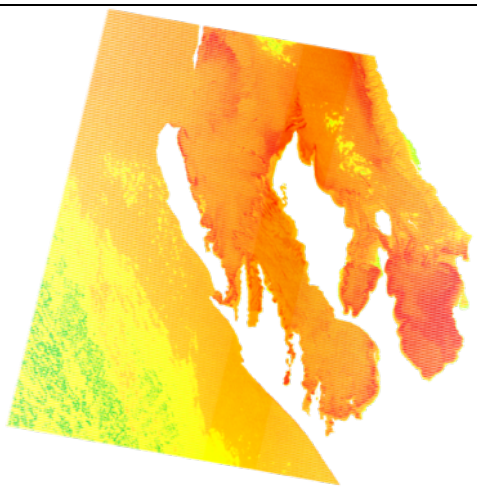
03.09.2008	24.12.2008
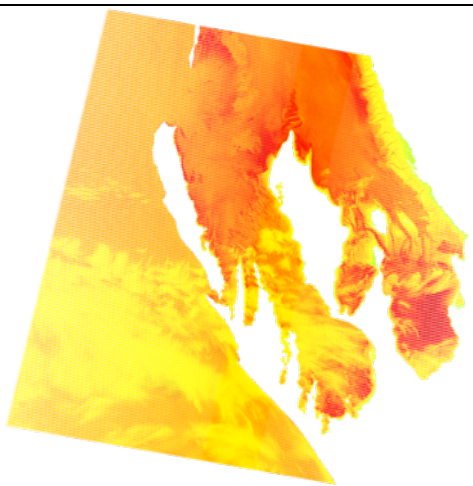	

NDCI 14.03.2009	18.06.2009
	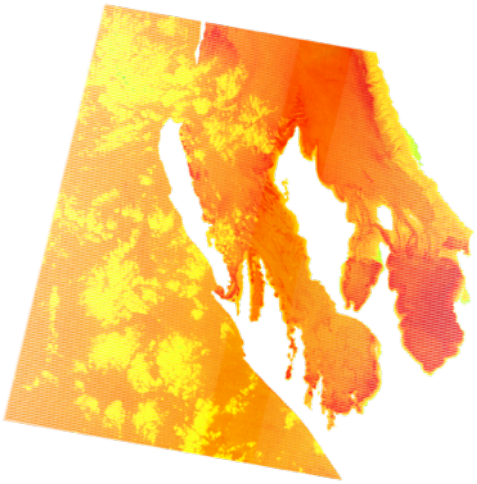
22.09.2009	11.12.2009
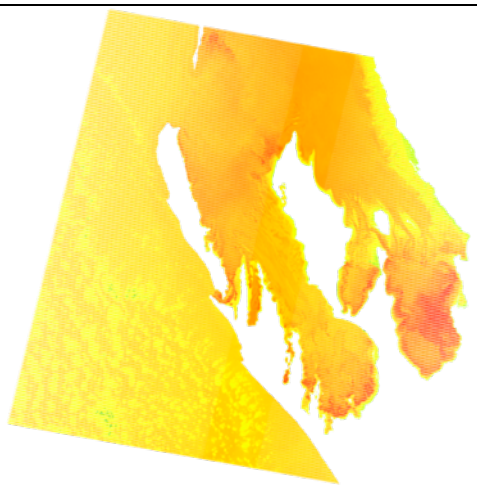	
17.03.2010	21.06.2010
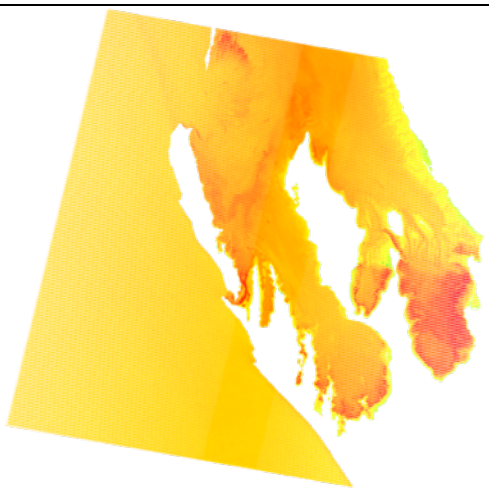	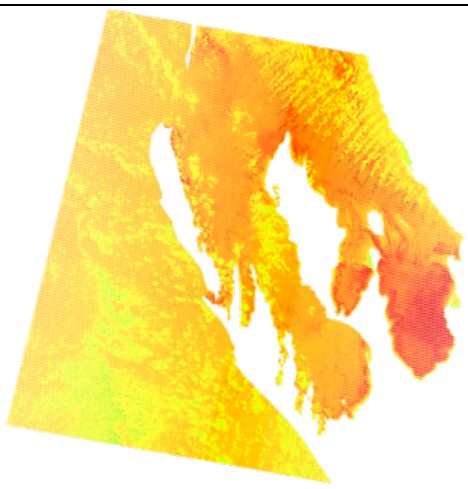

NDCI 25.09.2010	30.12.2010
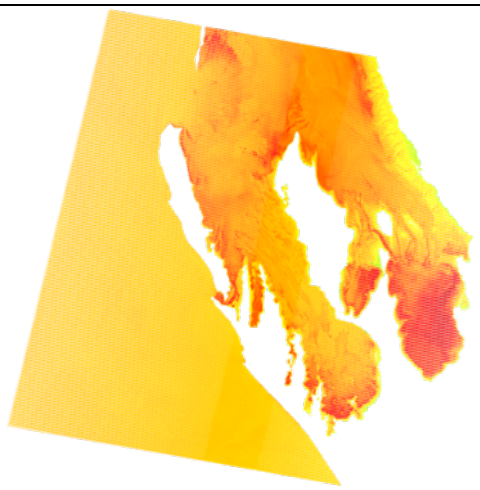	
04.03.2011	08.06.2011
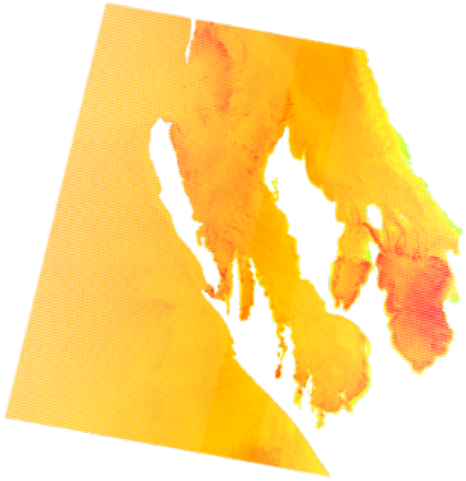	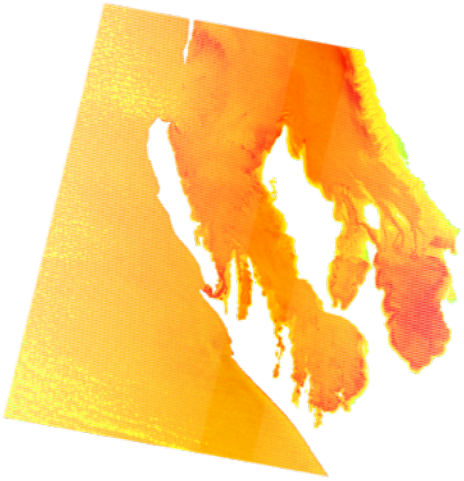
12.09.2011	01.12.2011
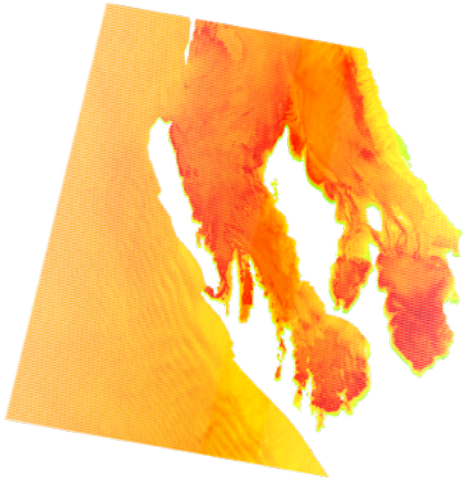	

NDCI 06.03.2012	10.06.2012
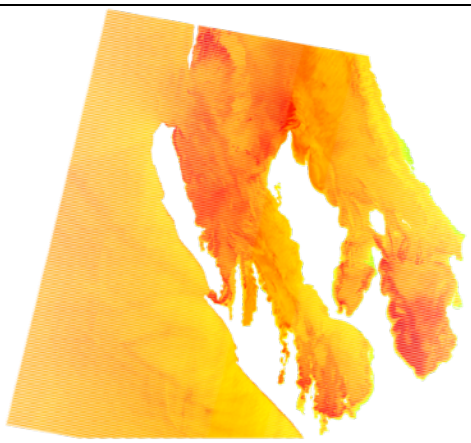	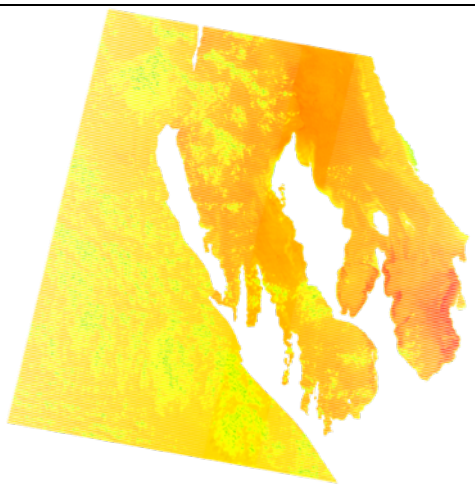
30.09.2012	03.12.2012
25.03.2013	29.06.2013
	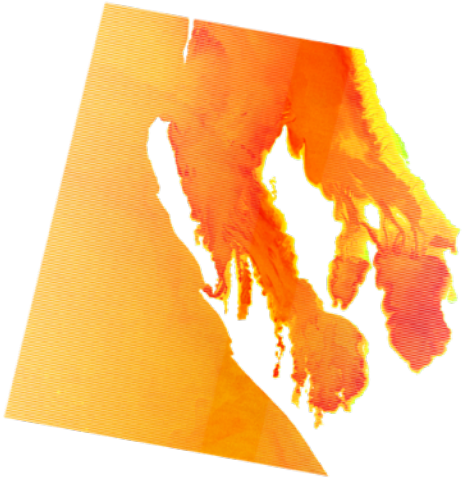

NDCI 09.09.2013 L8	22.12.2013
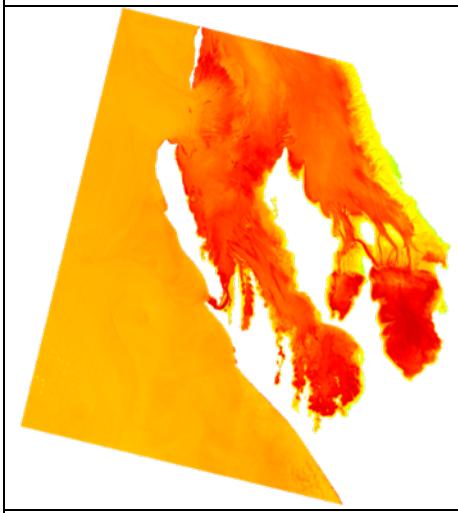	
12.03.2014 (Error in Image)	16.06.2014
	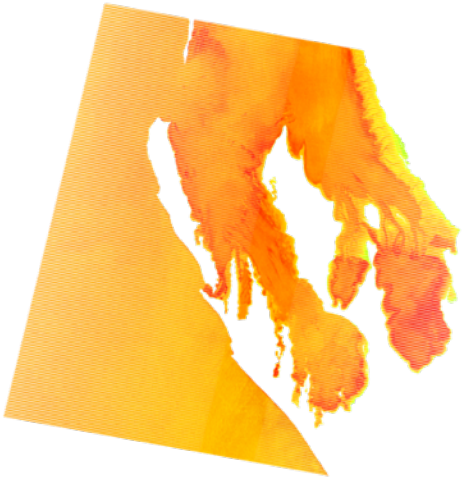
20.09.2014	25.12.2014

NDCI 15.03.2015	03.06.2015
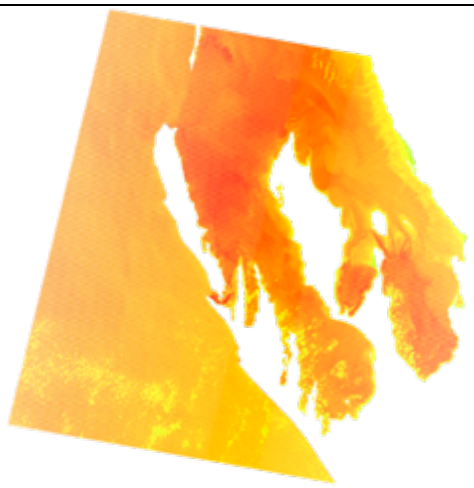	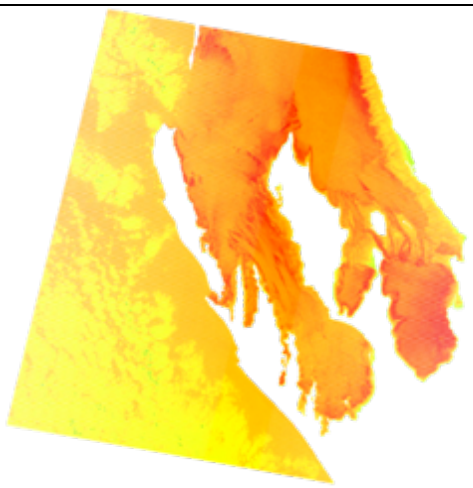
07.09.2015	12.12.2015
01.03.2016	13.06.2016 L8
	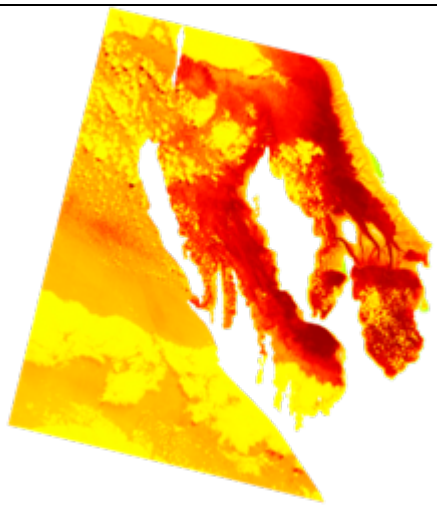

NDCI 09.09.2016	14.12.2012
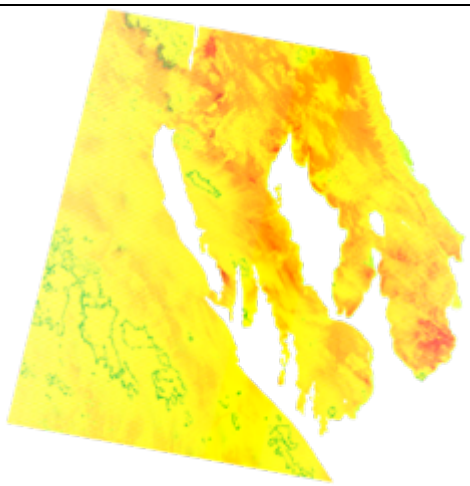	
04.03.2017	08.06.2017
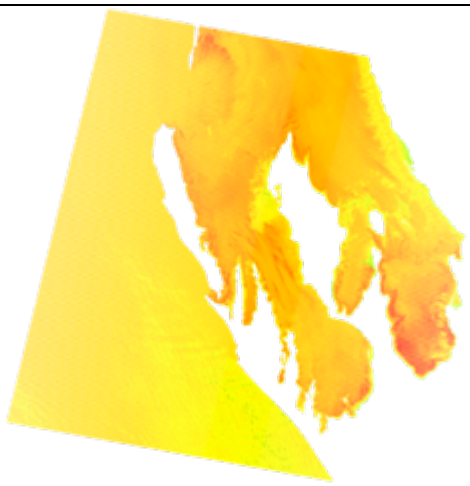	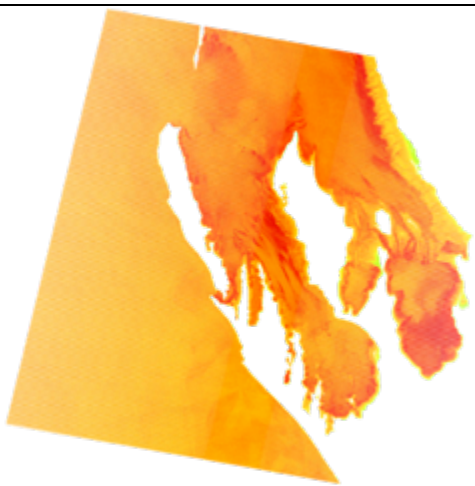
12.09.2017	01.12.2017
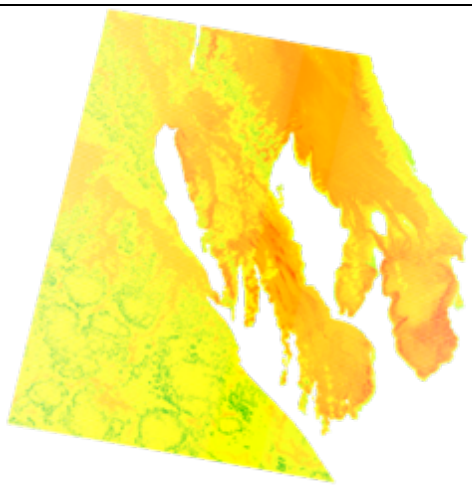	

NDCI 07.03.2018	

8.1.2 Plots

NDCI at West 1 (June)	NDCI at West 2 (June)
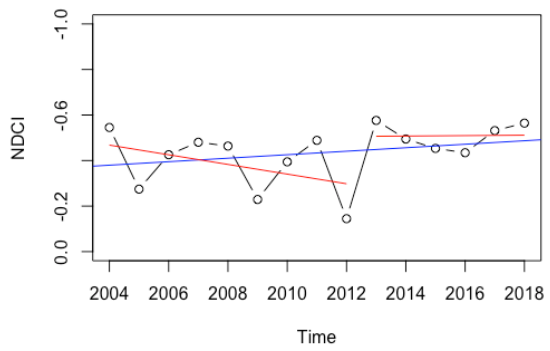	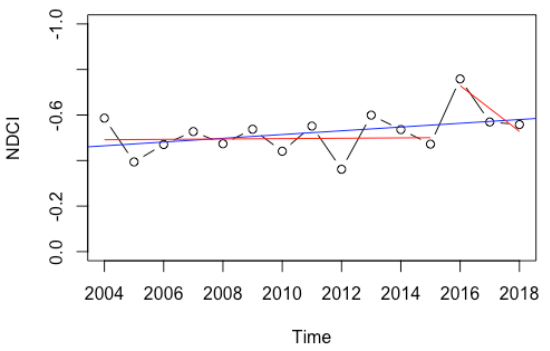
NDCI at West 3 (June)	NDCI at West 4 (June)
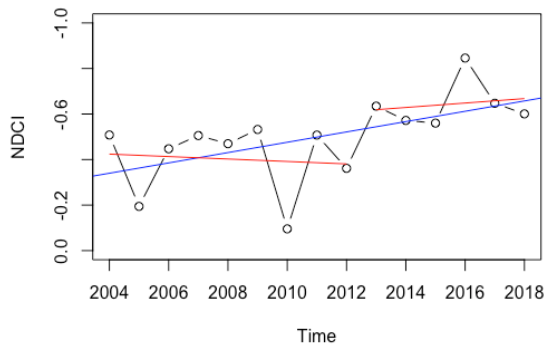	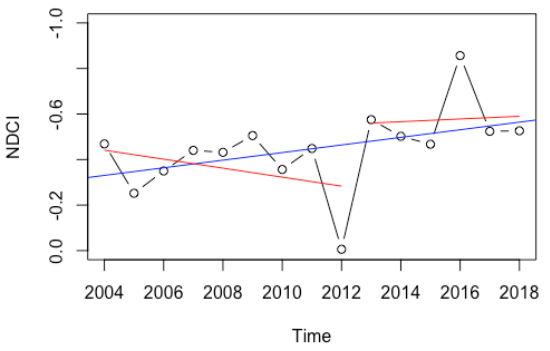
NDCI at West 5 (June)	NDCI at East 1 (June)
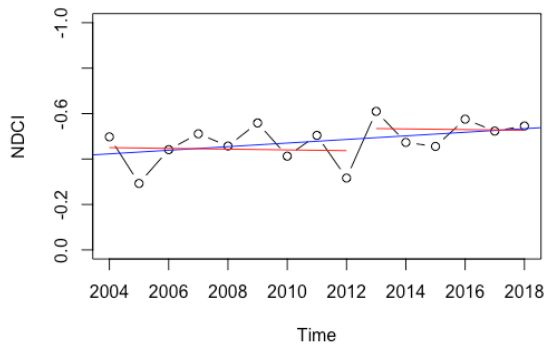	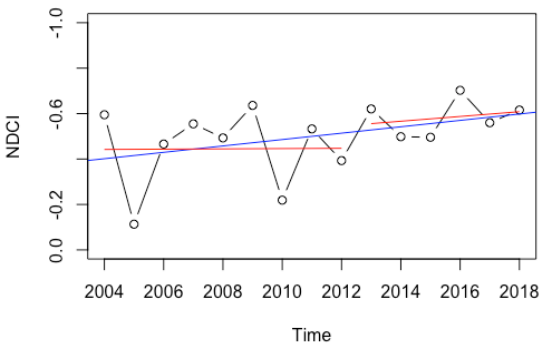

NDCI at East 2 (June)	NDCI at East 3 (June)
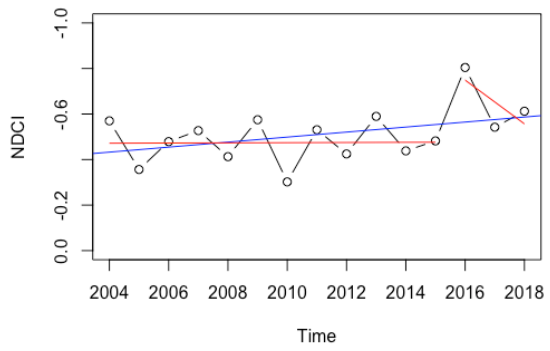	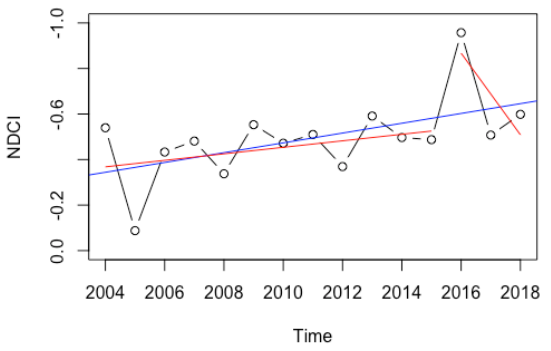
NDCI at East 4 (June)	NDCI at East 5 (June)
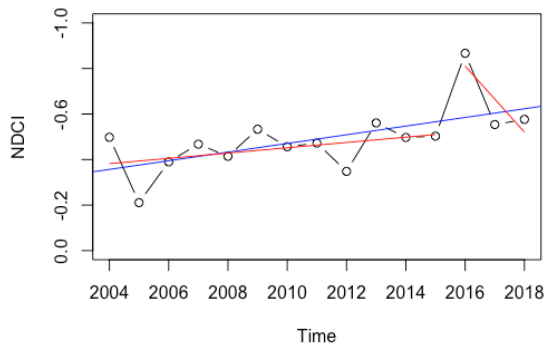	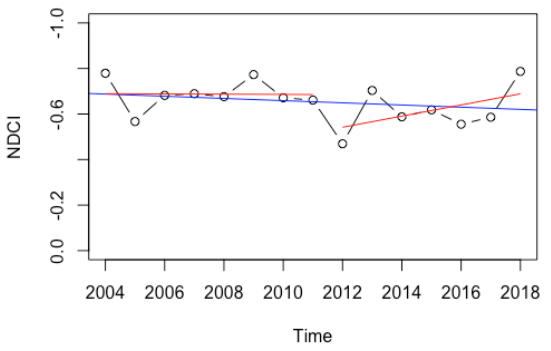

8.2 TSS

8.2.1 Images

TSS 05.03.2000	29.09.2000
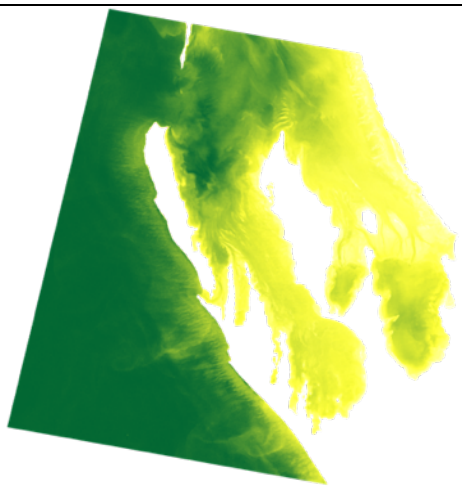	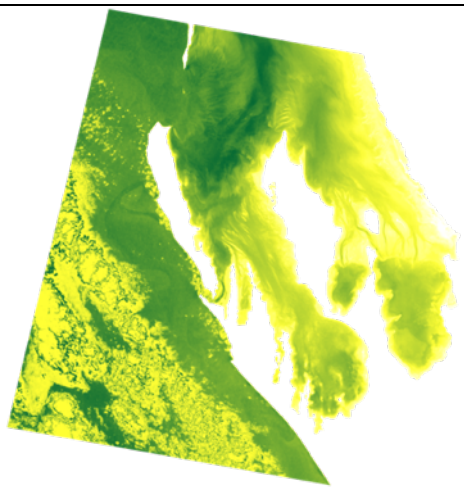
No Data	18.12.2000
	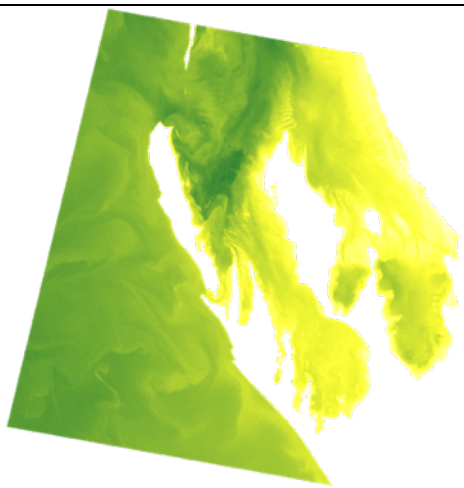
24.03.2001	12.06.2001
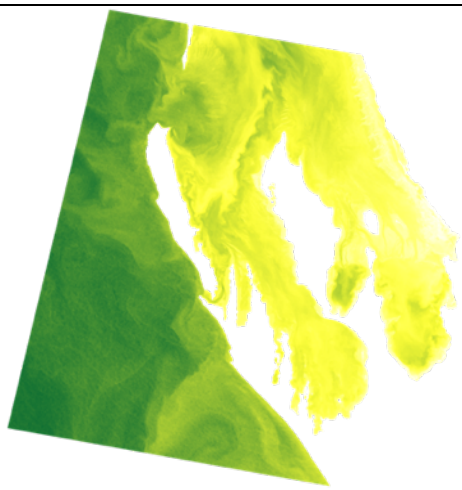	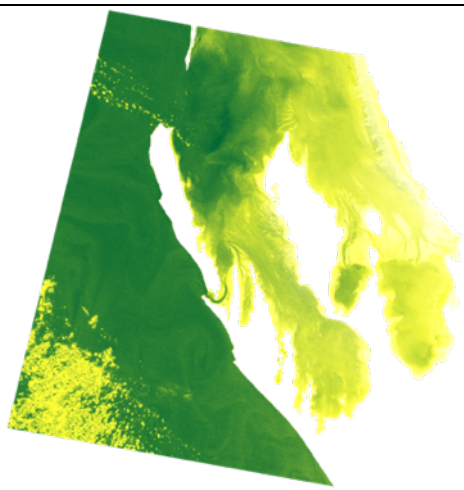

TSS 16.09.2001	21.12.2001
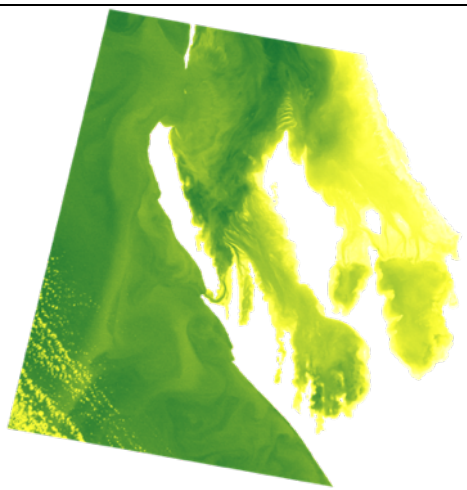	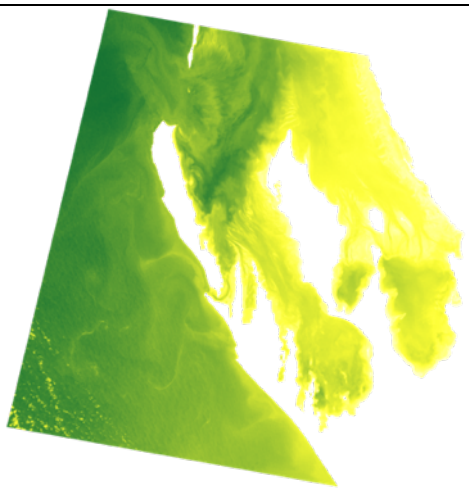
11.03.2002	No Data
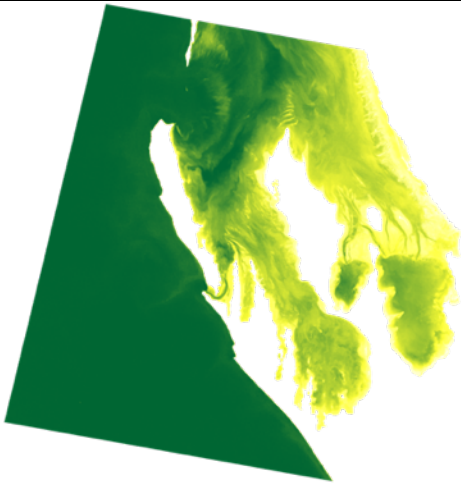	
19.09.2002	08.12.2002
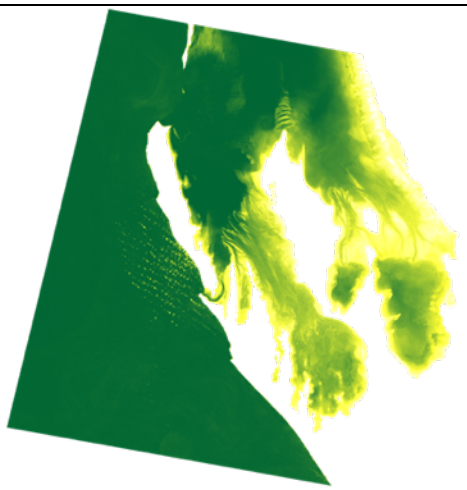	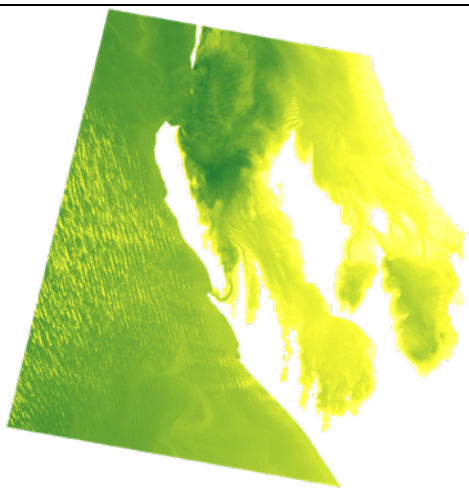

TSS 14.03.2003	No Data
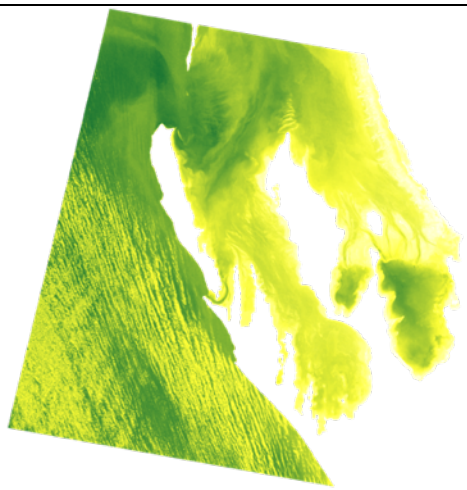	
22.09.2003 (Cloudy Sample)	11.12.2003
	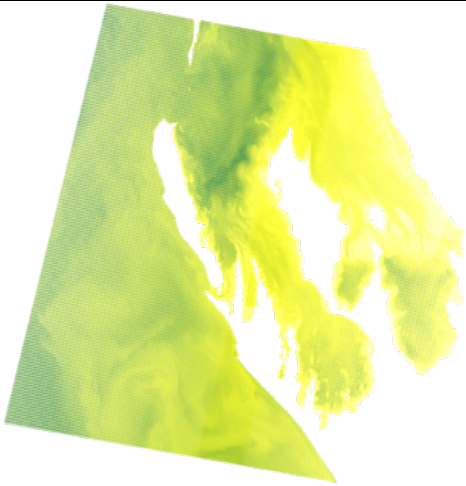
16.03.2004	04.06.2004
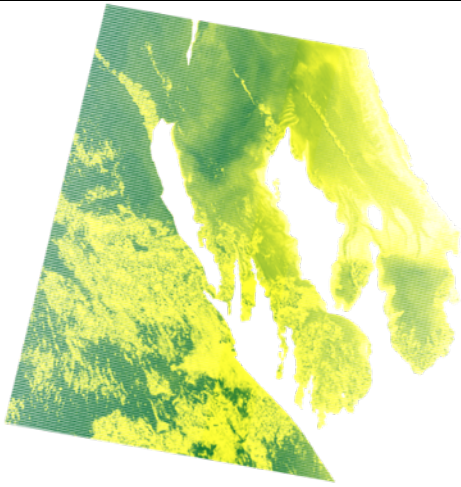	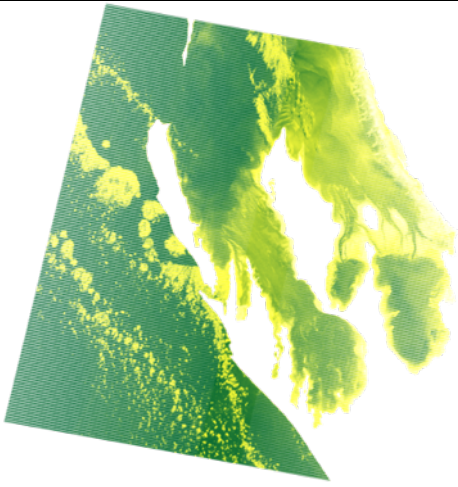

TSS 08.09.2004	13.12.2004
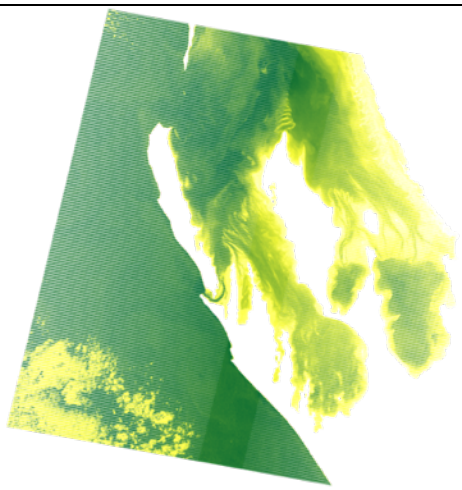	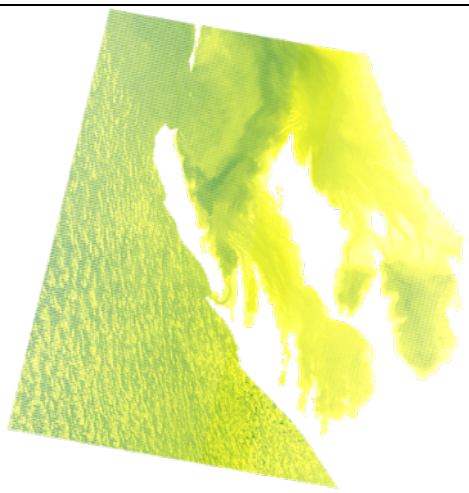
19.03.2005	07.06.2005
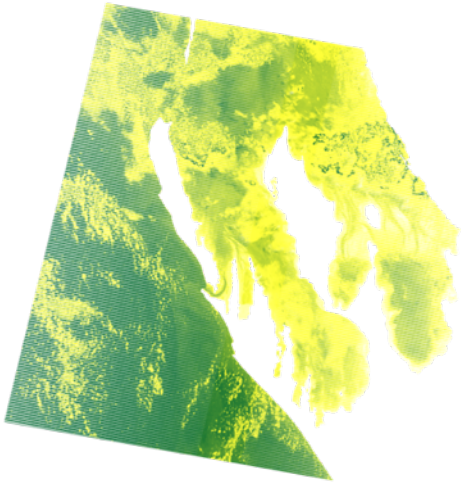	
11.09.2005	16.12.2005
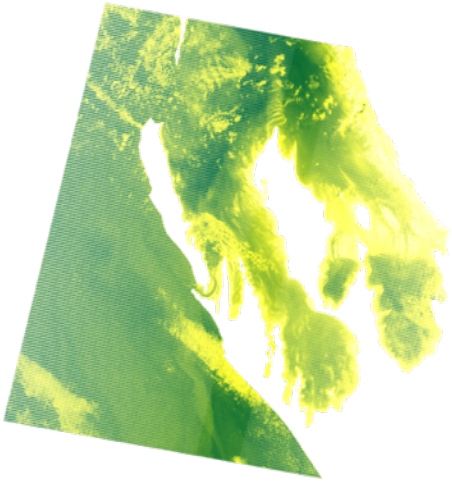	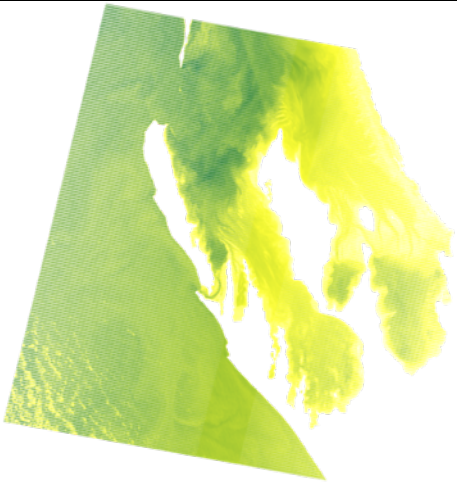

TSS 06.03.2006	10.06.2006
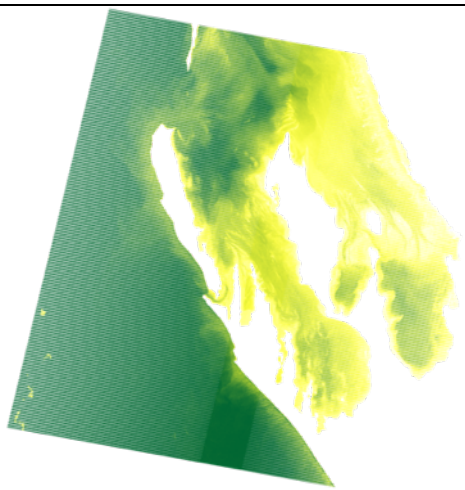	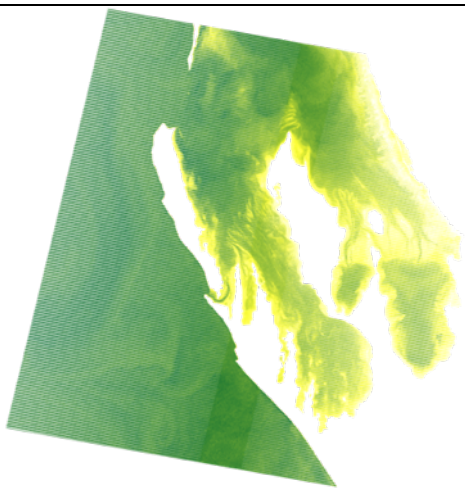
14.09.2006	03.12.2006
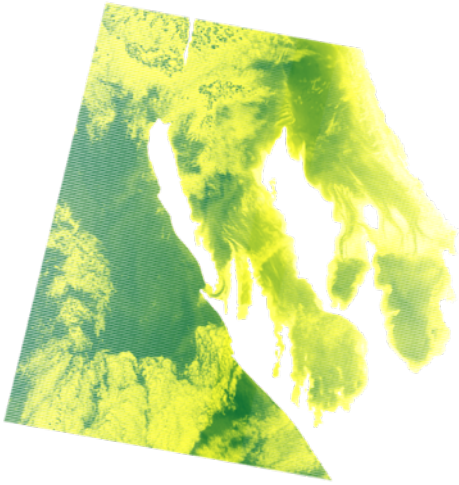	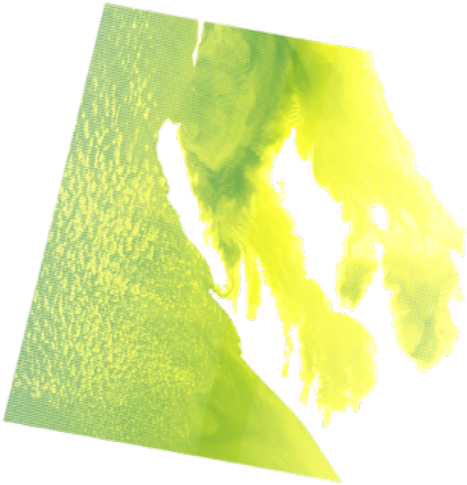
25.03.2007	13.06.2007
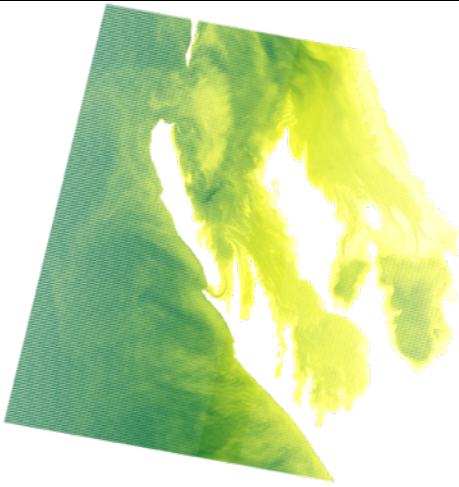	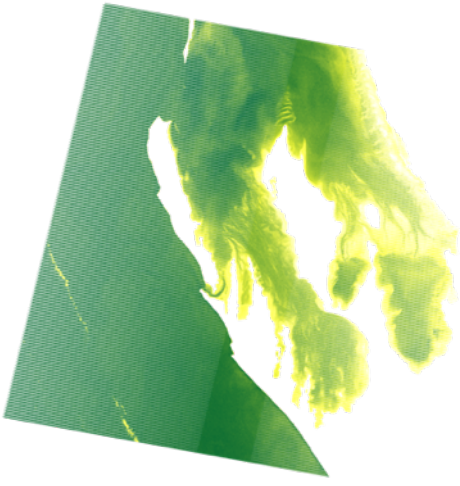

TSS 01.09.2007	22.12.2007
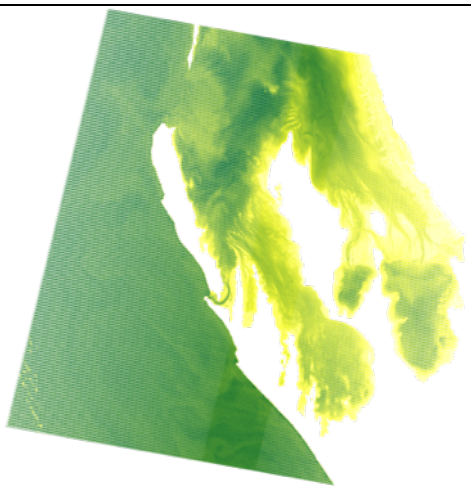	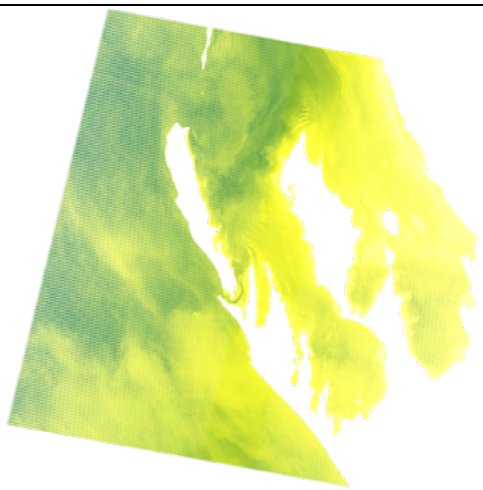
No Data	15.06.2008
	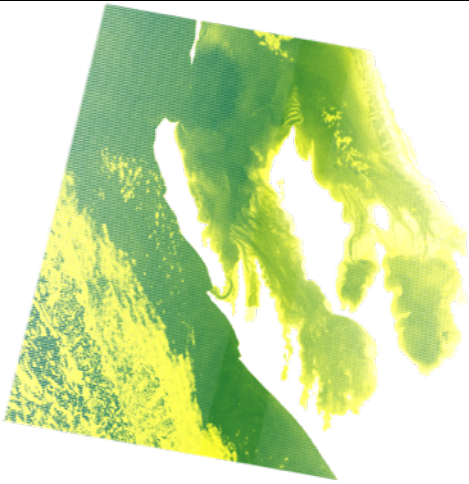
03.09.2008	24.12.2008
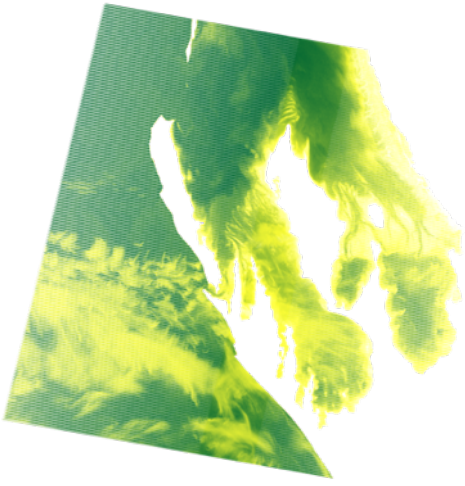	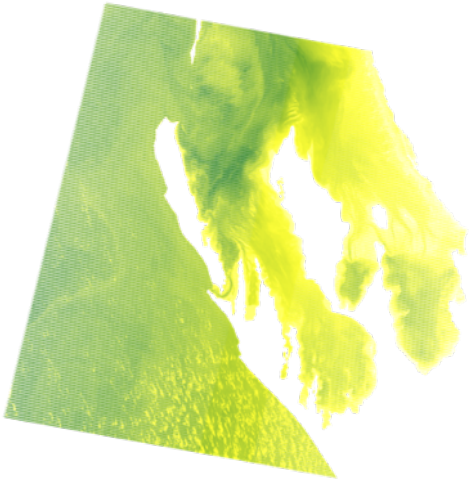

TSS 14.03.2009	18.06.2009
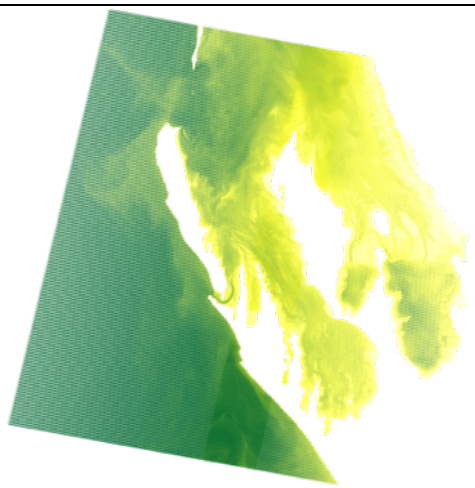	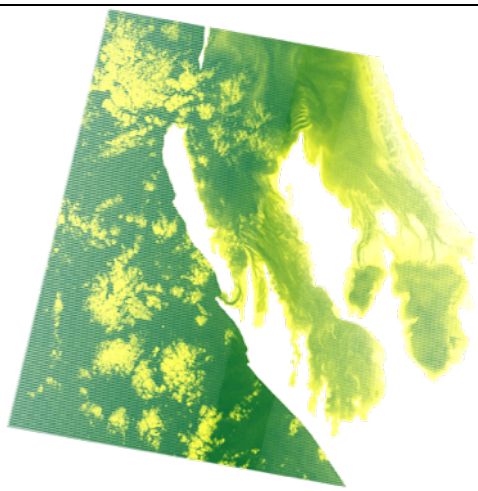
22.09.2009	11.12.2009
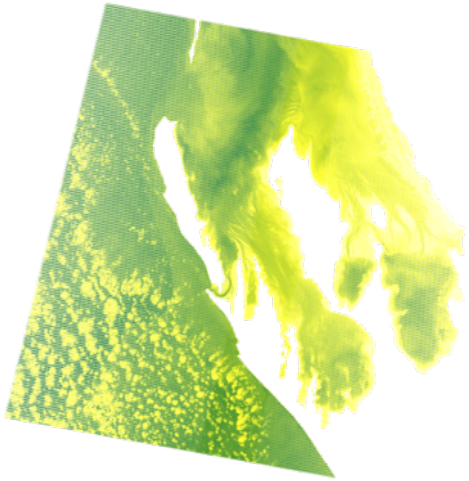	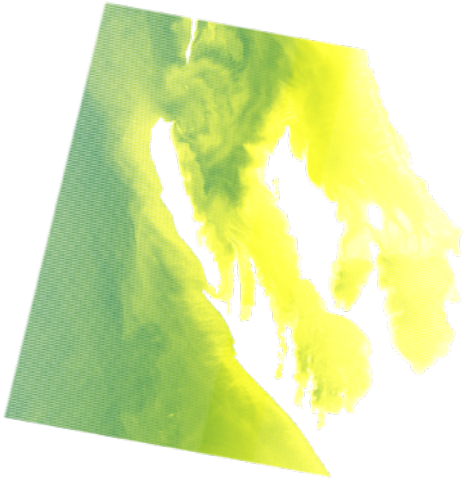
17.03.2010	21.06.2010
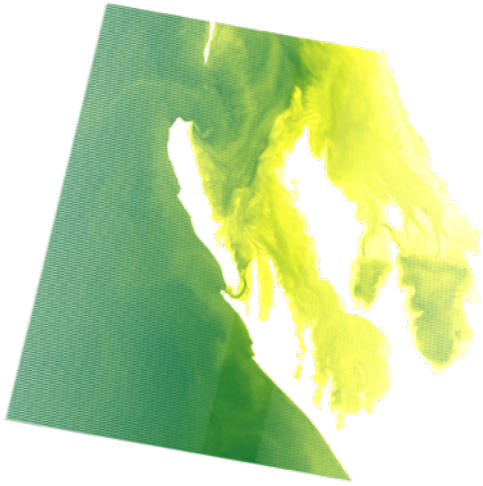	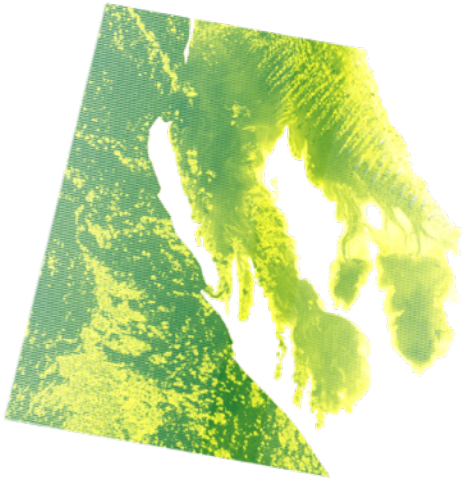

TSS 25.09.2010	30.12.2010
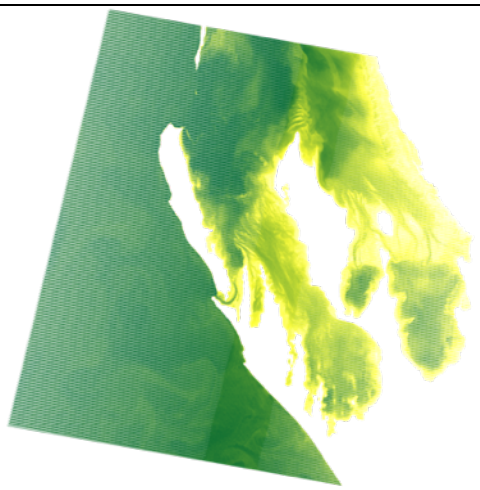	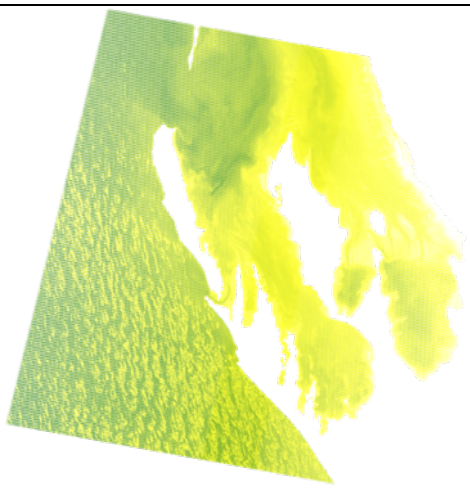
04.03.2011	08.06.2011
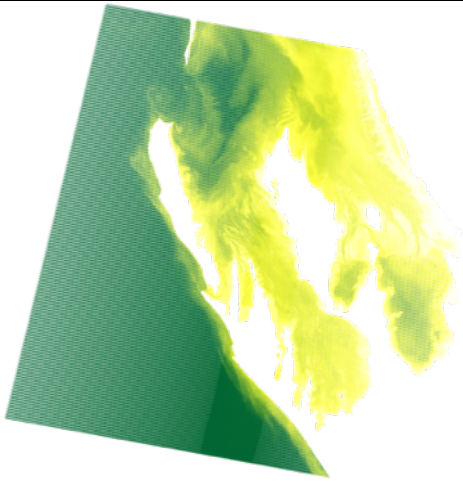	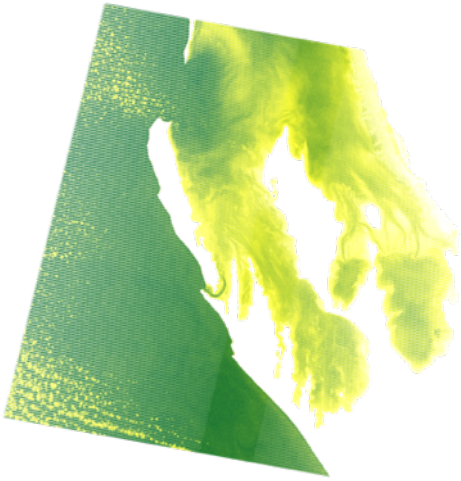
12.09.2011	01.12.2011
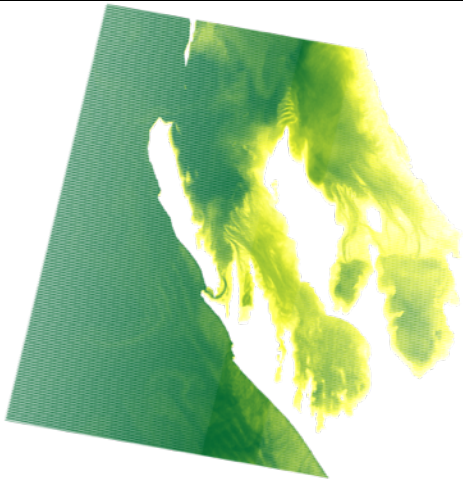	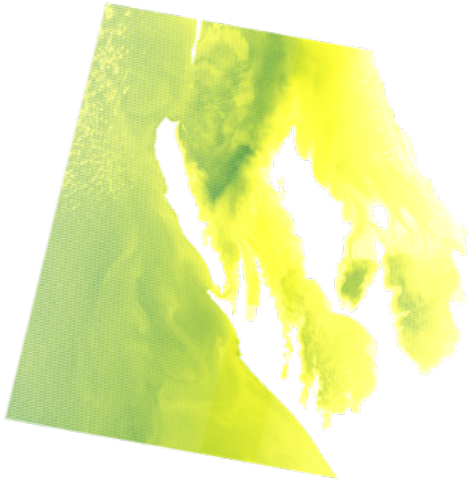

TSS 06.03.2012	10.06.2012
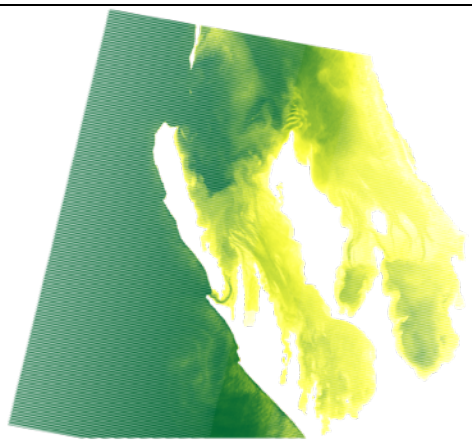	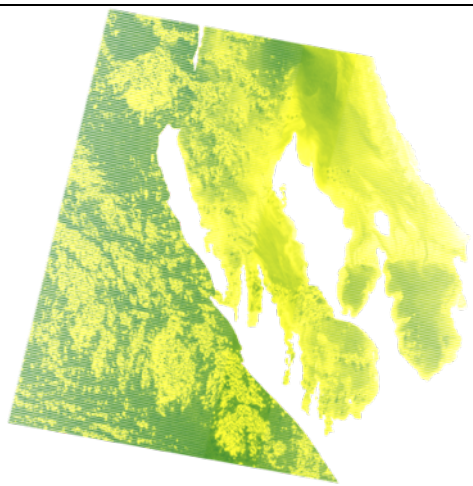
30.09.2012	03.12.2012
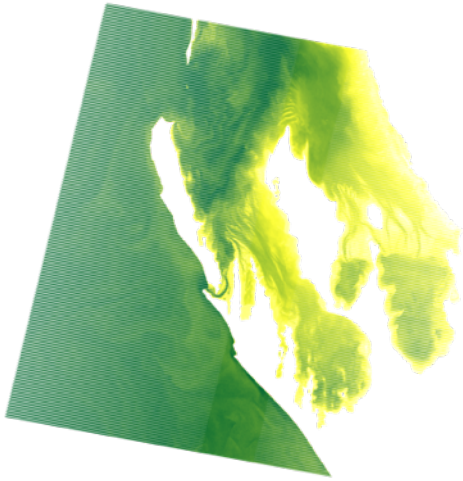	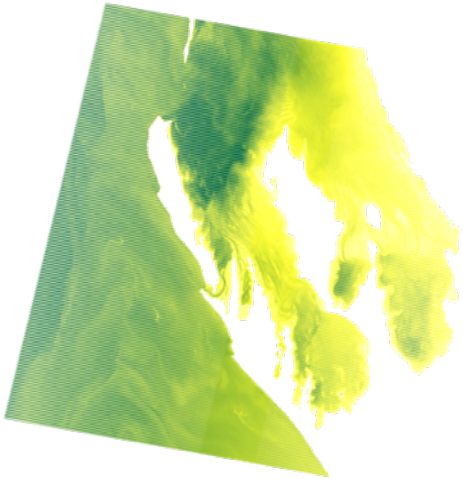
25.03.2013	29.06.2013
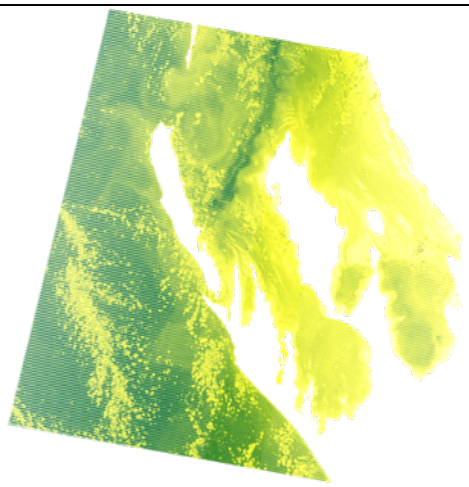	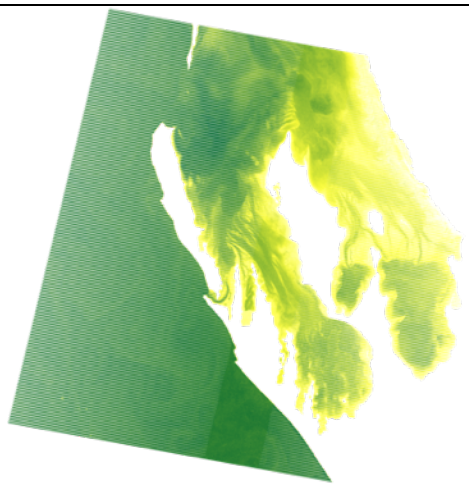

TSS 09.09.2013 L8	22.12.2013
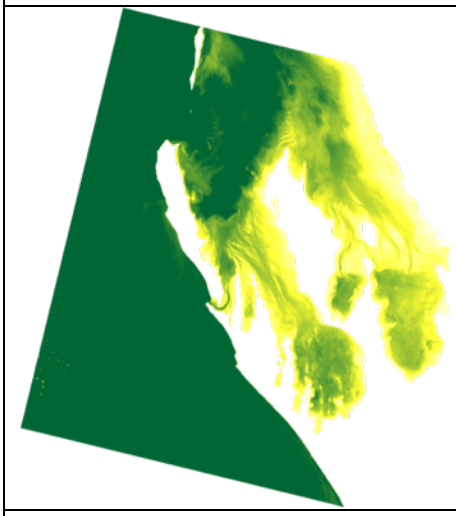	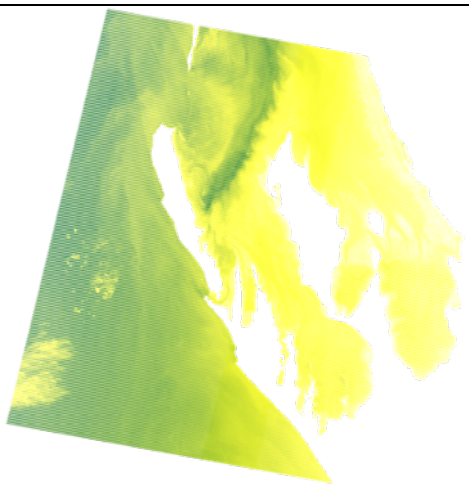
12.03.2014 (Error in Image)	16.06.2014
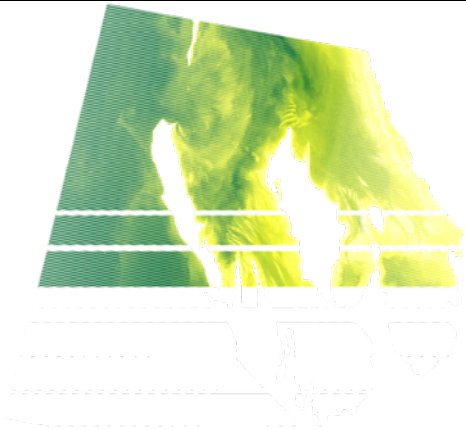	
20.09.2014	25.12.2014
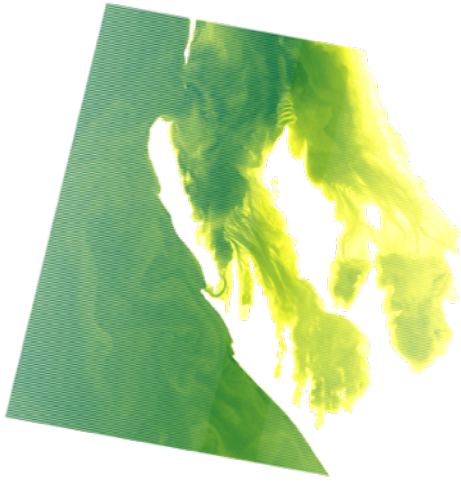	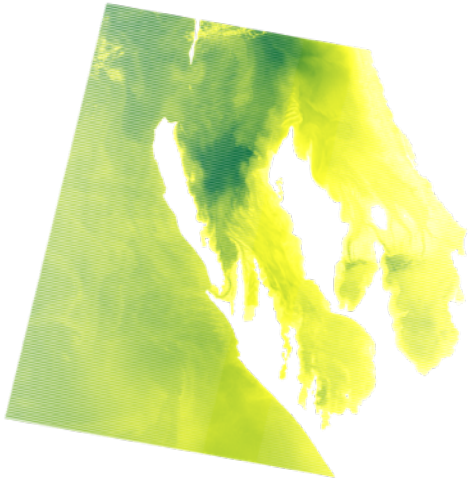

TSS 15.03.2015	03.06.2015
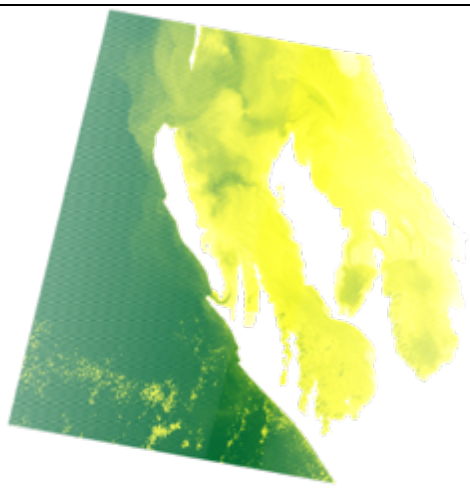	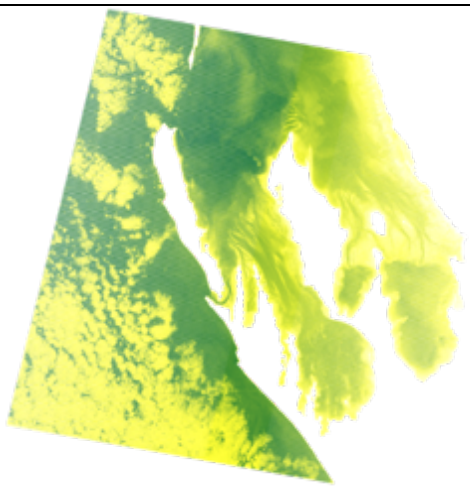
07.09.2015	12.12.2015
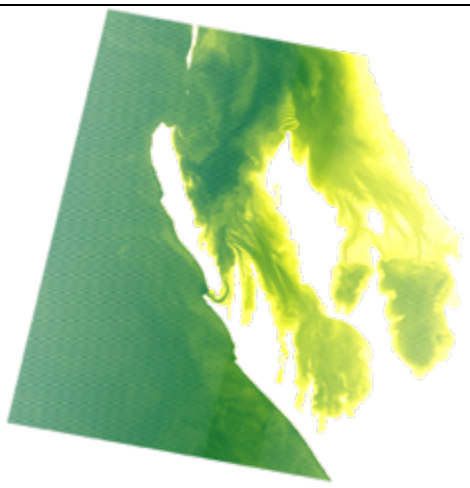	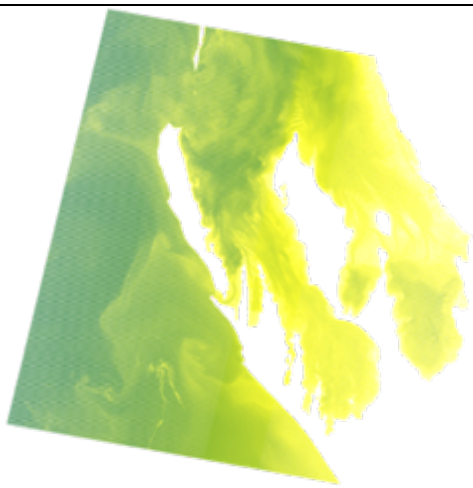
01.03.2016	13.06.2016 L8
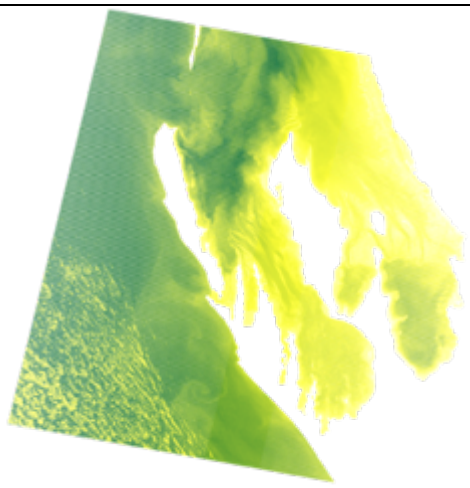	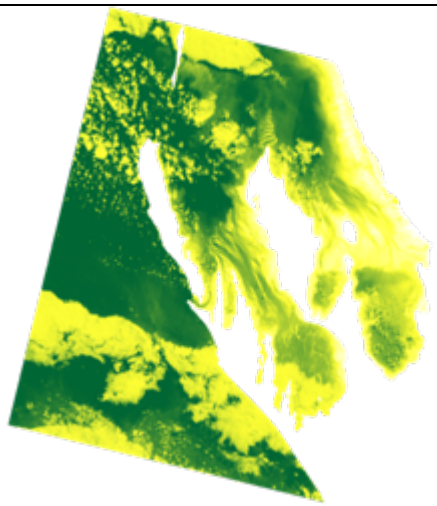

TSS 09.09.2016	14.12.2012
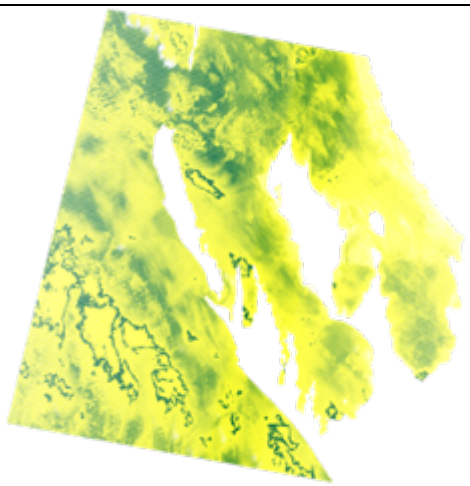	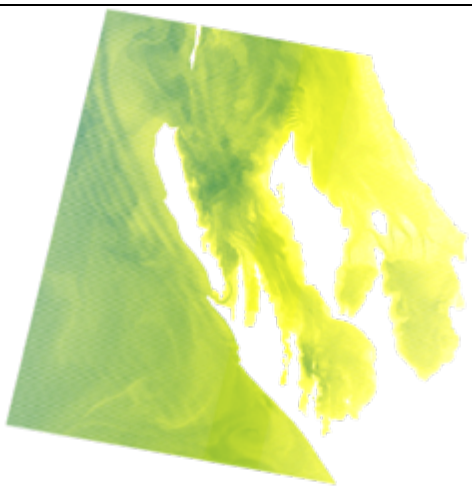
04.03.2017	08.06.2017
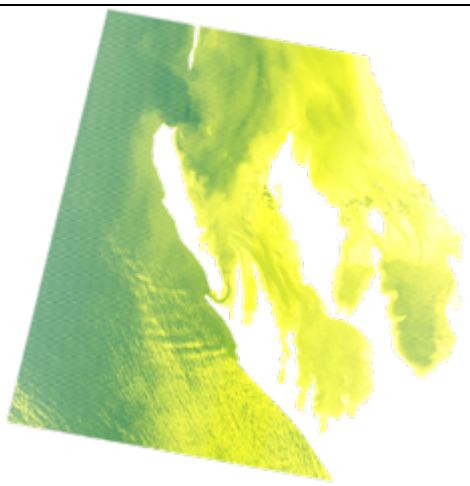	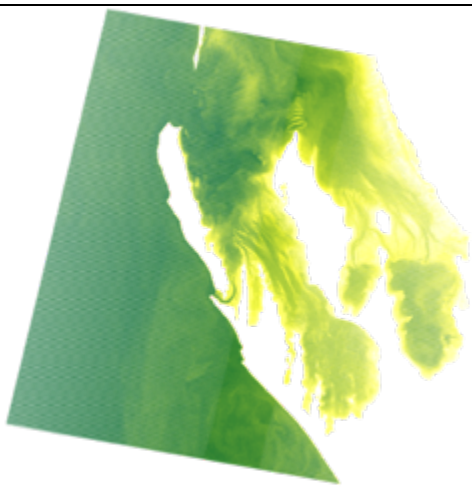
12.09.2017	01.12.2017
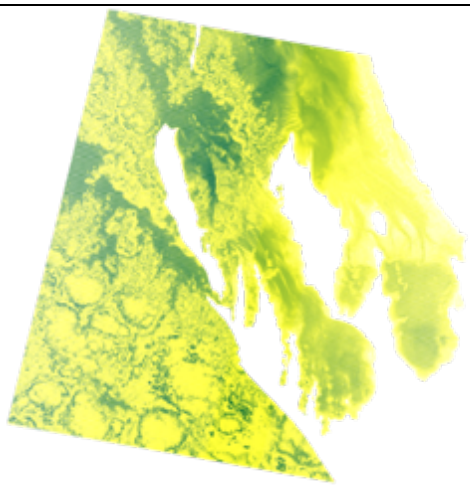	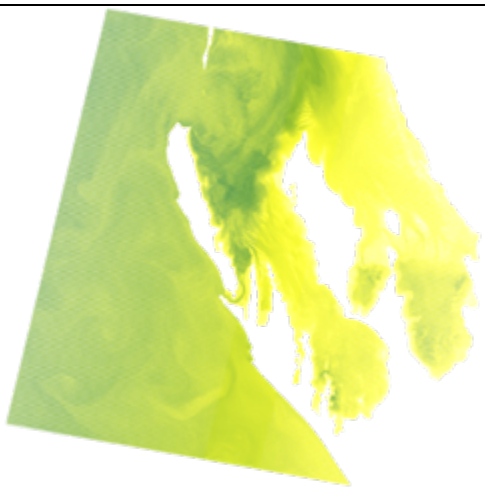

TSS 07.03.2018	
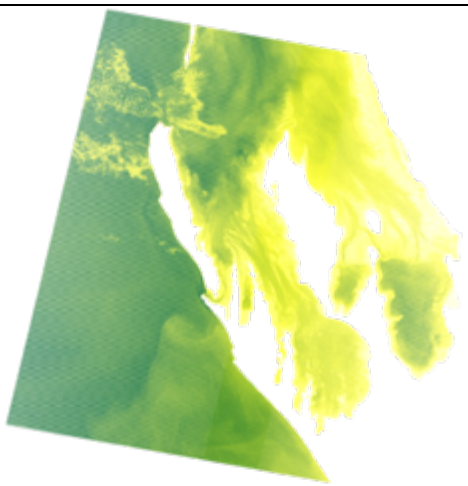	

8.2.2 Plots

TSS at West 1 (June)	TSS at West 2 (June)
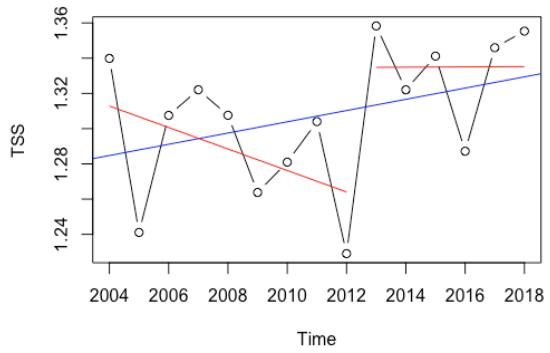	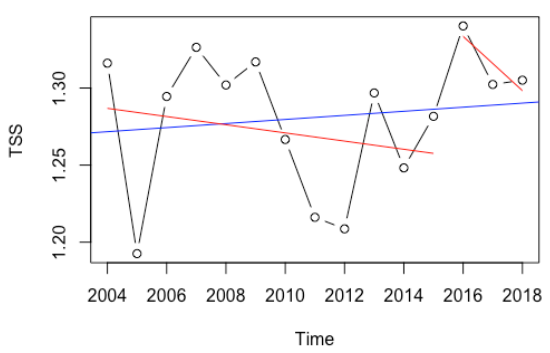
TSS at West 3 (June)	**TSS at West 4 (June)**
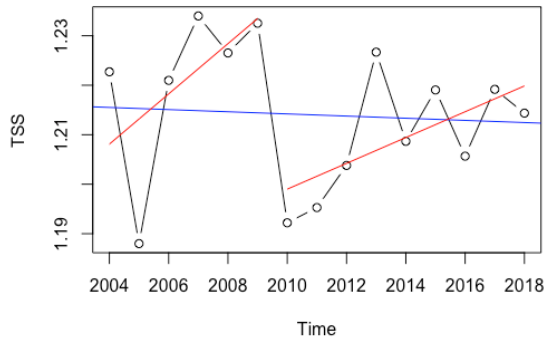	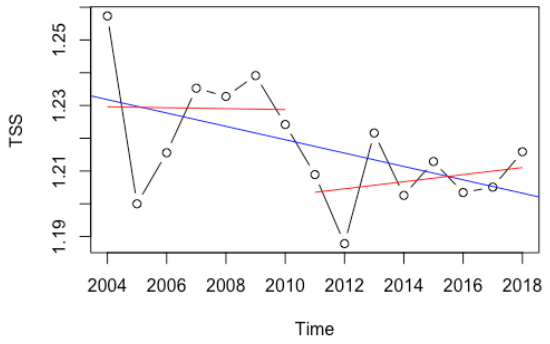
TSS at West 5 (June)	**TSS at East 1 (June)**
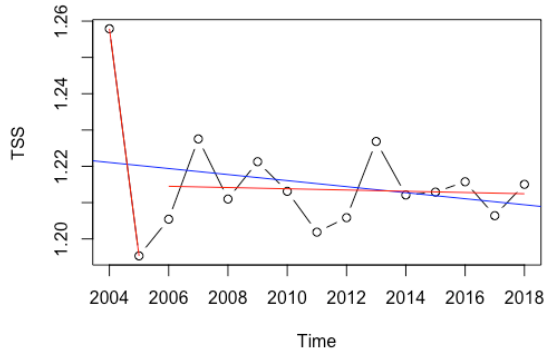	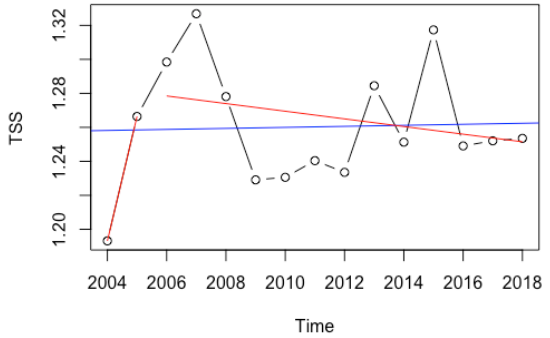

TSS at East 2 (June)	TSS at East 3 (June)
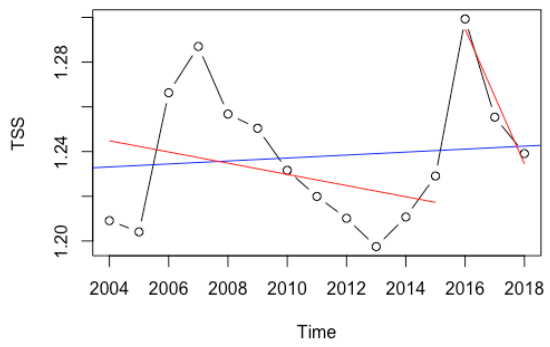	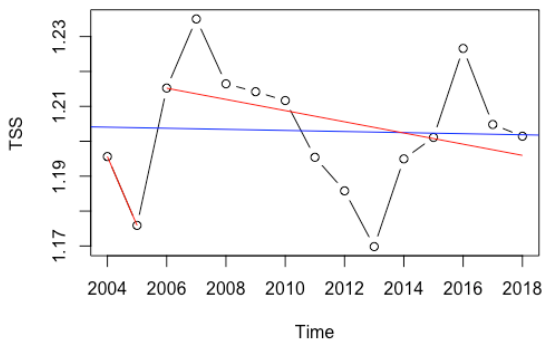
TSS at East 4 (June)	TSS at East 5 (June)
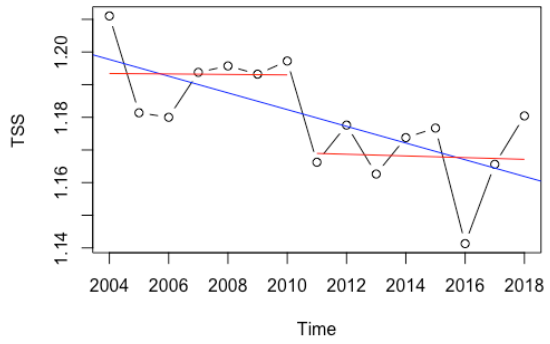	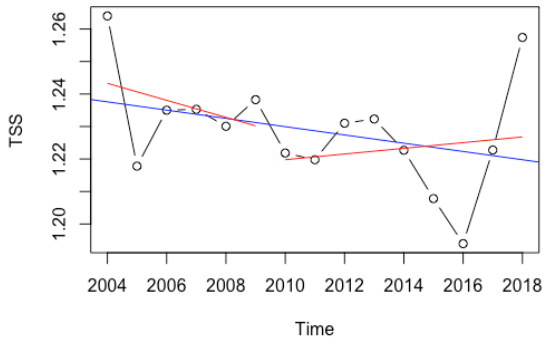

8.3 CDOM

8.3.1 Images

CDOM 05.03.2000	29.09.2000
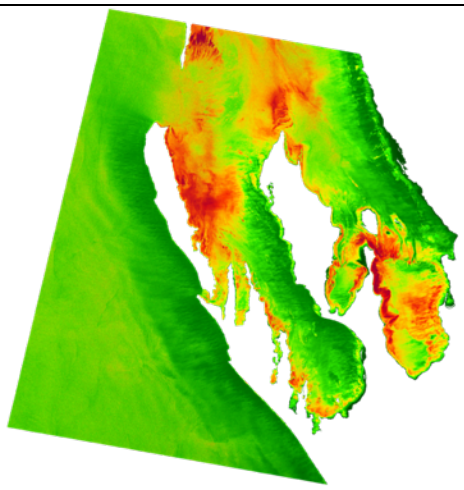	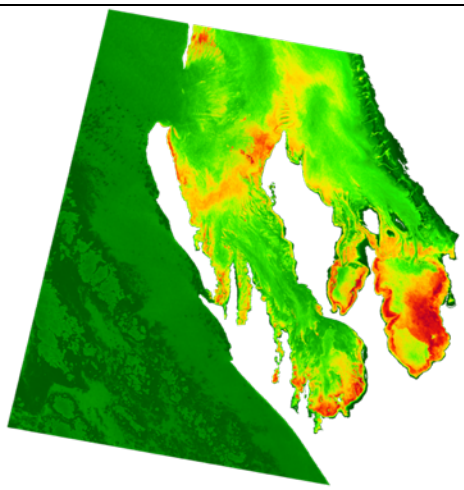
No Data	18.12.2000
	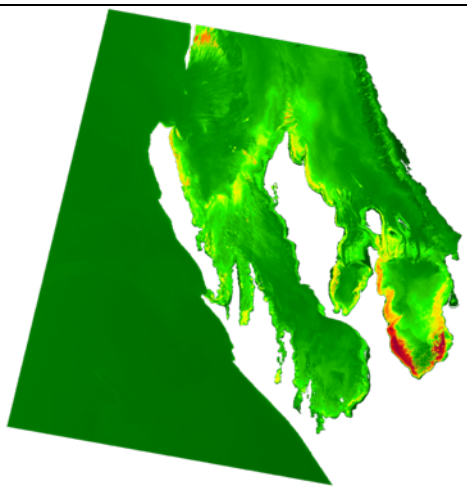
24.03.2001	12.06.2001
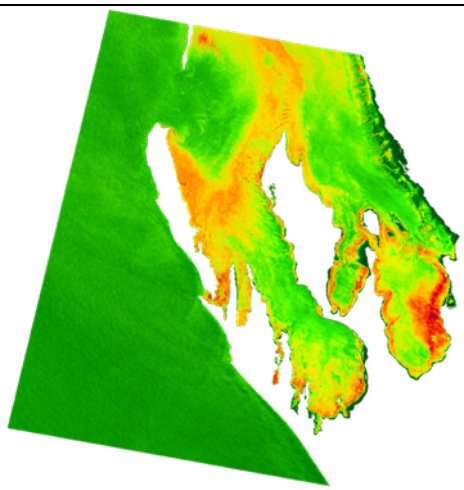	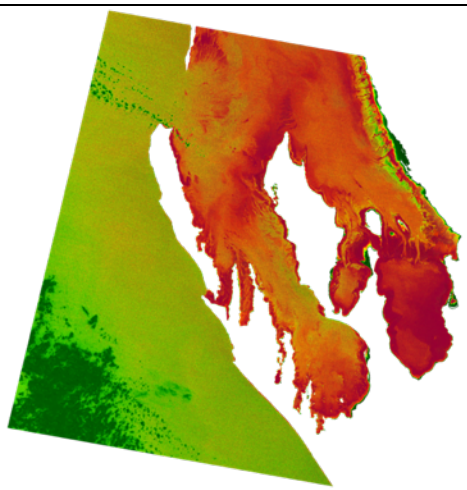

CDOM 16.09.2001	21.12.2001
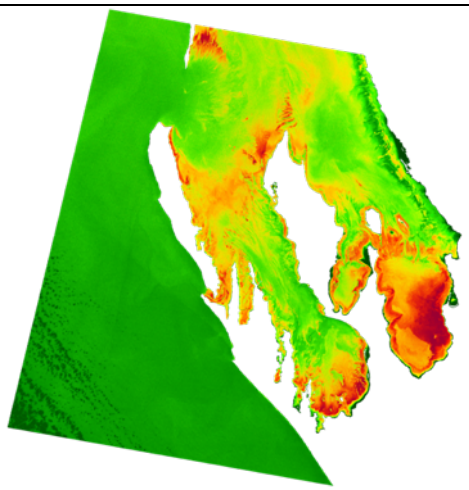	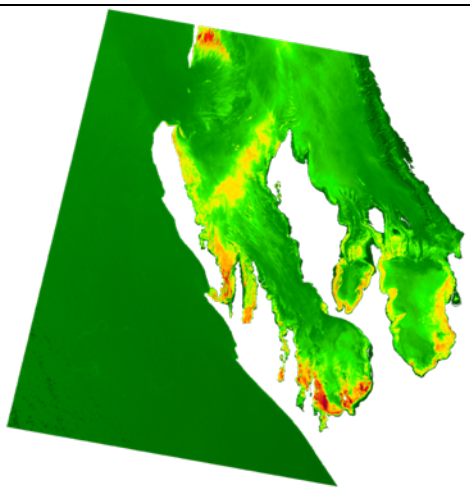
11.03.2002	No Data
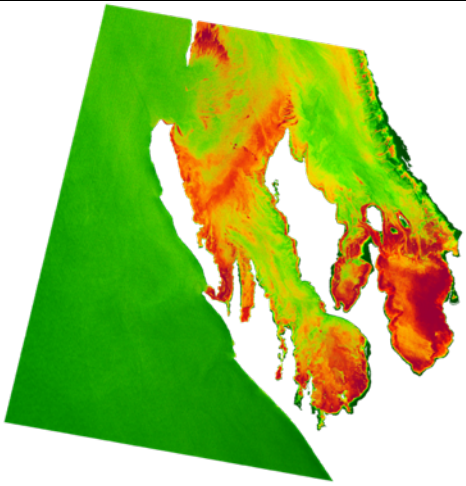	
19.09.2002	08.12.2002
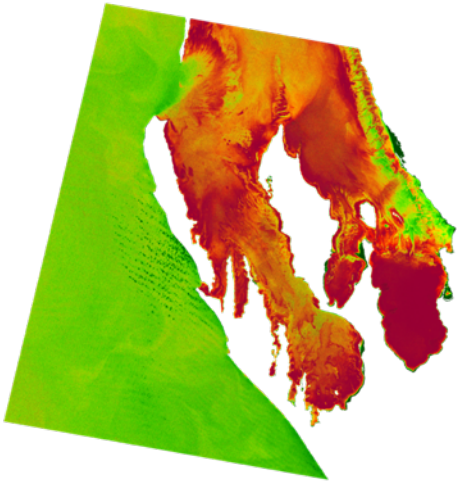	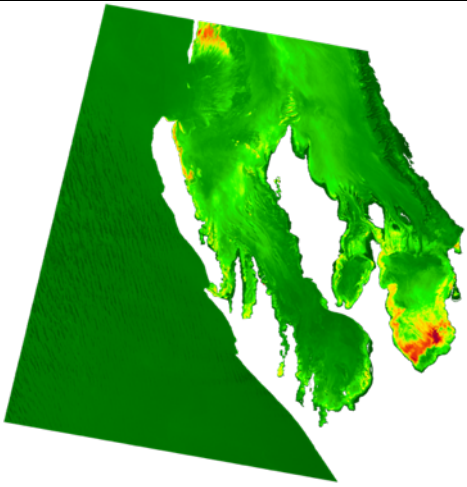

CDOM 14.03.2003	No Data
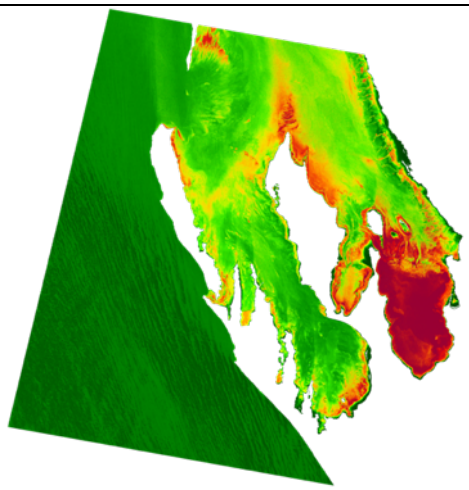	
22.09.2003 (Cloudy Sample)	11.12.2003
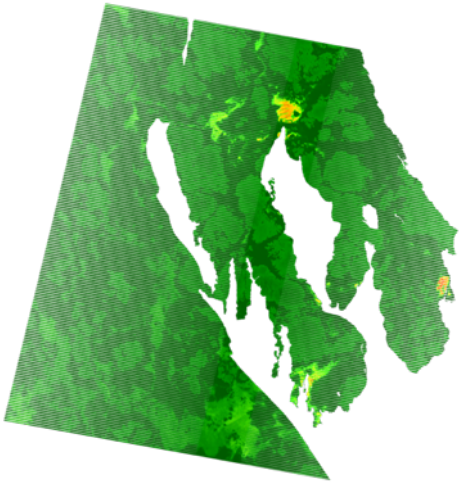	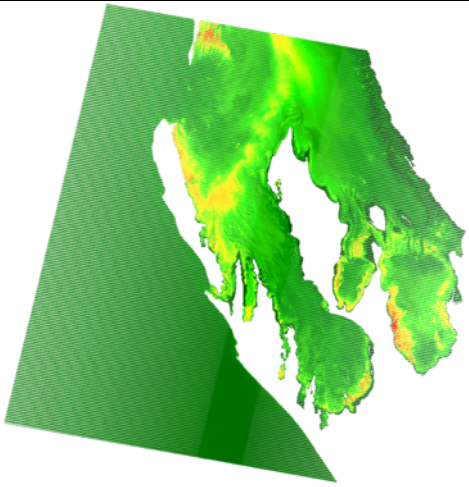
16.03.2004	04.06.2004
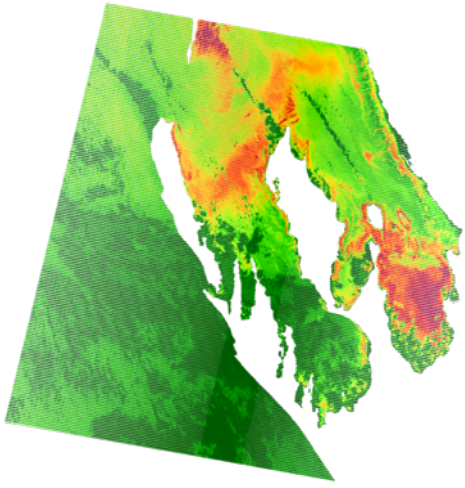	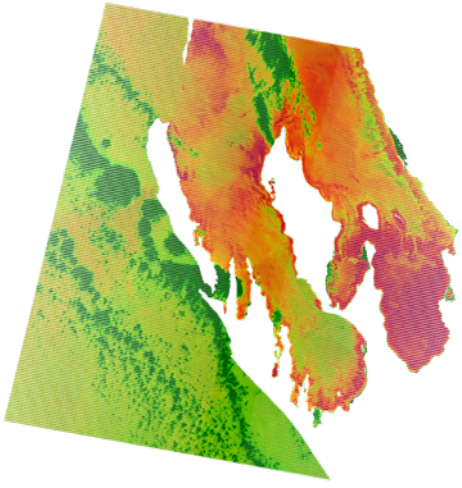

CDOM 08.09.2004	13.12.2004
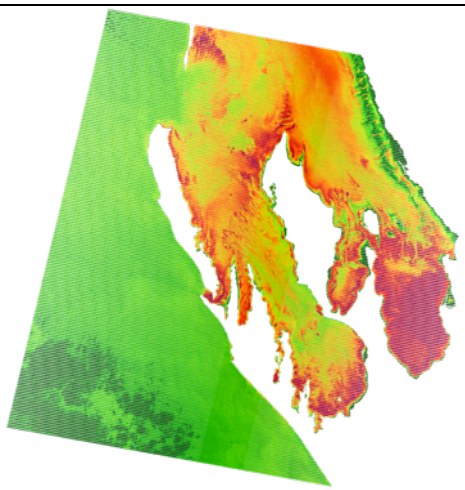	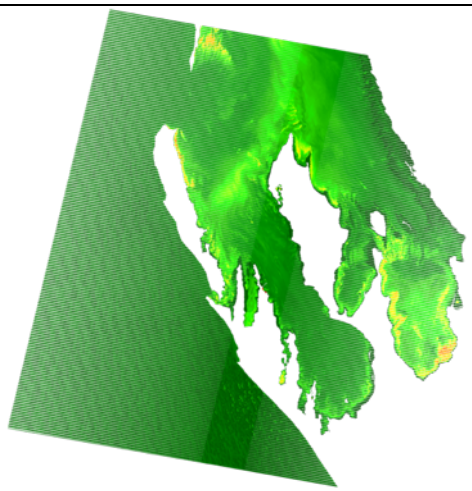
19.03.2005	07.06.2005
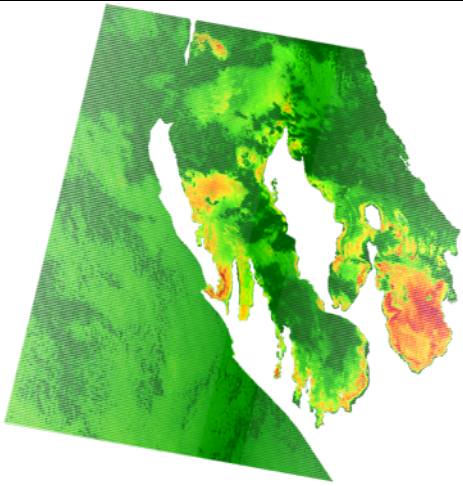	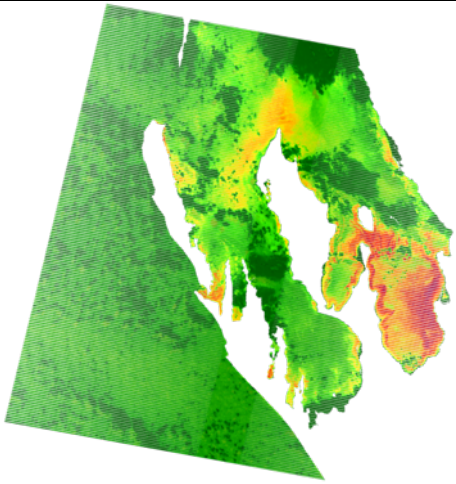
11.09.2005	16.12.2005
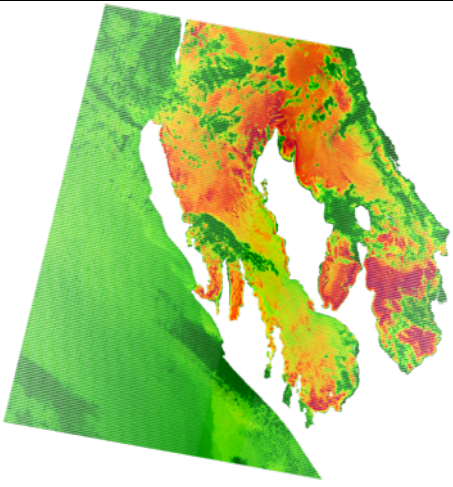	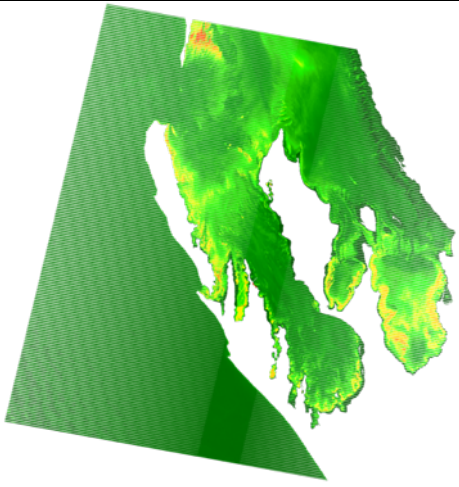

CDOM 06.03.2006	10.06.2006
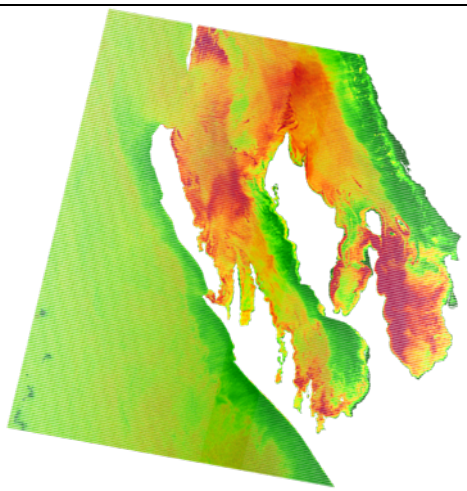	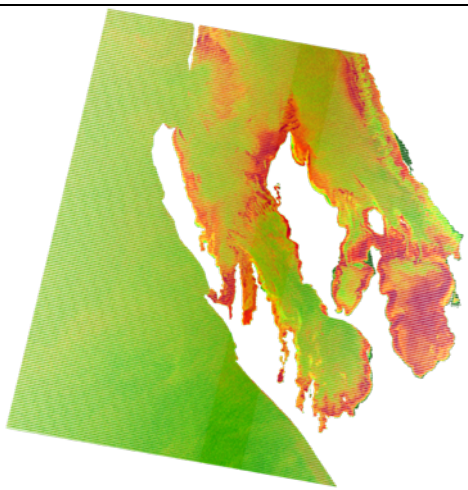
14.09.2006	03.12.2006
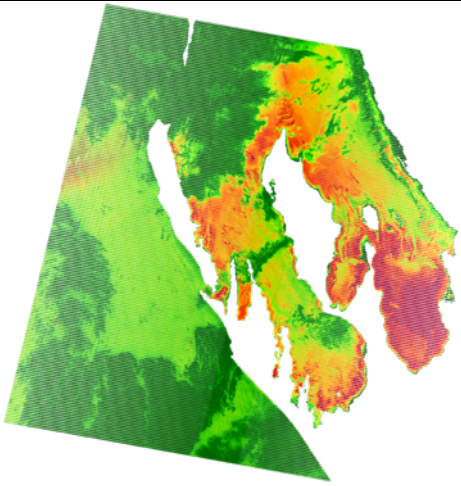	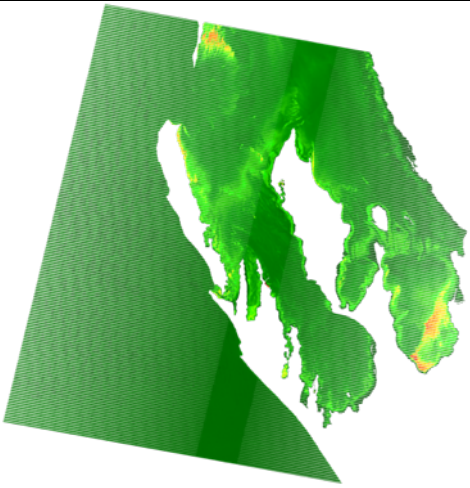
25.03.2007	13.06.2007
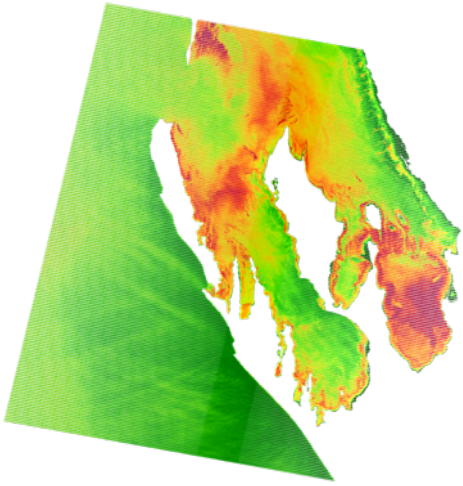	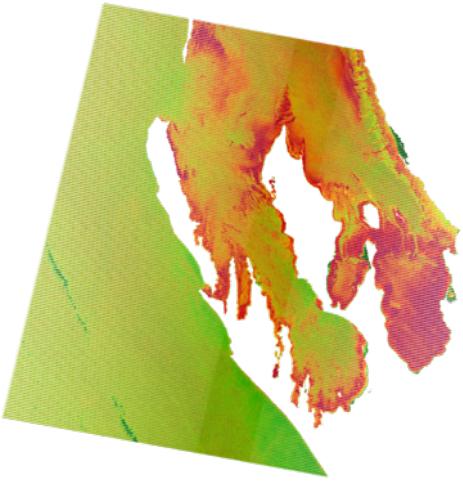

CDOM 01.09.2007	22.12.2007
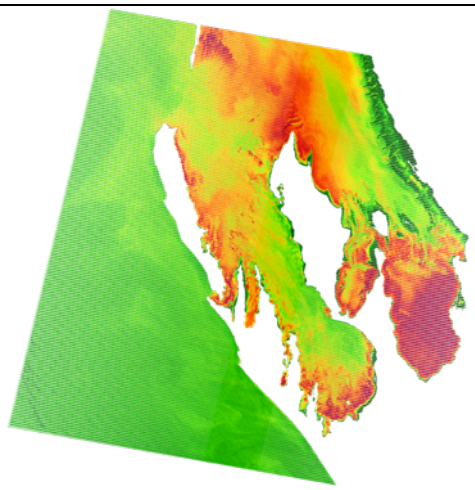	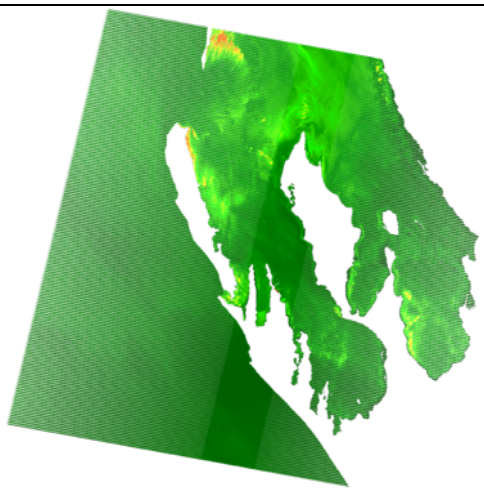
No Data	15.06.2008
	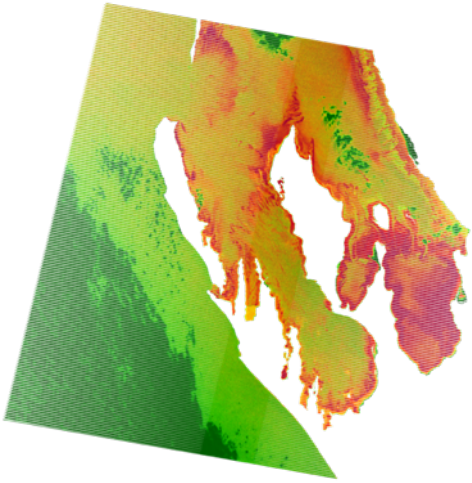
03.09.2008	24.12.2008
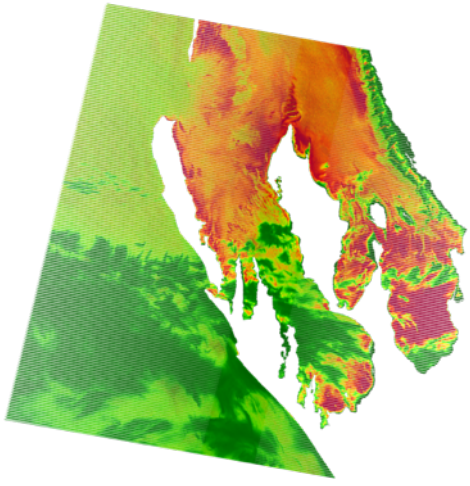	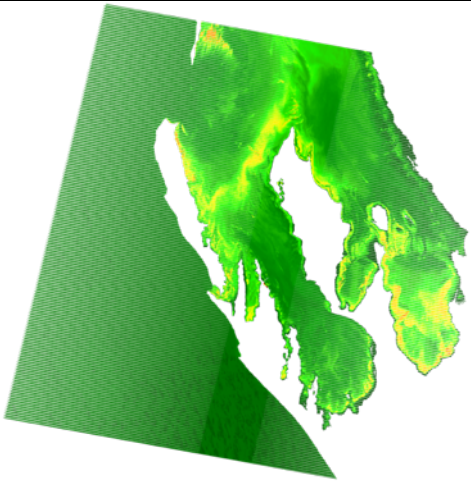

CDOM 14.03.2009	18.06.2009
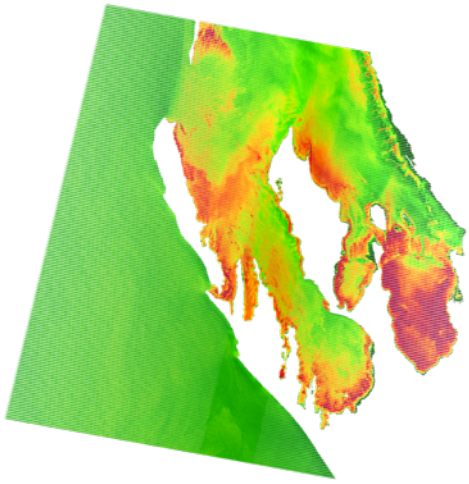	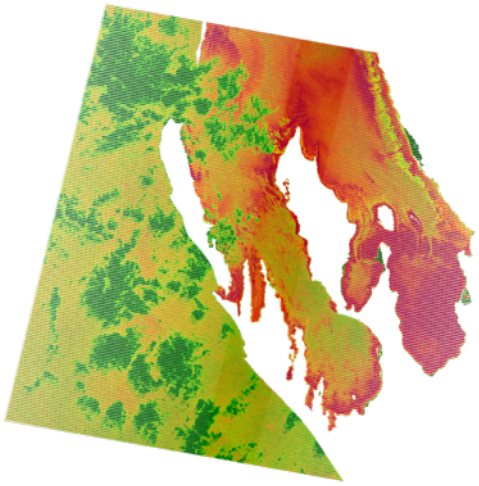
22.09.2009	11.12.2009
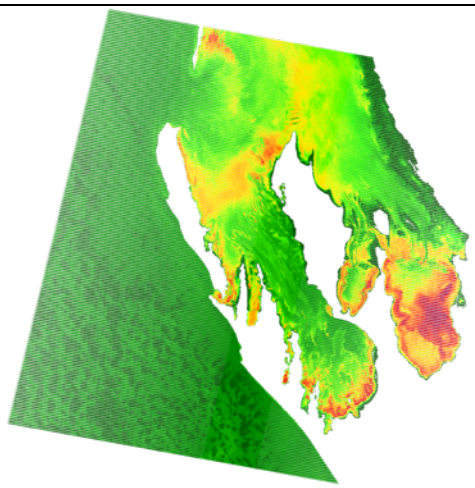	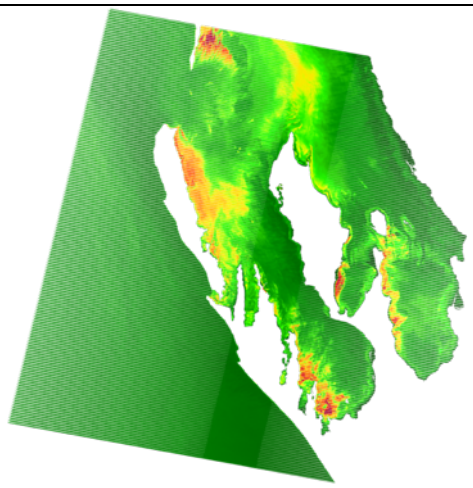
17.03.2010	21.06.2010
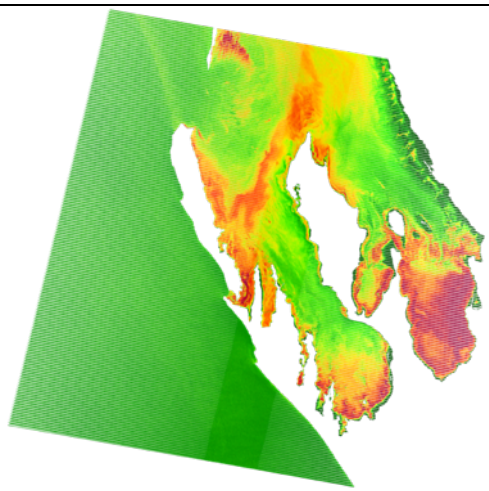	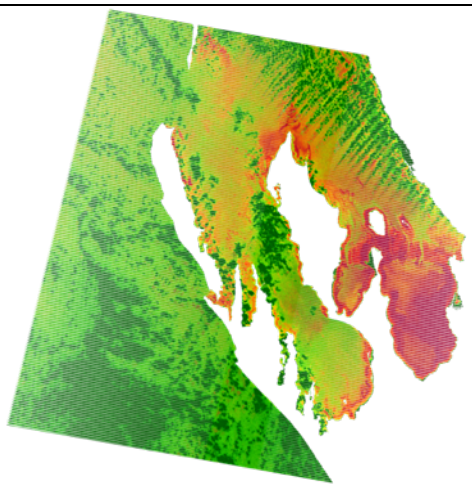

CDOM 25.09.2010	30.12.2010
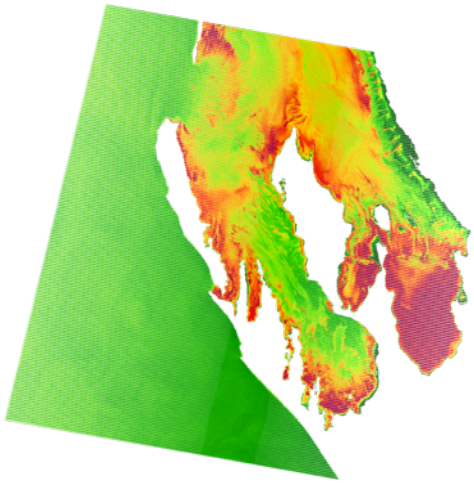	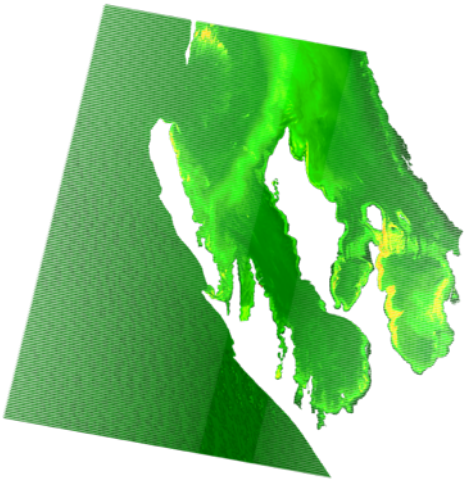
04.03.2011	08.06.2011
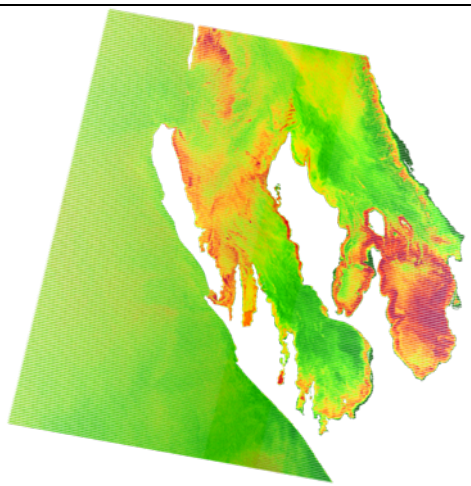	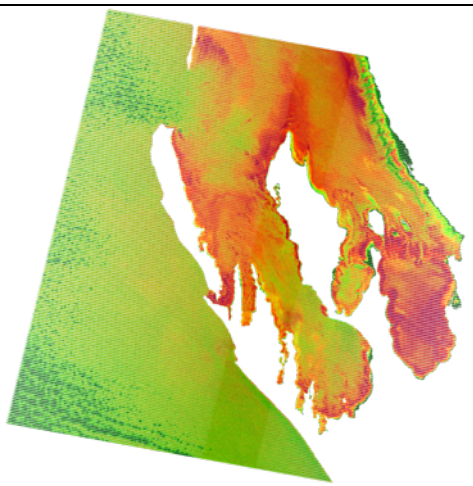
12.09.2011	01.12.2011
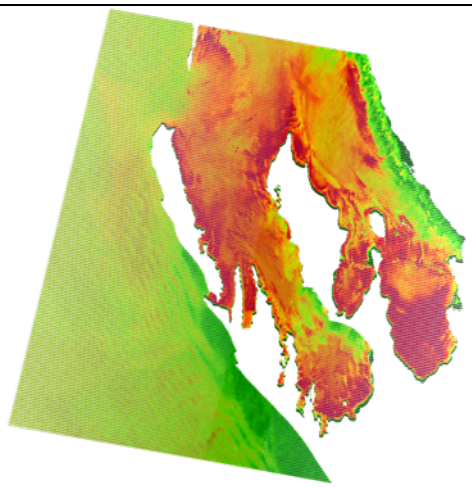	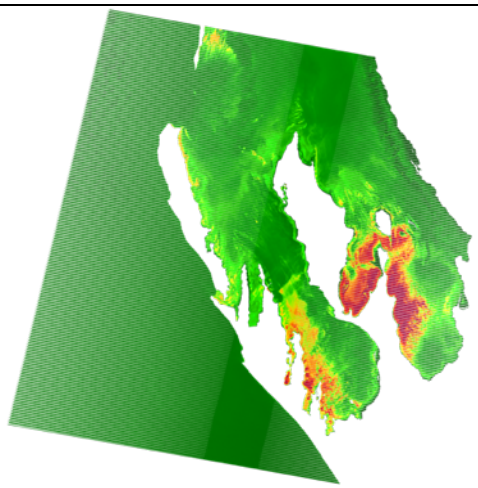

CDOM 06.03.2012	10.06.2012
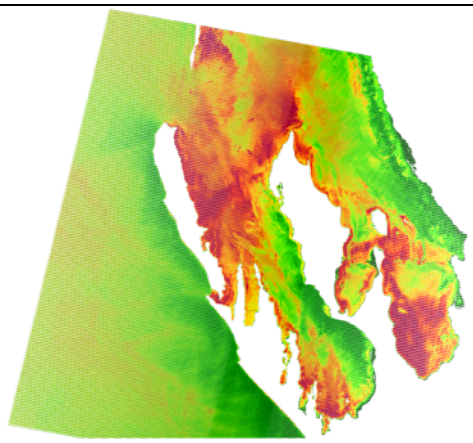	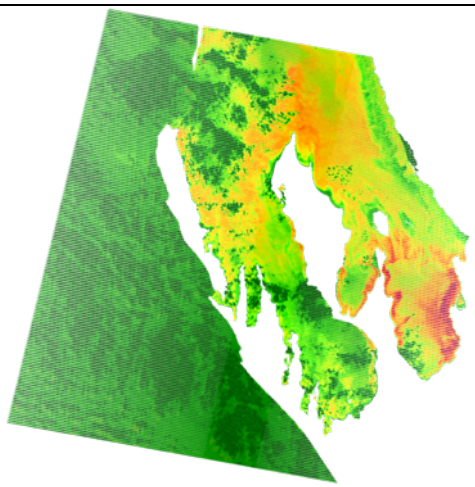
30.09.2012	03.12.2012
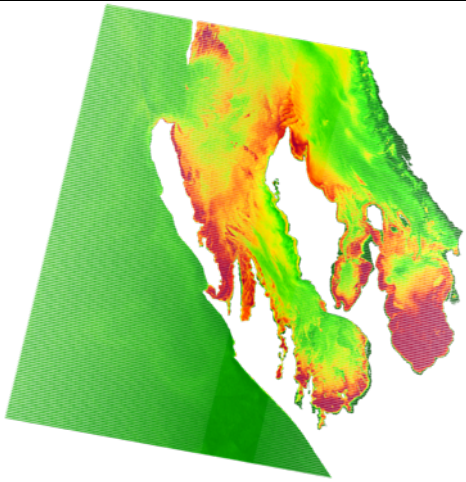	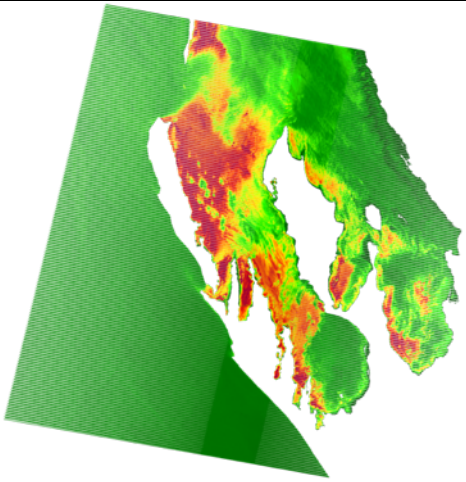
25.03.2013	29.06.2013
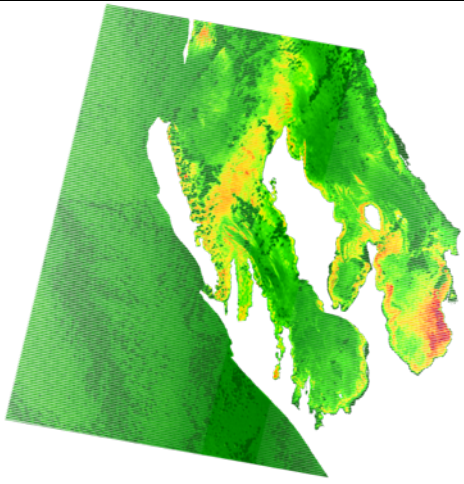	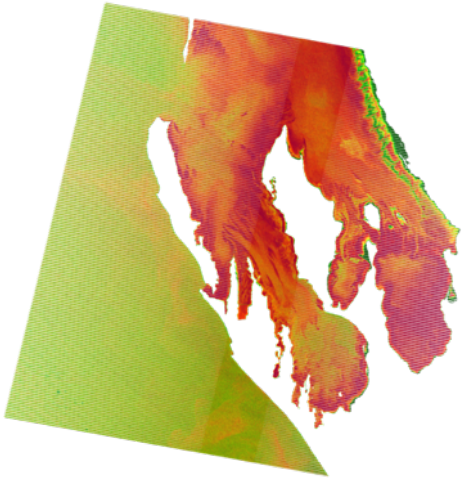

CDOM 09.09.2013 L8	22.12.2013
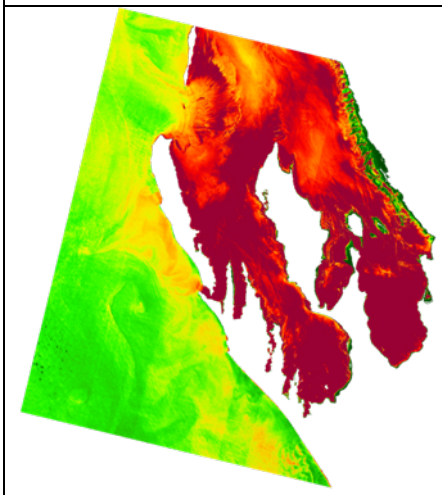	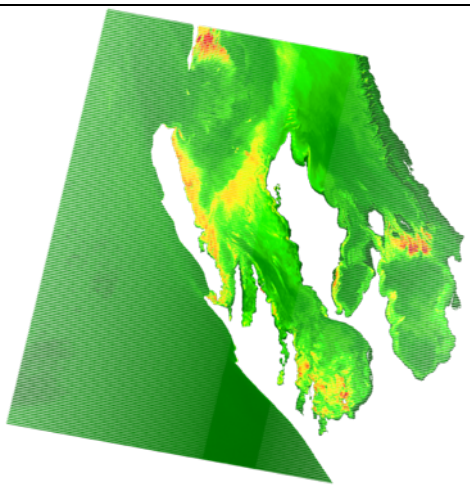
12.03.2014 (Error in Image)	16.06.2014
	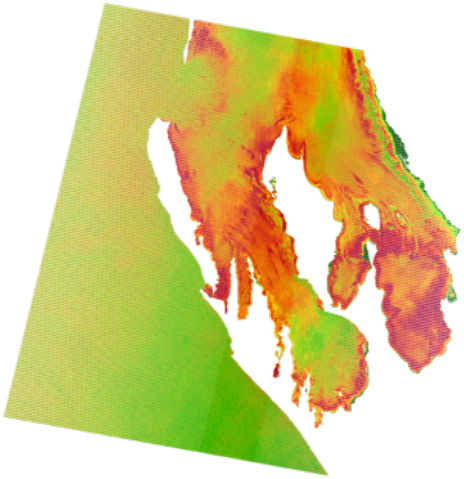
20.09.2014	25.12.2014
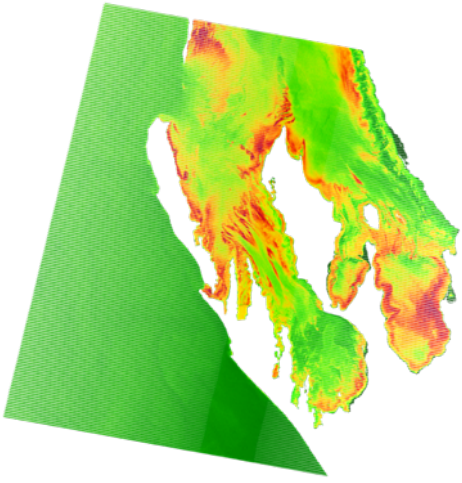	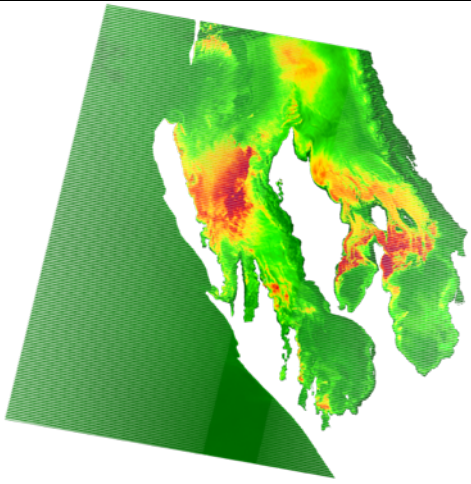

CDOM 15.03.2015	03.06.2015
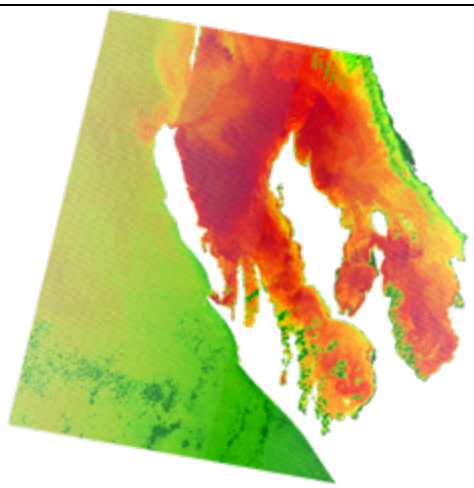	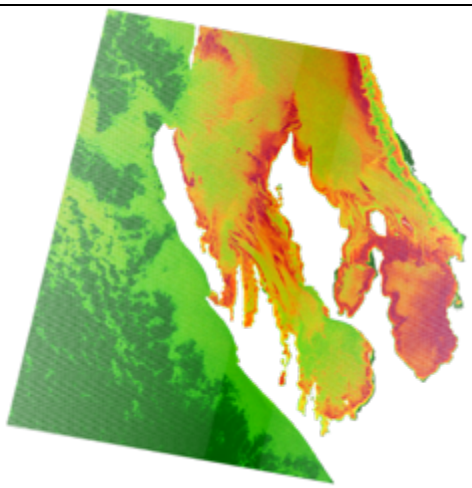
07.09.2015	12.12.2015
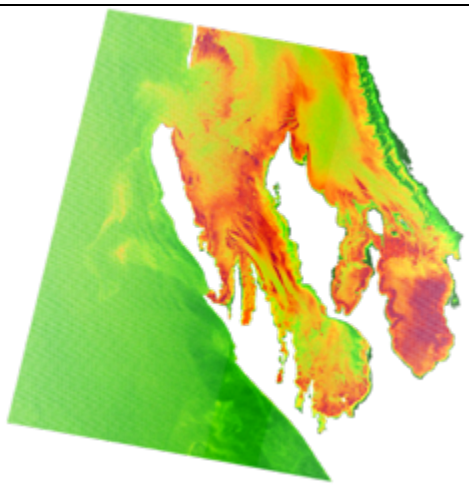	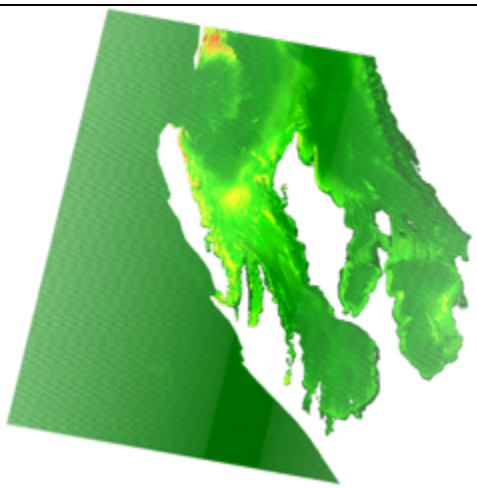
01.03.2016	13.06.2016 L8
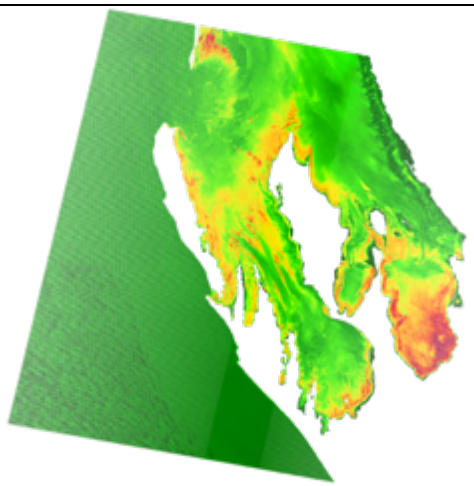	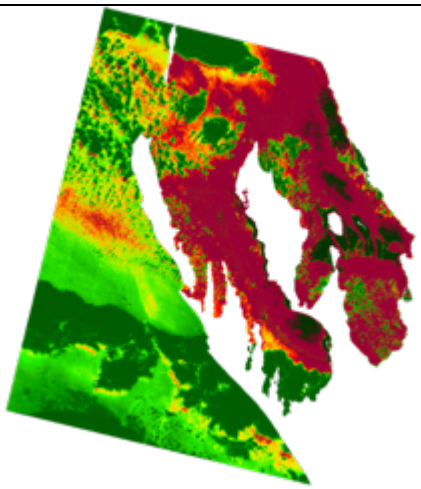

CDOM 09.09.2016	14.12.2012
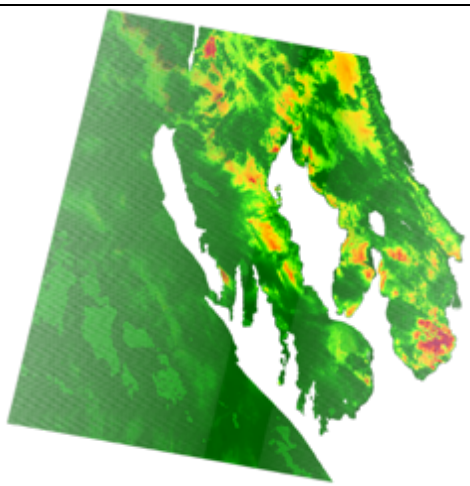	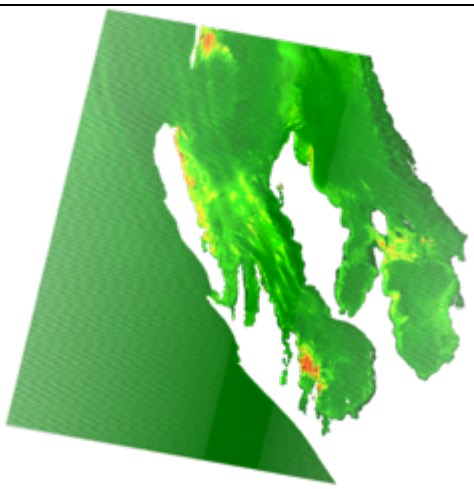
04.03.2017	08.06.2017
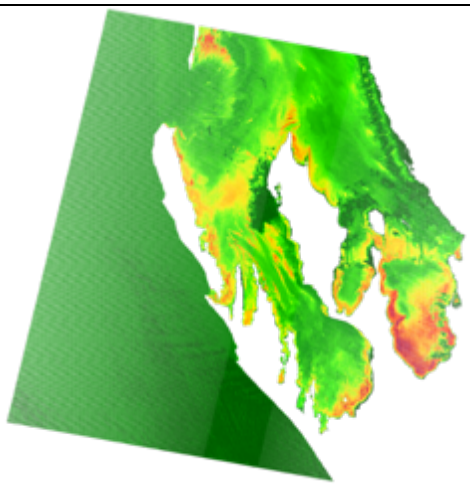	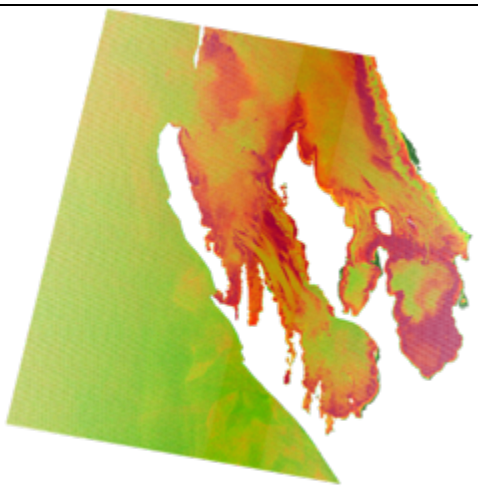
12.09.2017	01.12.2017
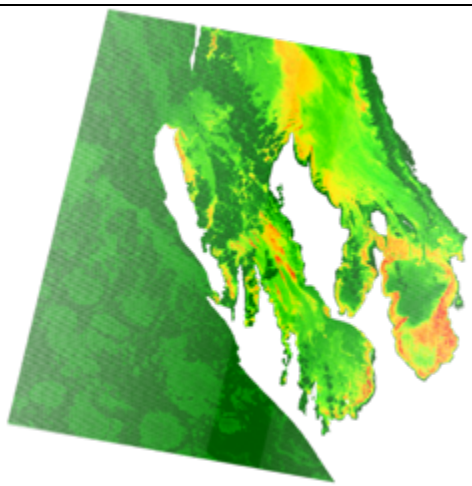	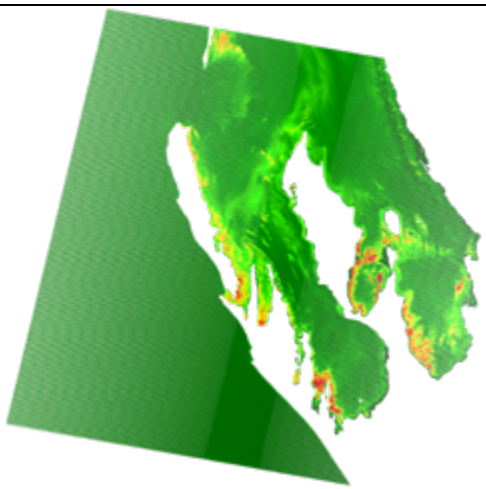

CDOM 07.03.2018

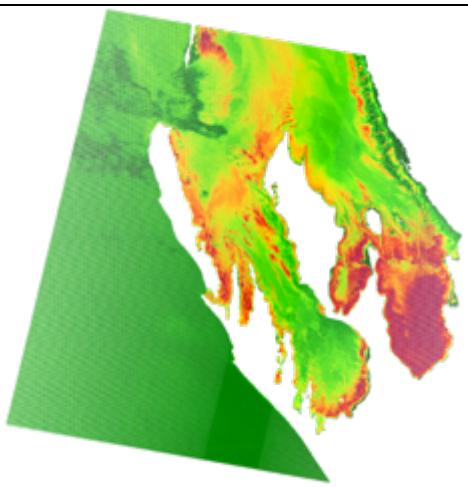

8.3.2 Plots

CDOM at West 1 (June)

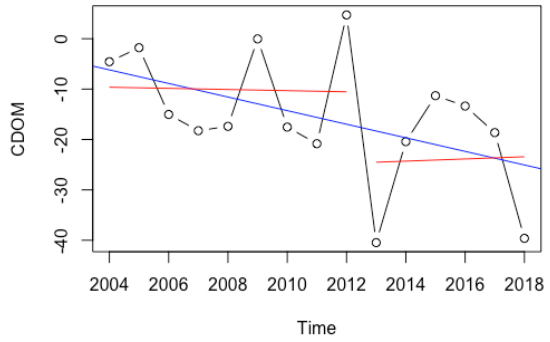

CDOM at West 2 (June)

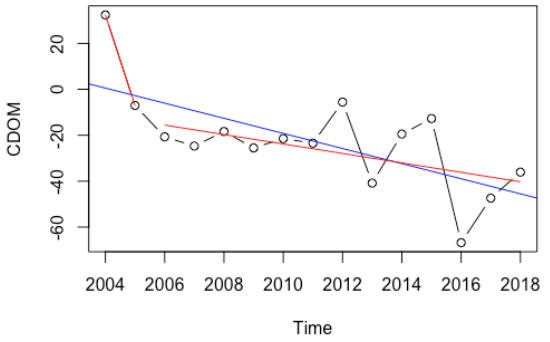

CDOM at West 3 (June)

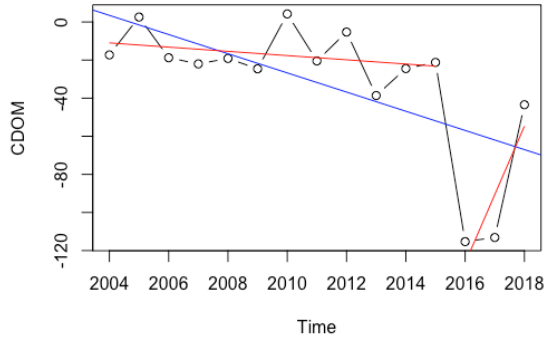

CDOM at West 4 (June)

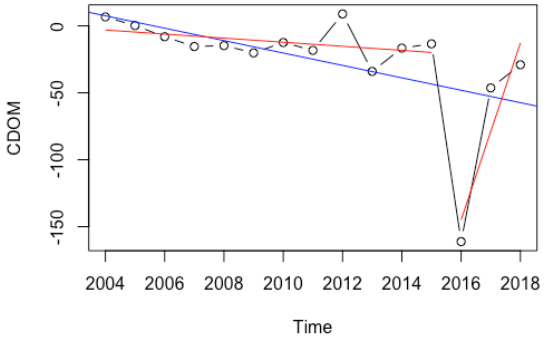

CDOM at West 5 (June)

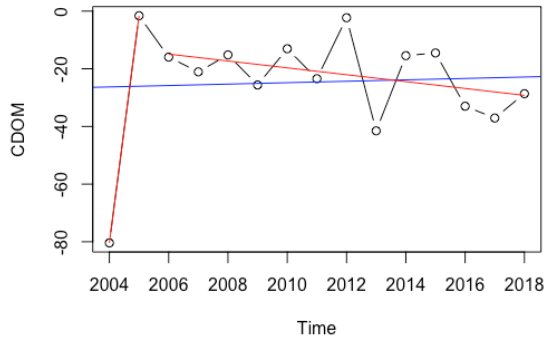

CDOM at East 1 (June)

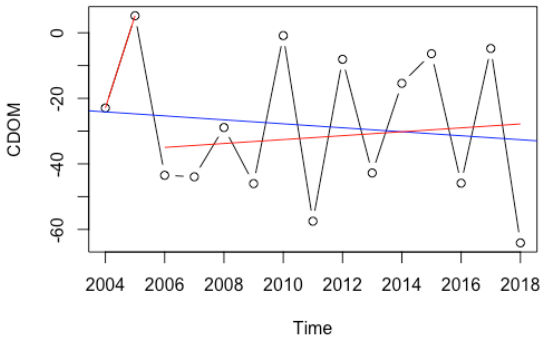

CDOM at East 2 (June)	CDOM at East 3 (June)
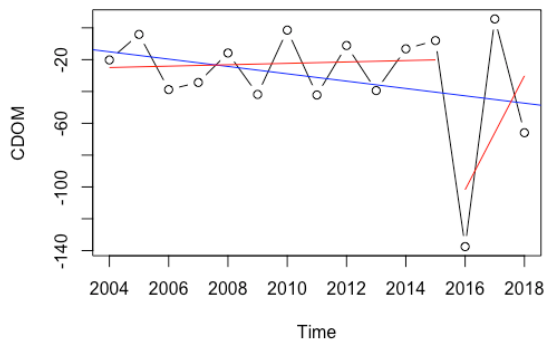	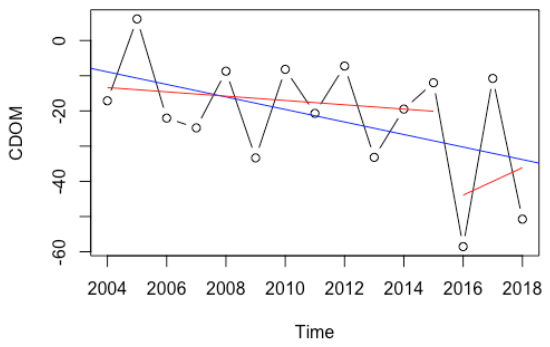
CDOM at East 4 (June)	CDOM at East 5 (June)
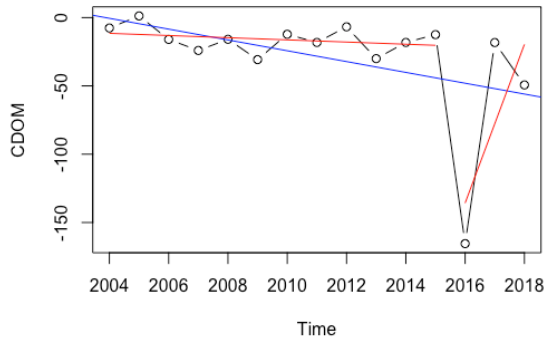	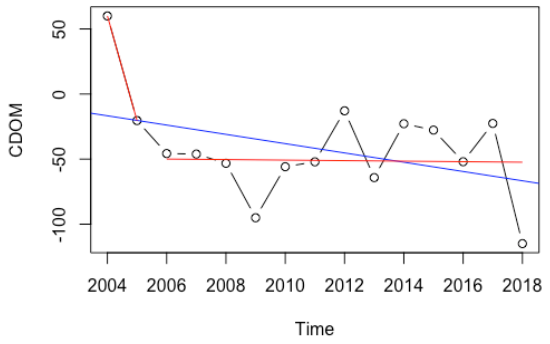

8.4 Correlation

East 1 CDOM and NDCI

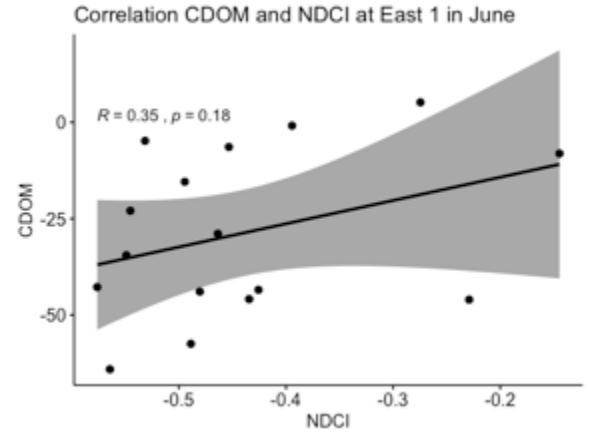

East 2 CDOM and NDCI

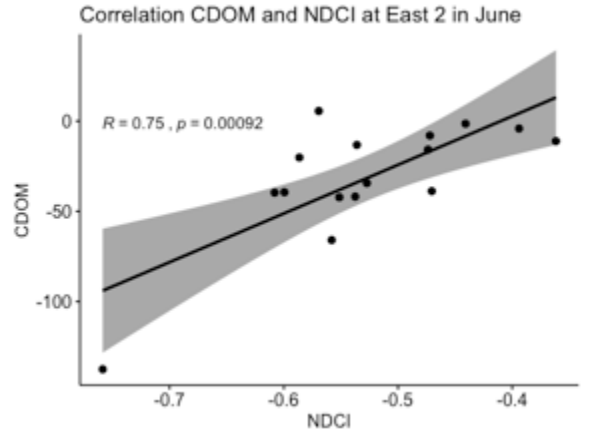

East 3 CDOM and NDCI

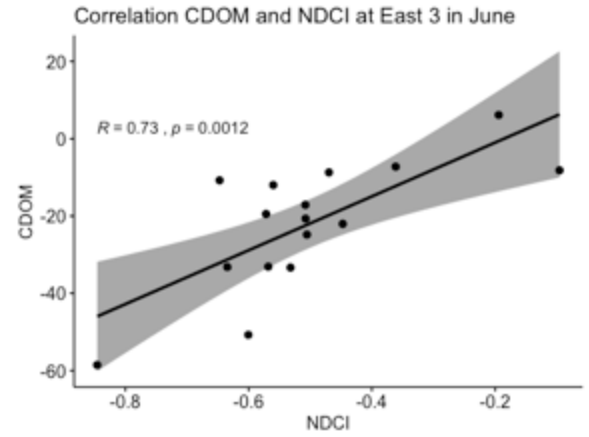

East 4 CDOM and NDCI

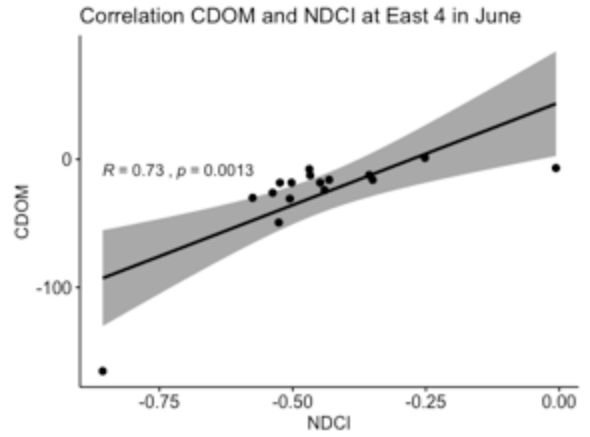

East 5 CDOM and NDCI

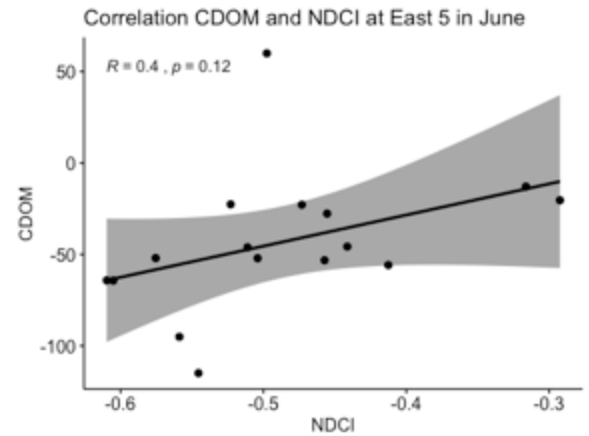

East 1 CDOM and TSS

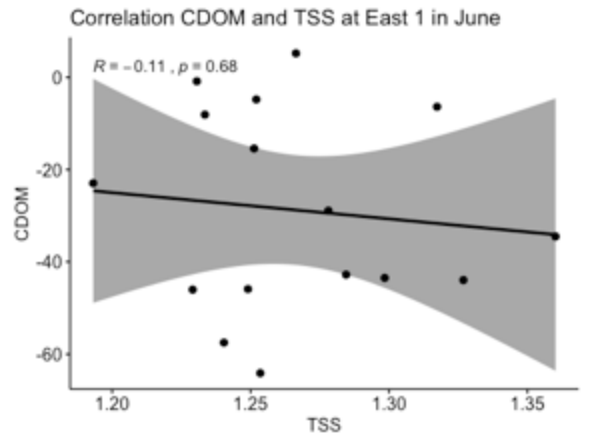

East 2 CDOM and TSS

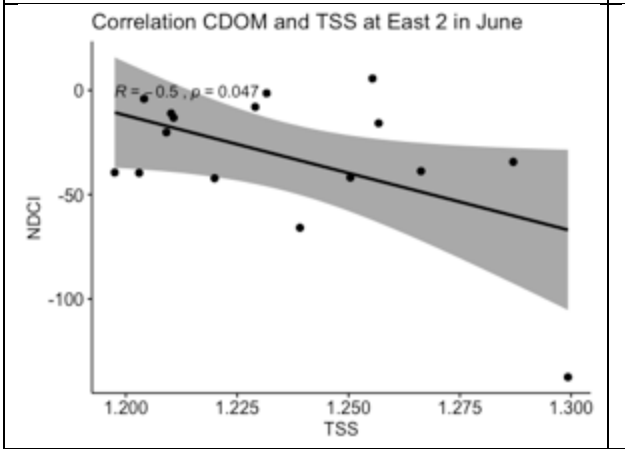

East 3 CDOM and TSS

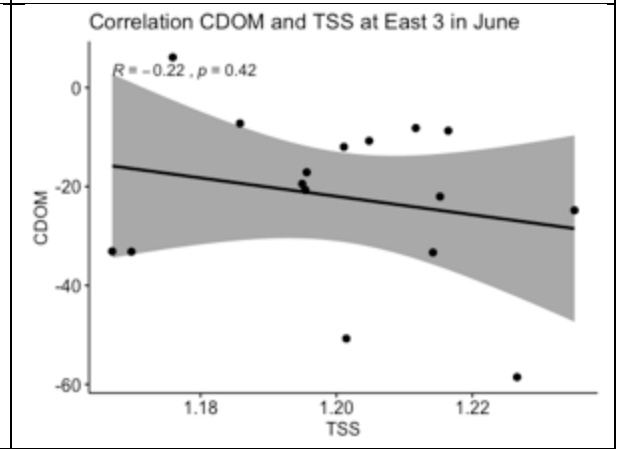

East 4 CDOM and TSS

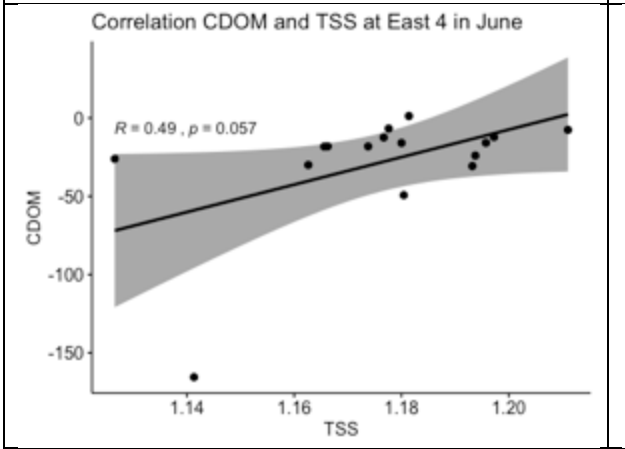

East 5 CDOM and TSS

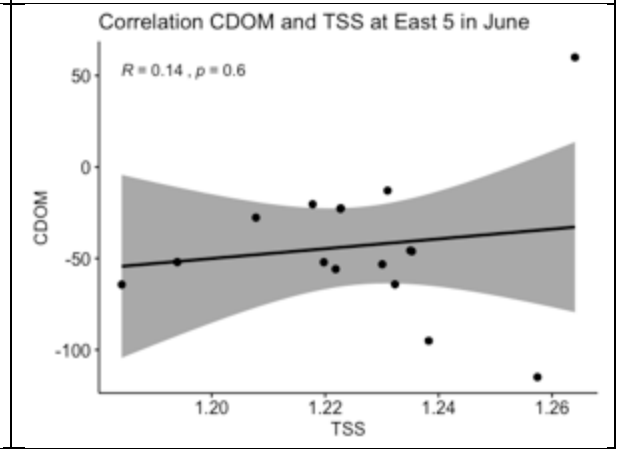

East 1 NDCI and TSS

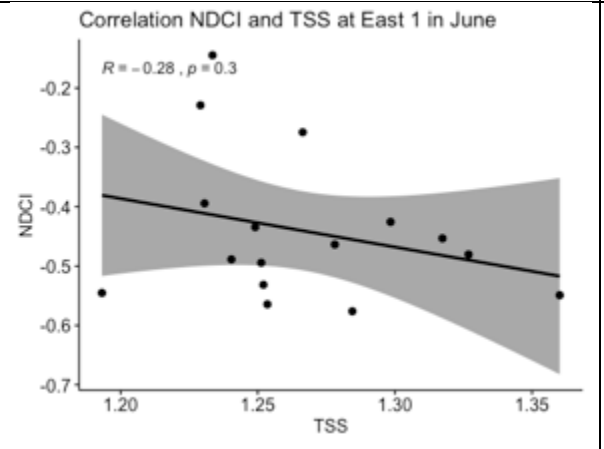

East 2 NDCI and TSS

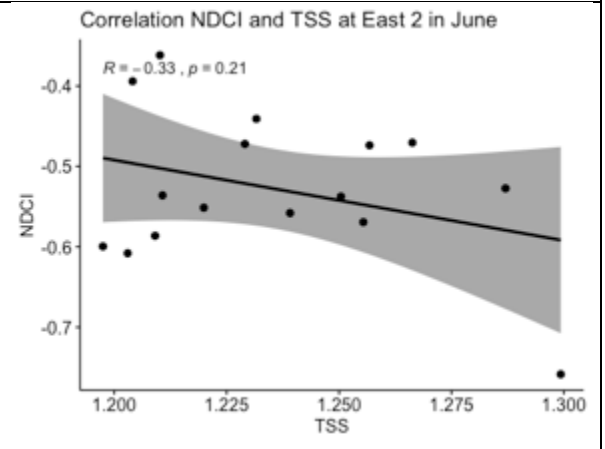

East 3 NDCI and TSS

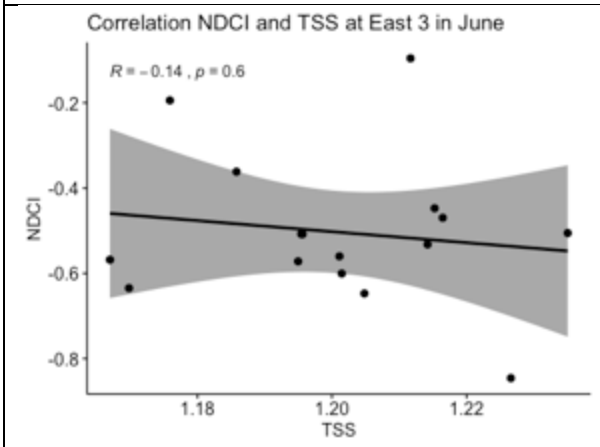

East 4 NDCI and TSS

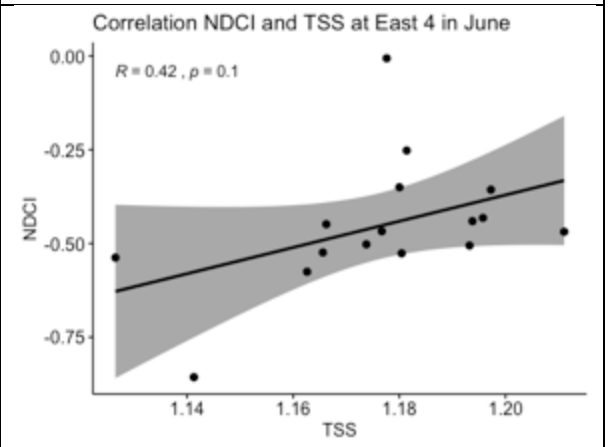

East 5 NDCI and TSS

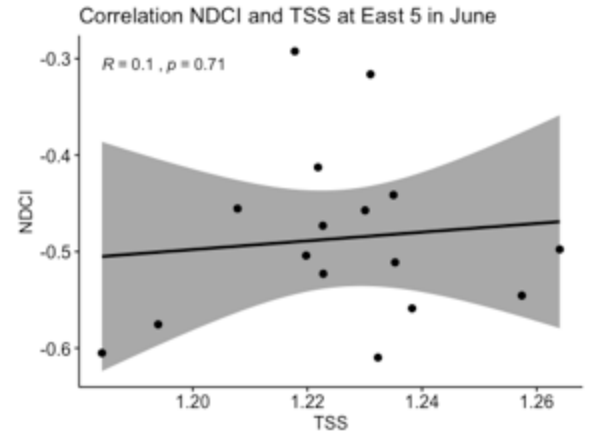

West 1 CDOM and NDCI

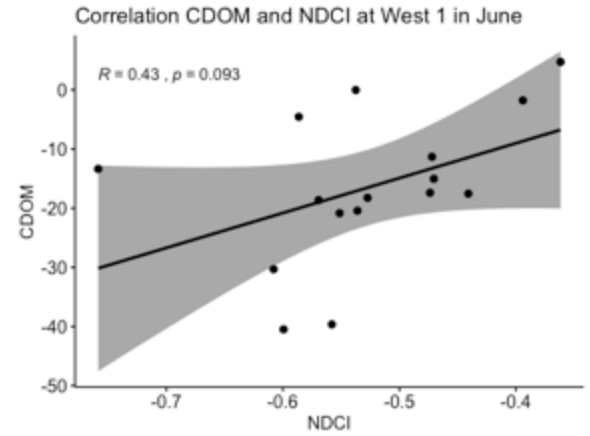

West 2 CDOM and NDCI

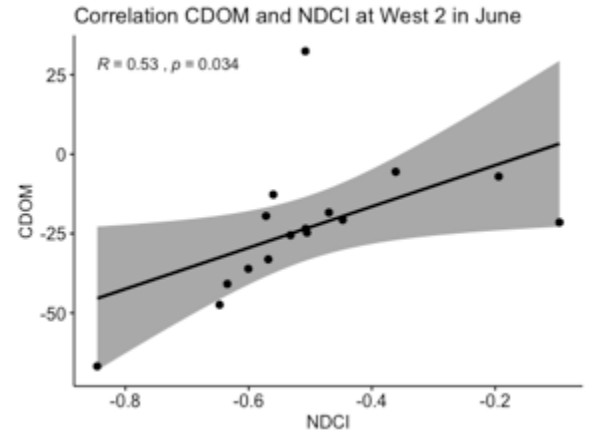

West 3 CDOM and NDCI

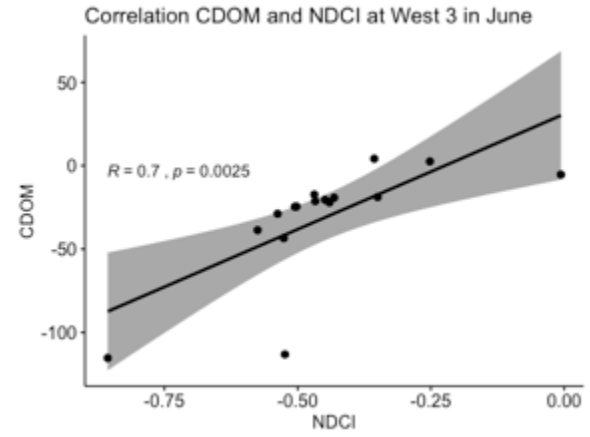

West 4 CDOM and NDCI

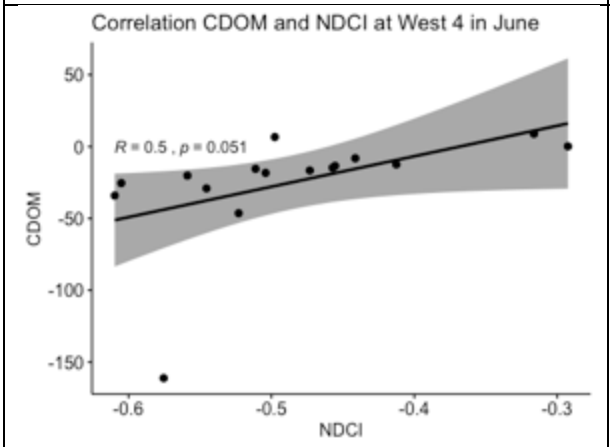

West 5 CDOM and NDCI

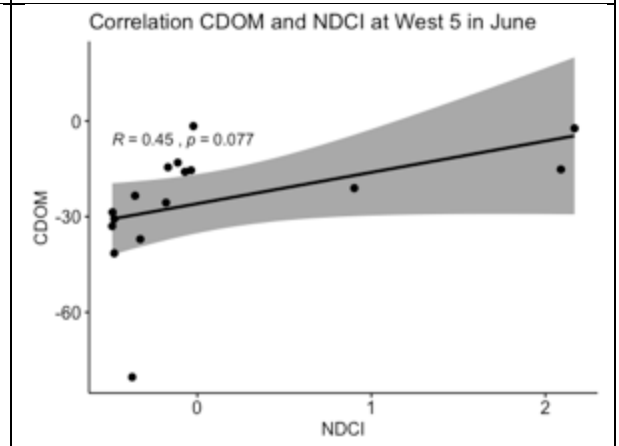

West 1 CDOM and TSS

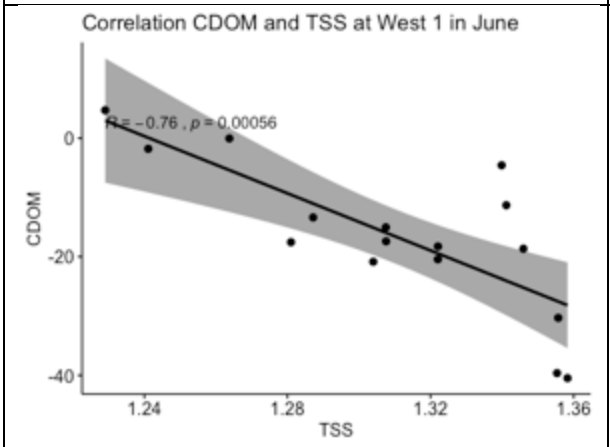

West 2 CDOM and TSS

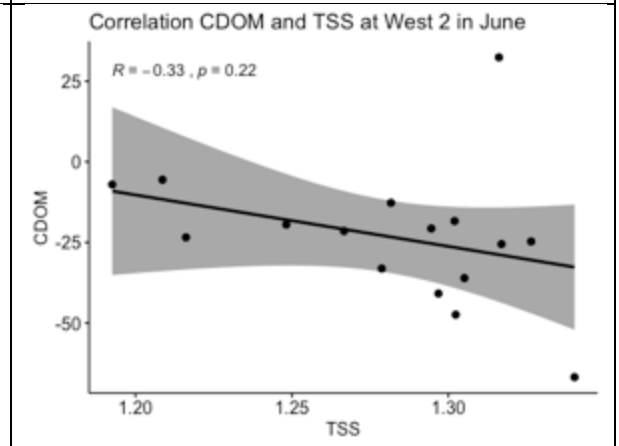

West 3 CDOM and TSS

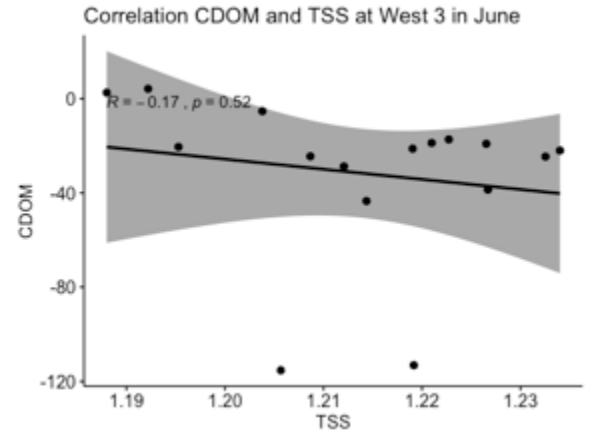

West 4 CDOM and TSS

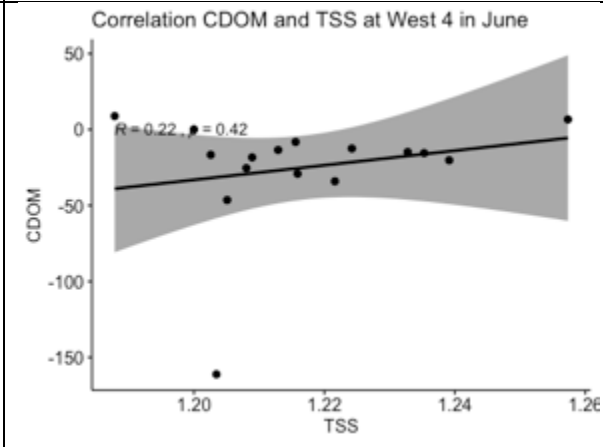

West 5 CDOM and TSS

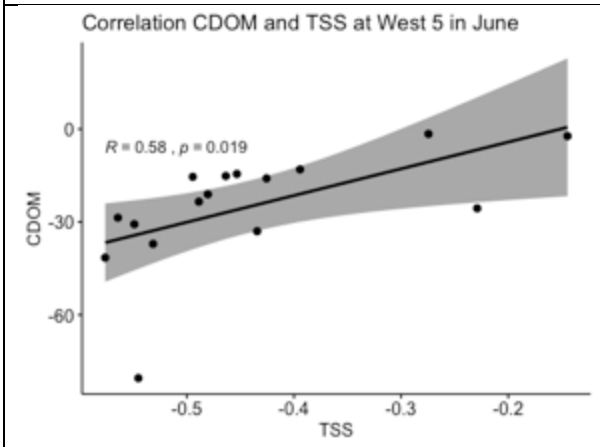

West 1 NDCI and TSS

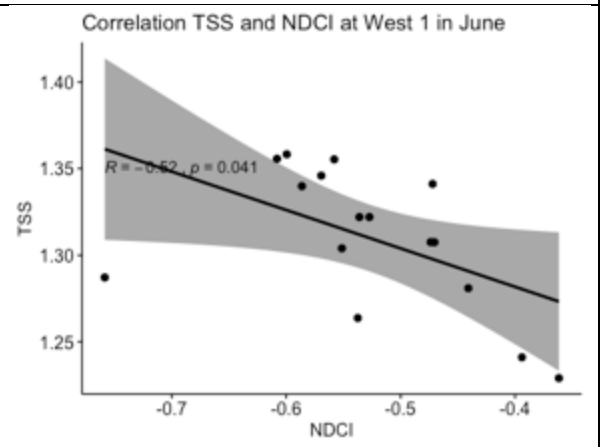

West 2 NDCI and TSS

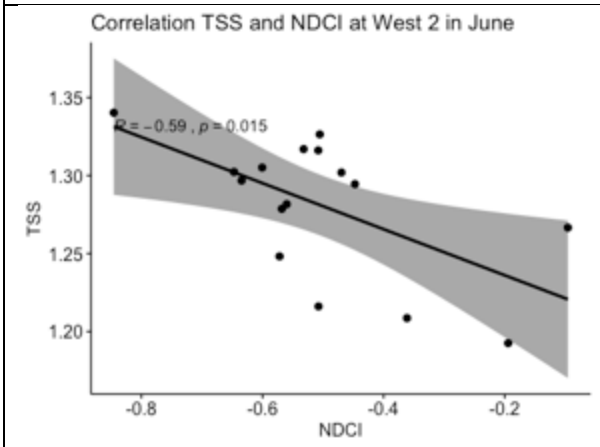

West 3 NDCI and TSS

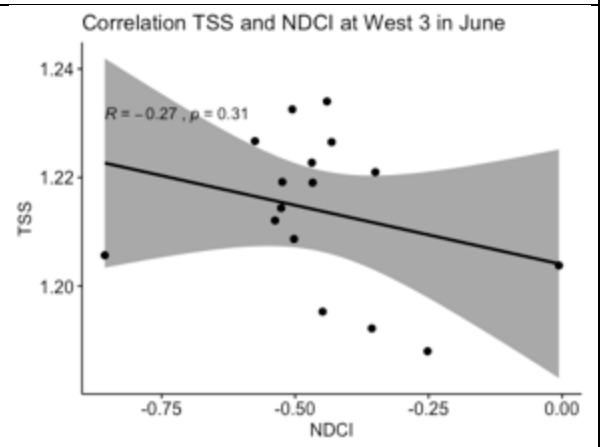

West 4 NDCI and TSS

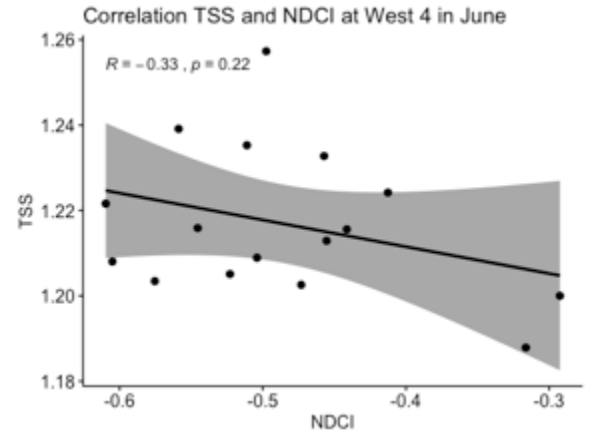

West 5 NDCI and TSS

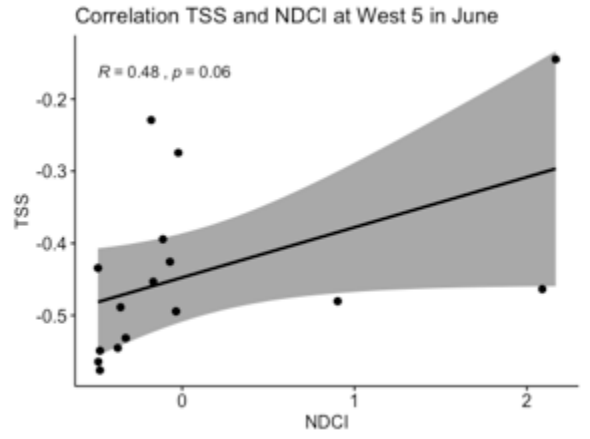

East 1 SST and NDCI

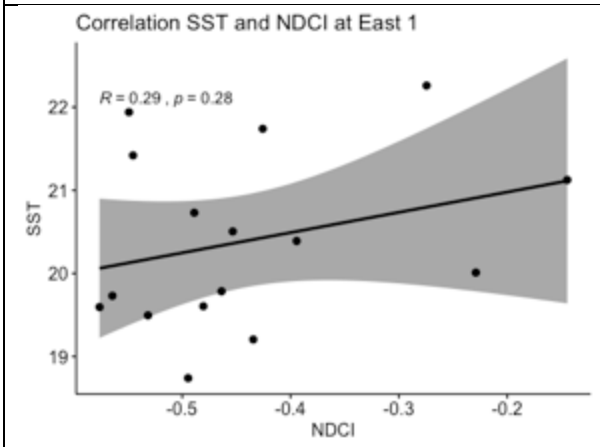

East 2 SST and NDCI

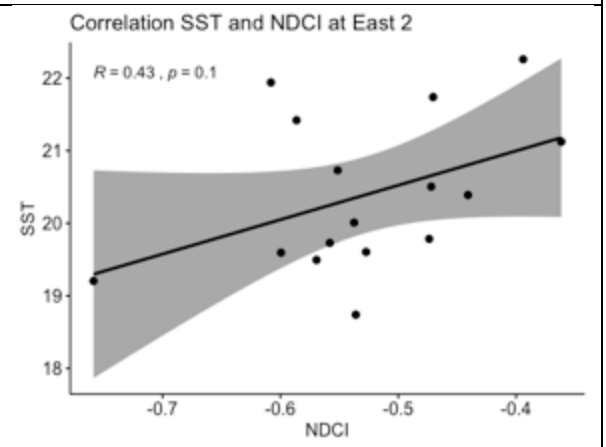

East 3 SST and NDCI

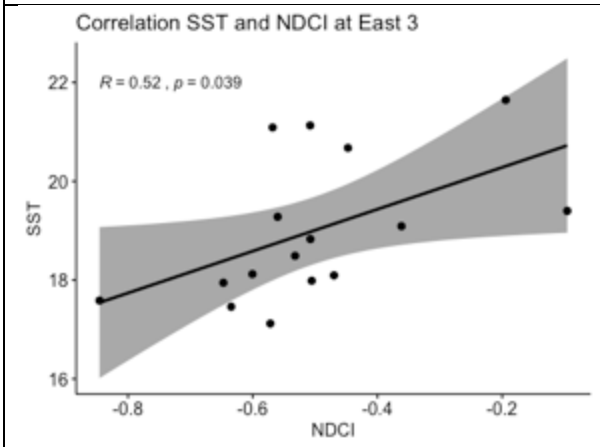

East 4 SST and NDCI

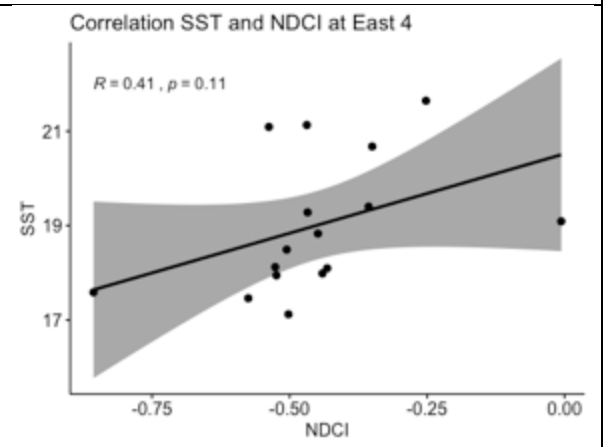

East 5 SST and NDCI

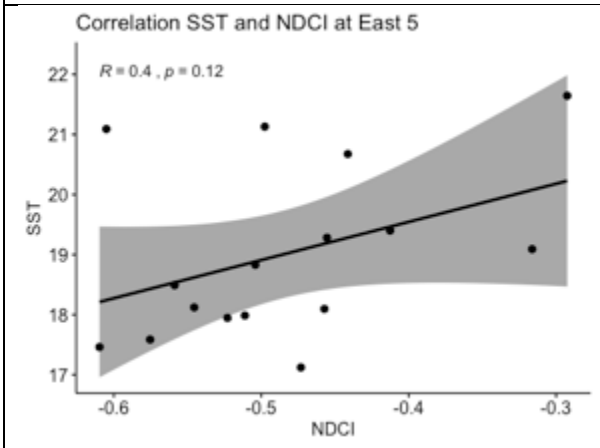

East 1 SST and TSS

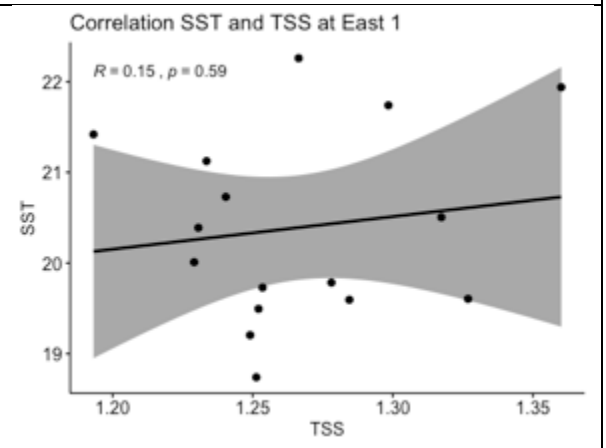

East 2 SST and TSS

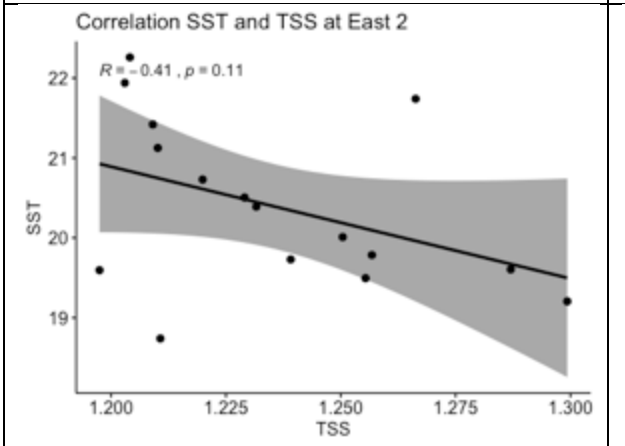

East 3 SST and TSS

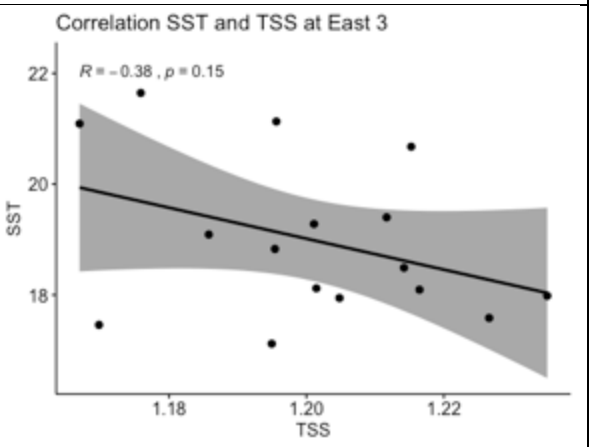

East 4 SST and TSS

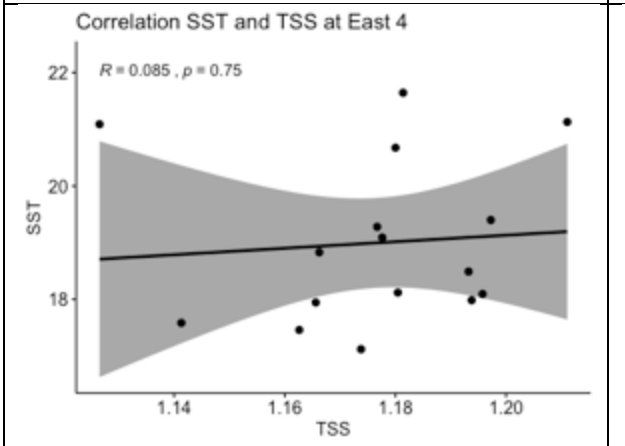

East 5 SST and TSS

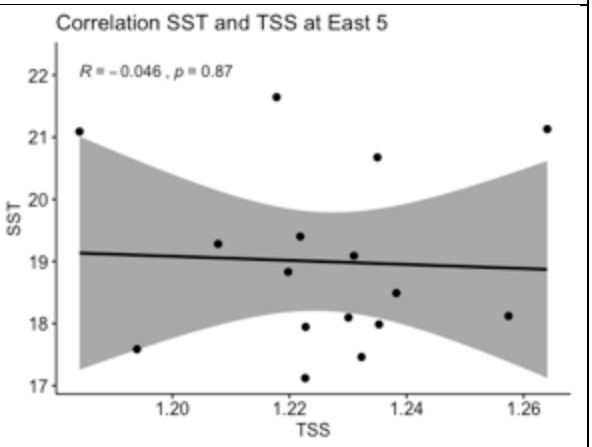

East 1 SST and CDOM

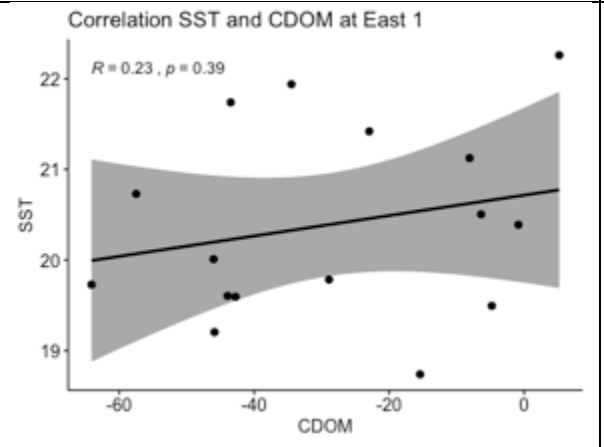

East 2 SST and CDOM

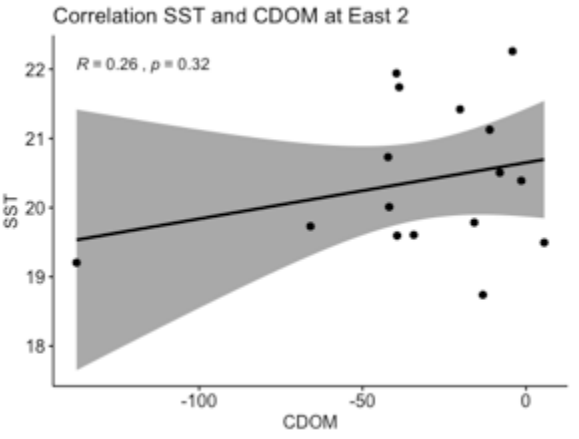

East 3 SST and CDOM

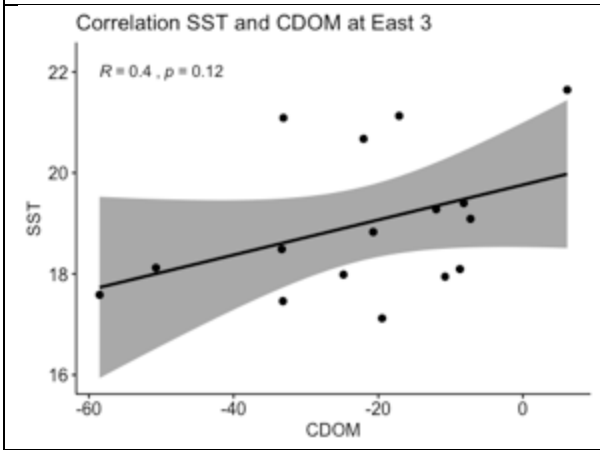

East 4 SST and CDOM

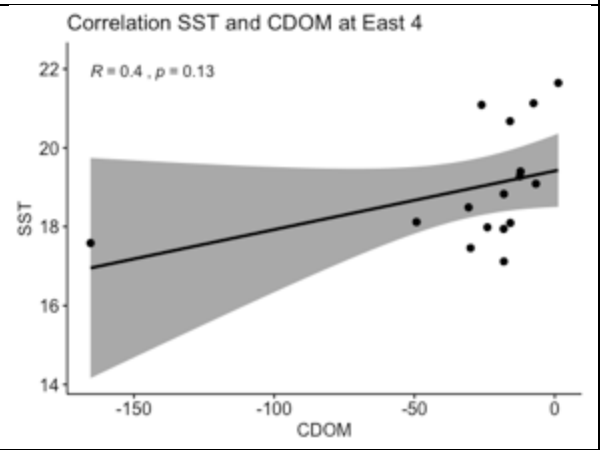

East 5 SST and CDOM

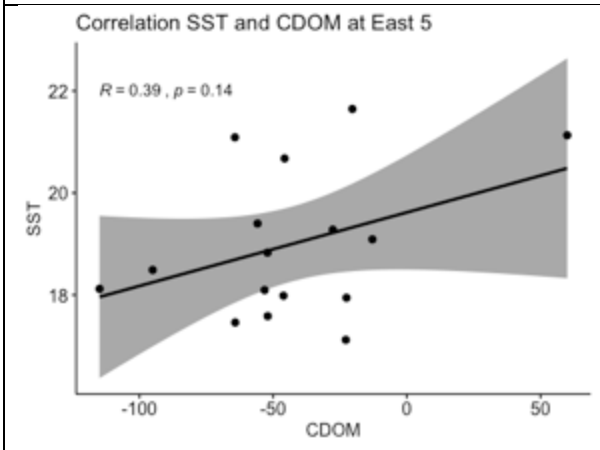

West 1 SST and NDCI

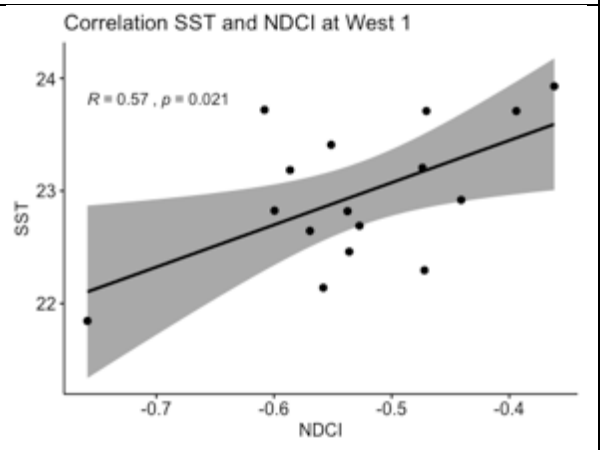

West 2 SST and NDCI

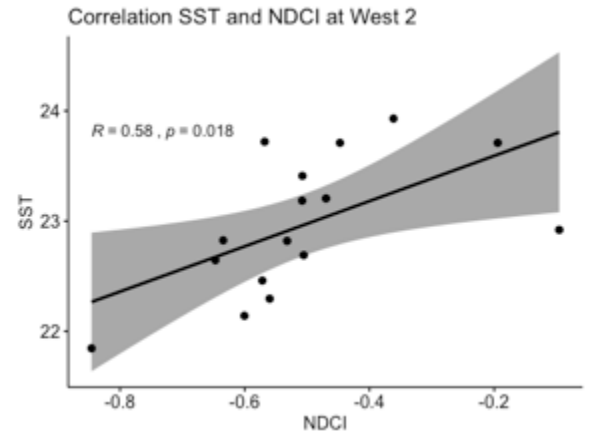

West 3 SST and NDCI

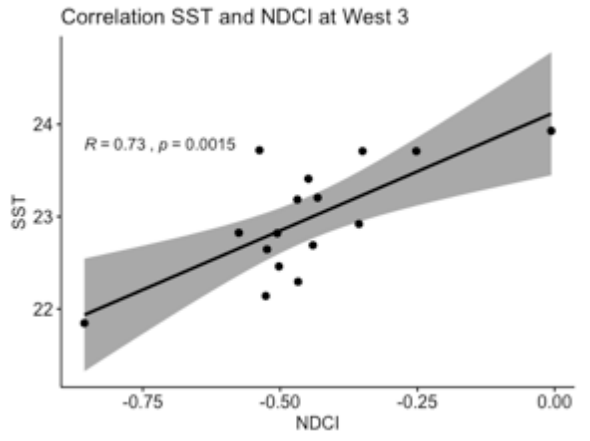

West 4 SST and NDCI

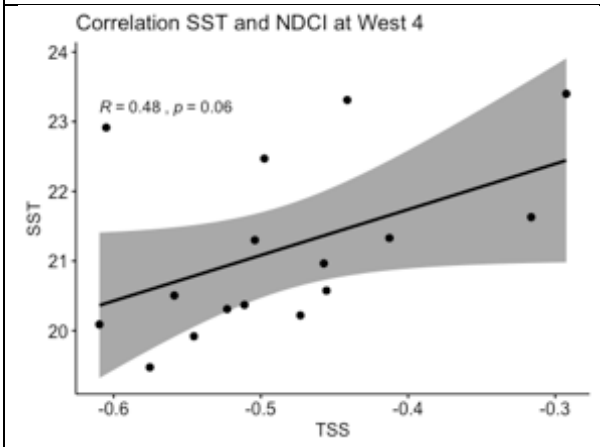

West 5 SST and NDCI

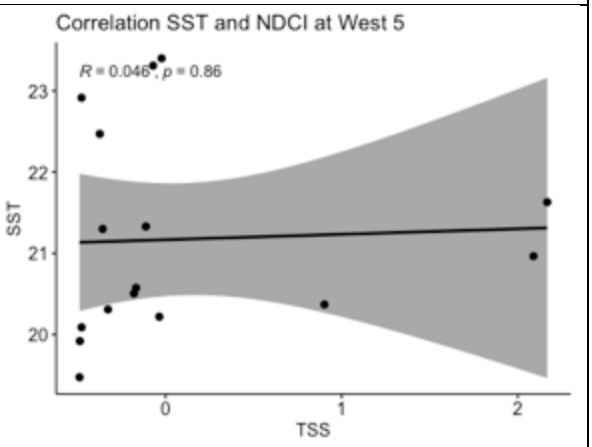

West 1 SST and TSS

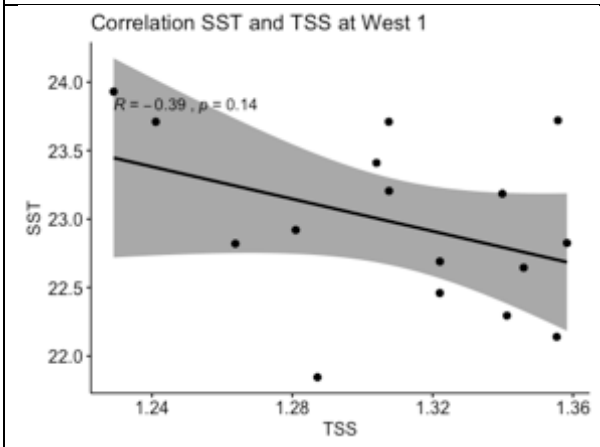

West 2 SST and TSS

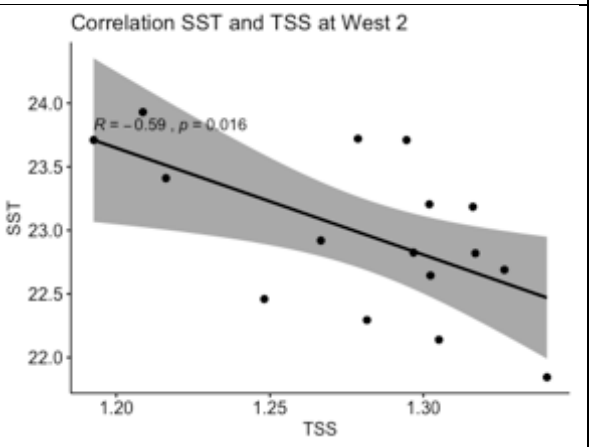

West 3 SST and TSS

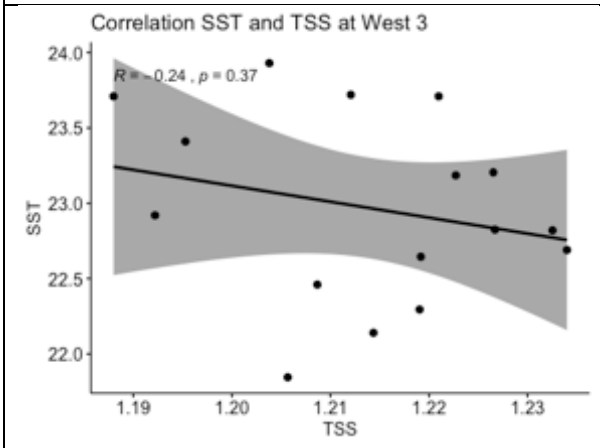

West 4 SST and TSS

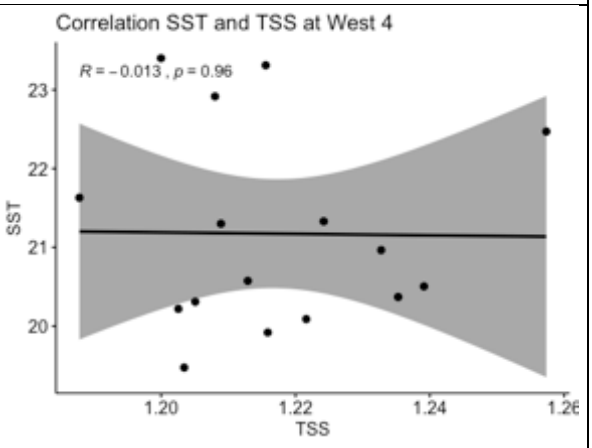

West 5 SST and TSS

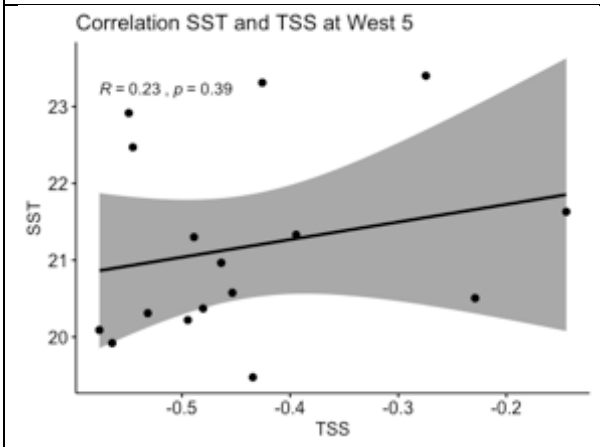

West 1 SST and CDOM

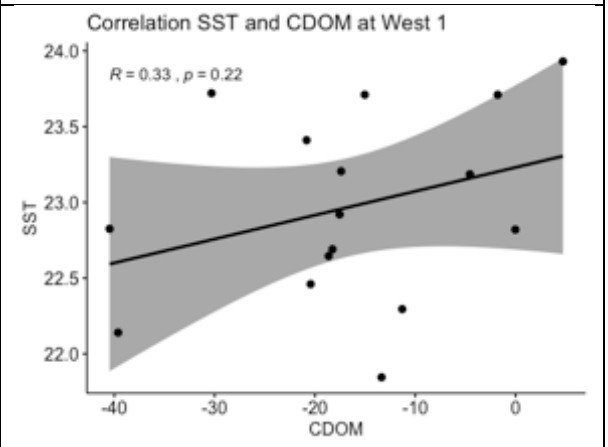

West 2 SST and CDOM

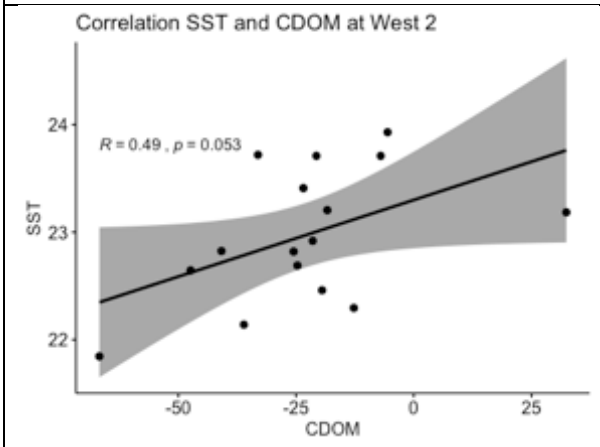

West 3 SST and CDOM

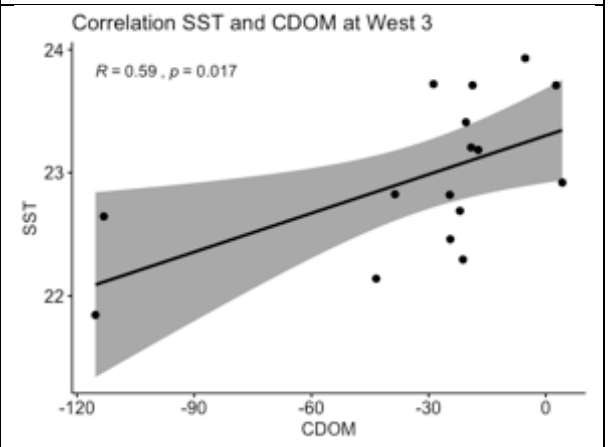

West 4 SST and CDOM

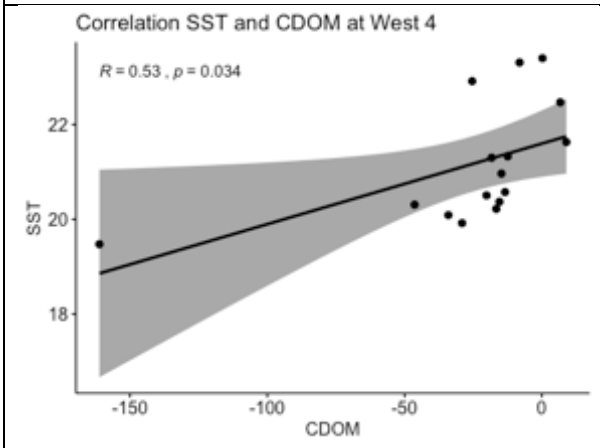

West 5 SST and CDOM

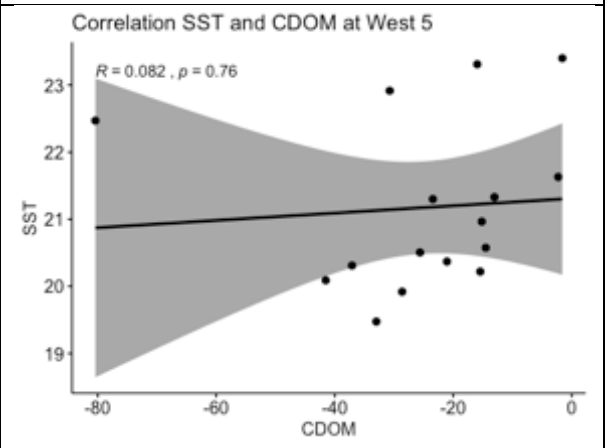

9. Personal declaration

I, Luca Brüderlin, hereby declare that the submitted thesis is the result of my own, independent work. All external sources are explicitly acknowledged in the thesis.

Luca Brüderlin